

CLIMATE DIAGNOSTICS BULLETIN



AUGUST 2010

NEAR REAL-TIME OCEAN / ATMOSPHERE

Monitoring, Assessments, and Prediction

U.S. DEPARTMENT OF COMMERCE
National Oceanic and Atmospheric Administration
National Weather Service
National Centers for Environmental Prediction

CLIMATE DIAGNOSTICS BULLETIN



CLIMATE PREDICTION CENTER
Attn: Climate Diagnostics Bulletin
W/NP52, Room 605, WWBG
Camp Springs, MD 20746-4304

Chief Editor: Gerald D. Bell

Editors: Wei Shi, Michelle L'Heureux, and Michael Halpert

Bulletin Production: Wei Shi

External Collaborators:

Center for Ocean-Atmospheric Prediction Studies (COAPS)

Cooperative Institute for Research in the Atmosphere (CIRA)

Earth & Space Research

International Research Institute for Climate and Society (IRI)

Joint Institute for the Study of the Atmosphere and Ocean (JISAO)

Lamont-Doherty Earth Observatory (LDEO)

NOAA-CIRES, Climate Diagnostics Center

NOAA-AOML, Atlantic Oceanographic and Meteorological Laboratory

NOAA-NESDIS-STAR, Center for Satellite Applications and Research

NOAA-NDBC, National Data Buoy Center

Scripps Institution of Oceanography

Software: Most of the bulletin figures generated at CPC are created using the Grid Analysis and Display System (GrADS).

- Climate Diagnostics Bulletin available on the World Wide Web

The CDB is available on the World Wide Web. The address of the online version of the CDB is:

<http://www.cpc.ncep.noaa.gov/products/CDB>

If you have any problems accessing the bulletin, contact Dr. Wei Shi by E-mail:

Wei.Shi@noaa.gov

Table of Contents

TROPICS

Highlights *page 6*
 Table of Atmospheric Indices *page 7*
 Table of Oceanic Indices *page 8*

FIGURE

Time Series

| | |
|--|----|
| Southern Oscillation Index (SOI) | T1 |
| Tahiti and Darwin SLP Anomalies | T1 |
| OLR Anomalies | T1 |
| CDAS/Reanalysis SOI & Equatorial SOI | T2 |
| 200-hPa Zonal Wind Anomalies | T3 |
| 500-hPa Temperature Anomalies | T3 |
| 30-hPa and 50-hPa Zonal Wind Anomalies | T3 |
| 850-hPa Zonal Wind Anomalies | T4 |
| Equatorial Pacific SST Anomalies | T5 |

Time-Longitude Sections

| | |
|---|-----|
| Mean and Anomalous Sea Level Pressure | T6 |
| Mean and Anomalous 850-hPa Zonal Wind | T7 |
| Mean and Anomalous OLR | T8 |
| Mean and Anomalous SST | T9 |
| Pentad SLP Anomalies | T10 |
| Pentad OLR Anomalies | T11 |
| Pentad 200-hPa Velocity Potential Anomalies | T12 |
| Pentad 850-hPa Zonal Wind Anomalies | T13 |
| Anomalous Equatorial Zonal Wind | T14 |
| Mean and Anomalous Depth of the 20°C Isotherm | T15 |

Mean & Anomaly Fields

| | |
|--|-----------|
| Depth of the 20°C Isotherm | T16 |
| Subsurface Equatorial Pacific Temperatures | T17 |
| SST | T18 |
| SLP | T19 |
| 850-hPa Vector Wind | T20 |
| 200-hPa Vector Wind | T21 |
| 200-hPa Streamfunction | T22 |
| 200-hPa Divergence | T23 |
| 200-hPa Velocity Potential and Divergent Wind | T24 |
| OLR | T25 |
| SSM/I Tropical Precipitation Estimates | T26 |
| Cloud Liquid Water | T27 |
| Precipitable Water | T28 |
| Divergence & E-W Divergent Circulation | T29 - T30 |
| Pacific Zonal Wind & N-S Divergent Circulation | T31 - T32 |

Appendix 1: Outside Contributions

| | |
|--|-------------|
| Tropical Drifting Buoys | A1.1 |
| Thermistor Chain Data | A1.2 |
| TAO/TRITON Array Time-Longitude Sections | A1.3 - A1.4 |

FIGURE

| | |
|------------------------------------|-------------|
| East Pacific SST and Sea Level | A1.5 |
| Pacific Wind Stress and Anomalies | A1.6 |
| Satellite-Derived Surface Currents | A1.7 - A1.8 |

FORECAST FORUM

Discussion *page 49*

| | |
|---|----------|
| Canonical Correlation Analysis Forecasts | F1 - F2 |
| NCEP Coupled Model Forecasts | F3 - F4 |
| NCEP Markov Model Forecasts | F5 - F6 |
| LDEO Model Forecasts | F7 - F8 |
| Linear Inverse Modeling Forecasts | F9 - F10 |
| Scripps/MPI Hybrid Coupled Model Forecast | F11 |
| ENSO-CLIPER Model Forecast | F12 |
| Model Forecasts of Niño 3.4 | F13 |

EXTRATROPICS

Highlights *page 64*

Table of Teleconnection Indices *page 66*

| | |
|-----------------------------------|---------|
| Global Surface Temperature | E1 |
| Temperature Anomalies (Land Only) | E2 |
| Global Precipitation | E3 |
| Regional Precipitation Estimates | E4 - E5 |
| U. S. Precipitation | E6 |

Northern Hemisphere

| | |
|---|-----|
| Teleconnection Indices | E7 |
| Mean and Anomalous SLP | E8 |
| Mean and Anomalous 500-hPa heights | E9 |
| Mean and Anomalous 300-hPa Wind Vectors | E10 |
| 500-hPa Persistence | E11 |
| Time-Longitude Sections of 500-hPa Height Anomalies | E12 |
| 700-hPa Storm Track | E13 |

Southern Hemisphere

| | |
|---|-----|
| Mean and Anomalous SLP | E14 |
| Mean and Anomalous 500-hPa heights | E15 |
| Mean and Anomalous 300-hPa Wind Vectors | E16 |
| 500-hPa Persistence | E17 |
| Time-Longitude Sections of 500-hPa Height Anomalies | E18 |

Stratosphere

| | |
|-------------------------------|---------|
| Height Anomalies | S1 - S2 |
| Temperatures | S3 - S4 |
| Ozone | S5 - S6 |
| Vertical Component of EP Flux | S7 |
| Ozone Hole | S8 |

Appendix 2: Additional Figures

| | |
|--|------|
| Arctic Oscillation and 500-hPa Anomalies | A2.1 |
| Snow Cover | A2.2 |

Tropical Highlights - August 2010

Negative sea surface temperature (SST) anomalies continued to strengthen across the equatorial Pacific Ocean during August 2010 (**Fig. T18**), and all of the monthly Niño indices were below -1.0°C (**Table T2, Fig. T5**). Consistent with this evolution, the oceanic thermocline (measured by the depth of the 20°C isotherm) remained much shallower than average across the central and eastern equatorial Pacific (**Figs. T15 and T16**), with sub-surface temperatures reaching 1°C to 5°C below average in these regions (**Fig. T17**).

Also during August, equatorial low-level easterly trade winds and upper-level westerly winds remained stronger than average over the western and central Pacific (**Table T1, Figs. T20 and T21**). This wind pattern was associated with enhanced convection over Indonesia and suppressed convection across the western and central equatorial Pacific (**Figs. T25 and E3**). Collectively, these oceanic and atmospheric anomalies reflect a strengthening of La Niña conditions.

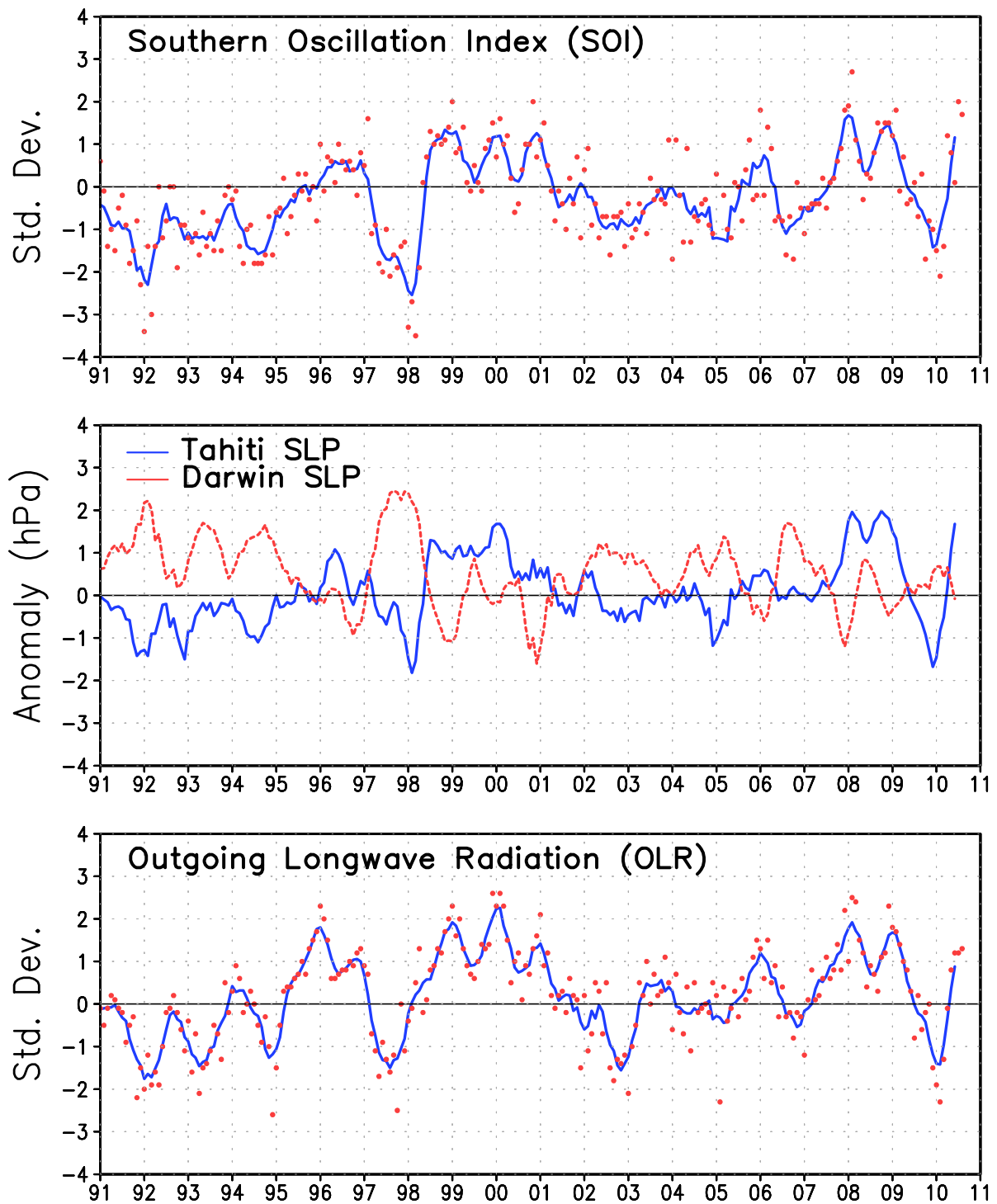
For the latest status of the ENSO cycle see the ENSO Diagnostic Discussion at:
http://www.cpc.ncep.noaa.gov/products/analysis_monitoring/enso_advisory/index.html

| MONTH | SLP ANOMALIES | | TAHITI minus DARWIN SOI | 850-hPa ZONAL WIND INDEX | | | 200-hPa WIND INDEX | OLR Index |
|---------------|---------------|--------|----------------------------------|--------------------------|--------------------|--------------------|--------------------------|---------------------------|
| | TAHITI | DARWIN | | 5N-5S 135E-180 | 5N-5S 175W-140W | 5N-5S 135W-120W | | |
| AUG 10 | 2.3 | -0.4 | 1.7 | 2.4 | 0.8 | -0.5 | 0.7 | 5N-5S 160E-160W 1.3 |
| JUL 10 | 2.6 | -0.4 | 2.0 | 2.5 | 0.8 | -0.7 | 0.1 | 1.2 |
| JUN 10 | 0.9 | 0.9 | 0.1 | 1.8 | 0.3 | -0.7 | -0.1 | 1.2 |
| MAY 10 | 0.6 | -0.7 | 0.8 | 2.1 | 0.7 | -0.8 | 0.5 | 0.8 |
| APR 10 | 2.0 | 0.2 | 1.2 | 1.3 | 0.1 | -0.8 | -0.6 | -0.1 |
| MAR 10 | -0.7 | 1.5 | -1.4 | 0.6 | 0.4 | -1.1 | -1.0 | -1.3 |
| FEB 10 | -1.9 | 1.4 | -2.1 | -0.2 | -0.8 | -1.7 | -0.5 | -2.3 |
| JAN 10 | -2.6 | -0.3 | -1.5 | 0.1 | 0.2 | -0.6 | -0.8 | -1.9 |
| DEC 09 | -1.0 | 0.6 | -1.0 | 0.3 | -0.7 | -1.8 | -1.2 | -1.5 |
| NOV 09 | -1.1 | 0.2 | -0.8 | 1.1 | 0.1 | -1.0 | -0.9 | 0.0 |
| OCT 09 | -1.8 | 0.8 | -1.7 | -0.9 | -1.2 | -1.5 | -1.4 | -0.2 |
| SEP 09 | 0.0 | -0.6 | 0.3 | -0.7 | 0.3 | 0.1 | 1.5 | -0.6 |
| AUG 09 | -0.7 | 0.3 | -0.7 | -0.1 | -0.6 | -1.0 | -0.6 | 0.2 |

TABLE T1 - Atmospheric index values for the most recent 12 months. Indices are standardized by the mean annual standard deviation, except for the Tahiti and Darwin SLP anomalies which are in units of hPa. Positive (negative) values of 200-hPa zonal wind index imply westerly (easterly) anomalies. Positive (negative) values of 850-hPa zonal wind indices imply easterly (westerly) anomalies.

| MONTH | PACIFIC SST | | | | ATLANTIC SST | | Global | | | | | | | |
|---------------|---------------------------------|--------------------------------------|---|---------------------------------------|-----------------------------|----------------------------|--------|------|-----|------|-----|------|-----|------|
| | NIÑO 1+2 0-10°S 90°W-80°W | NIÑO 3 5°N-5°S 150°W-90- °W | NIÑO 3.4 5°N-5°S 170°W-12- 0°W | NIÑO 4 5°N-5°S 160°E-150- °W | N. ATL 5N-20N 60W-30W | S. ATL 0-20S 30W-10E | | | | | | | | |
| AUG 10 | -1.5 | 19.3 | -1.1 | 23.9 | -1.2 | 25.5 | -1.0 | 27.5 | 1.1 | 28.6 | 0.2 | 23.3 | 0.0 | 27.0 |
| JUL 10 | -1.7 | 20.2 | -1.0 | 24.6 | -0.9 | 26.1 | -0.5 | 28.1 | 1.2 | 28.3 | 0.5 | 24.2 | 0.2 | 27.5 |
| JUN 10 | -0.2 | 22.8 | -0.5 | 25.9 | -0.4 | 27.1 | 0.1 | 28.7 | 1.3 | 28.0 | 0.9 | 25.7 | 0.5 | 28.3 |
| MAY 10 | 0.1 | 24.5 | 0.0 | 27.1 | 0.0 | 27.7 | 0.4 | 29.1 | 1.4 | 27.6 | 0.7 | 26.7 | 0.5 | 28.9 |
| APR 10 | 0.6 | 26.1 | 0.7 | 28.7 | 0.7 | 28.4 | 0.8 | 29.2 | 1.4 | 27.2 | 0.8 | 27.6 | 0.7 | 29.1 |
| MAR 10 | -0.2 | 26.2 | 0.7 | 27.7 | 1.1 | 28.3 | 1.1 | 29.2 | 1.3 | 26.8 | 1.0 | 27.9 | 0.7 | 28.8 |
| FEB 10 | 0.0 | 26.0 | 0.7 | 27.1 | 1.2 | 27.9 | 1.1 | 29.1 | 1.0 | 26.5 | 0.6 | 27.0 | 0.6 | 28.3 |
| JAN 10 | 0.2 | 24.7 | 1.0 | 26.6 | 1.6 | 28.1 | 1.4 | 29.6 | 0.7 | 26.5 | 0.7 | 26.2 | 0.7 | 28.2 |
| DEC 09 | 0.3 | 23.1 | 1.6 | 26.7 | 1.8 | 28.3 | 1.4 | 29.7 | 0.5 | 27.1 | 0.5 | 25.1 | 0.7 | 28.2 |
| NOV 09 | 0.5 | 22.1 | 1.3 | 26.2 | 1.7 | 28.2 | 1.5 | 29.9 | 0.5 | 27.9 | 0.2 | 24.1 | 0.6 | 28.1 |
| OCT 09 | 0.0 | 20.9 | 0.8 | 25.7 | 1.0 | 27.6 | 1.2 | 29.6 | 0.6 | 28.5 | 0.3 | 23.6 | 0.5 | 27.8 |
| SEP 09 | 0.3 | 20.8 | 0.8 | 25.7 | 0.8 | 27.5 | 0.8 | 29.3 | 0.5 | 28.4 | 0.2 | 23.2 | 0.5 | 27.6 |
| AUG 09 | 0.8 | 21.6 | 1.0 | 25.9 | 0.8 | 27.5 | 0.8 | 29.2 | 0.3 | 27.9 | 0.2 | 23.2 | 0.5 | 27.5 |

TABLE T2. Mean and anomalous sea surface temperature (°C) for the most recent 12 months. Anomalies are departures from the 1971–2000 adjusted OI climatology (Smith and Reynolds 1998, *J. Climate*, **11**, 3320–3323).



Data updated through August 2010

FIGURE T1. Five-month running mean of the Southern Oscillation Index (SOI) (top), sea-level pressure anomaly (hPa) at Darwin and Tahiti (middle), and outgoing longwave radiation anomaly (OLR) averaged over the area 5N-5S, 160E-160W (bottom). Anomalies in the top and middle panels are departures from the 1951-1980 base period means and are normalized by the mean annual standard deviation. Anomalies in the bottom panel are departures from the 1979-1995 base period means. Individual monthly values are indicated by “x”s in the top and bottom panels. The x-axis labels are centered on July.

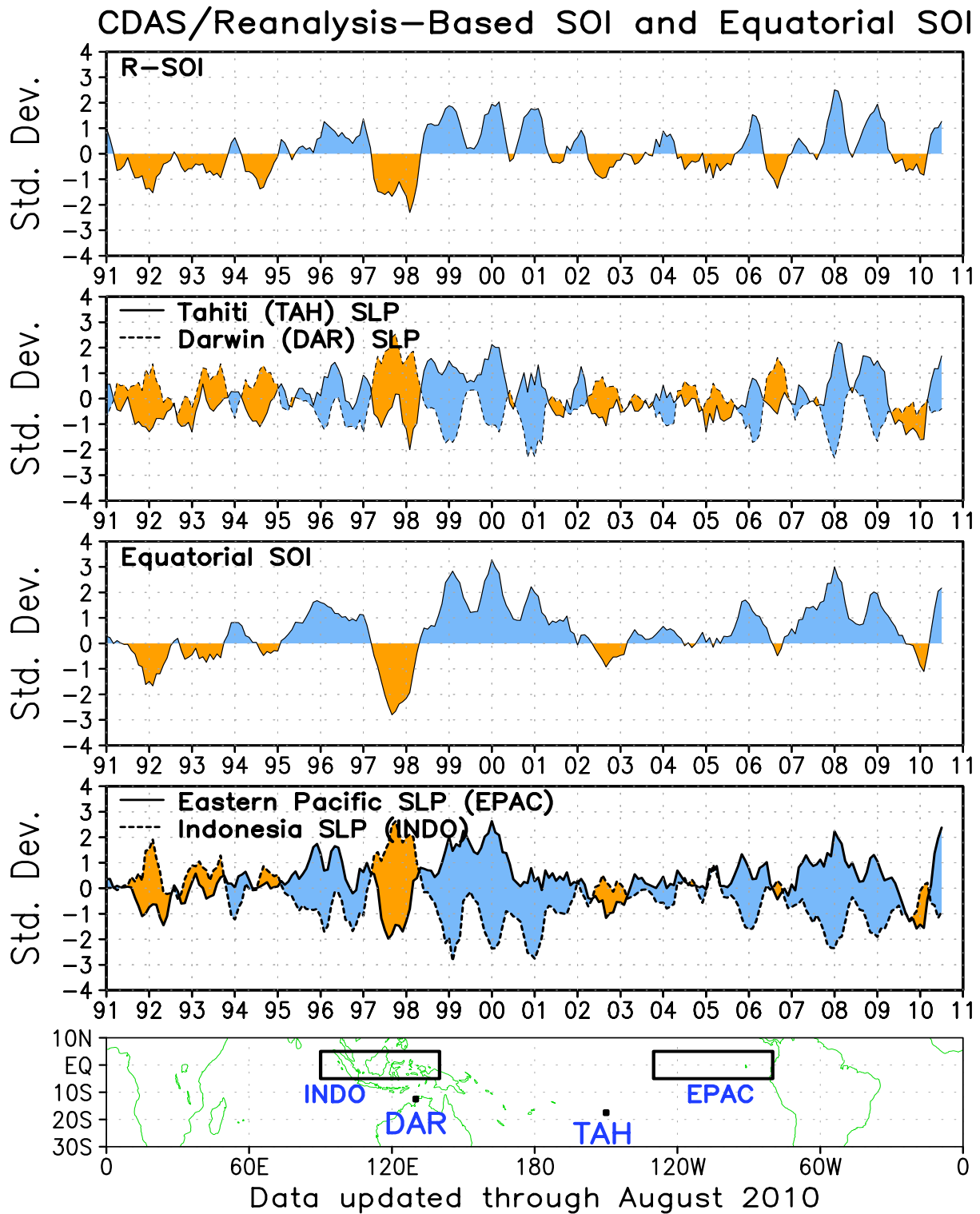


FIGURE T2. Three-month running mean of a CDAS/Reanalysis-derived (a) Southern Oscillation Index (RSOI), (b) standardized pressure anomalies near Tahiti (solid) and Darwin (dashed), (c) an equatorial SOI ([EPAC] - [INDO]), and (d) standardized equatorial pressure anomalies for (EPAC) (solid) and (INDO) (dashed). Anomalies are departures from the 1979–95 base period means and are normalized by the mean annual standard deviation. The equatorial SOI is calculated as the normalized difference between the standardized anomalies averaged between 5°N–5°S, 80°W–130°W (EPAC) and 5°N–5°S, 90°E–140°E (INDO).

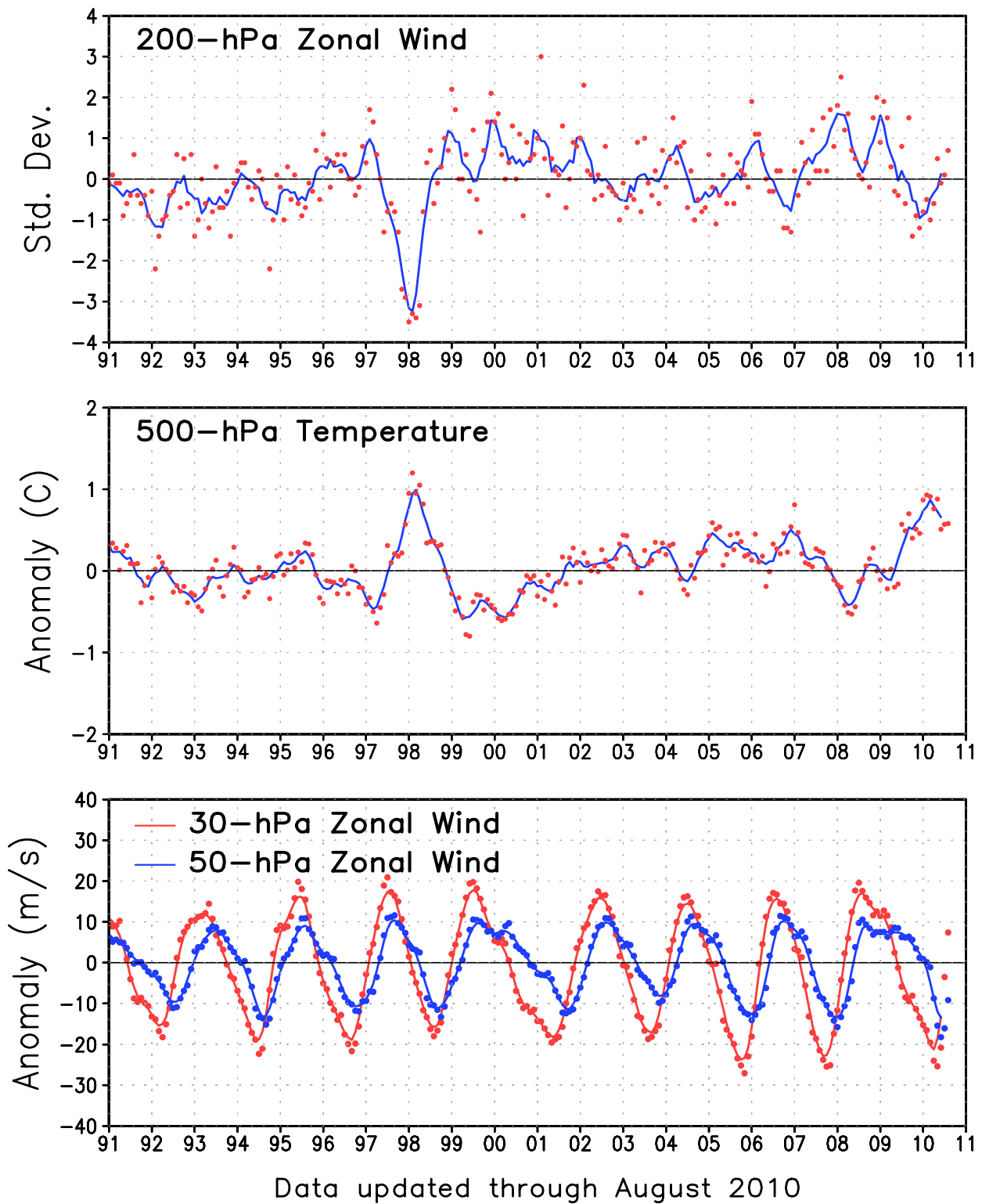


FIGURE T3. Five-month running mean (solid lines) and individual monthly mean (dots) of the 200-hPa zonal wind anomalies averaged over the area 5N-5S, 165W-110W (top), the 500-hPa virtual temperature anomalies averaged over the latitude band 20N-20S (middle), and the equatorial zonally-averaged zonal wind anomalies at 30-hPa (red) and 50-hPa (blue) (bottom). In the top panel, anomalies are normalized by the mean annual standard deviation. Anomalies are departures from the 1979-1995 base period means. The x-axis labels are centered on January.

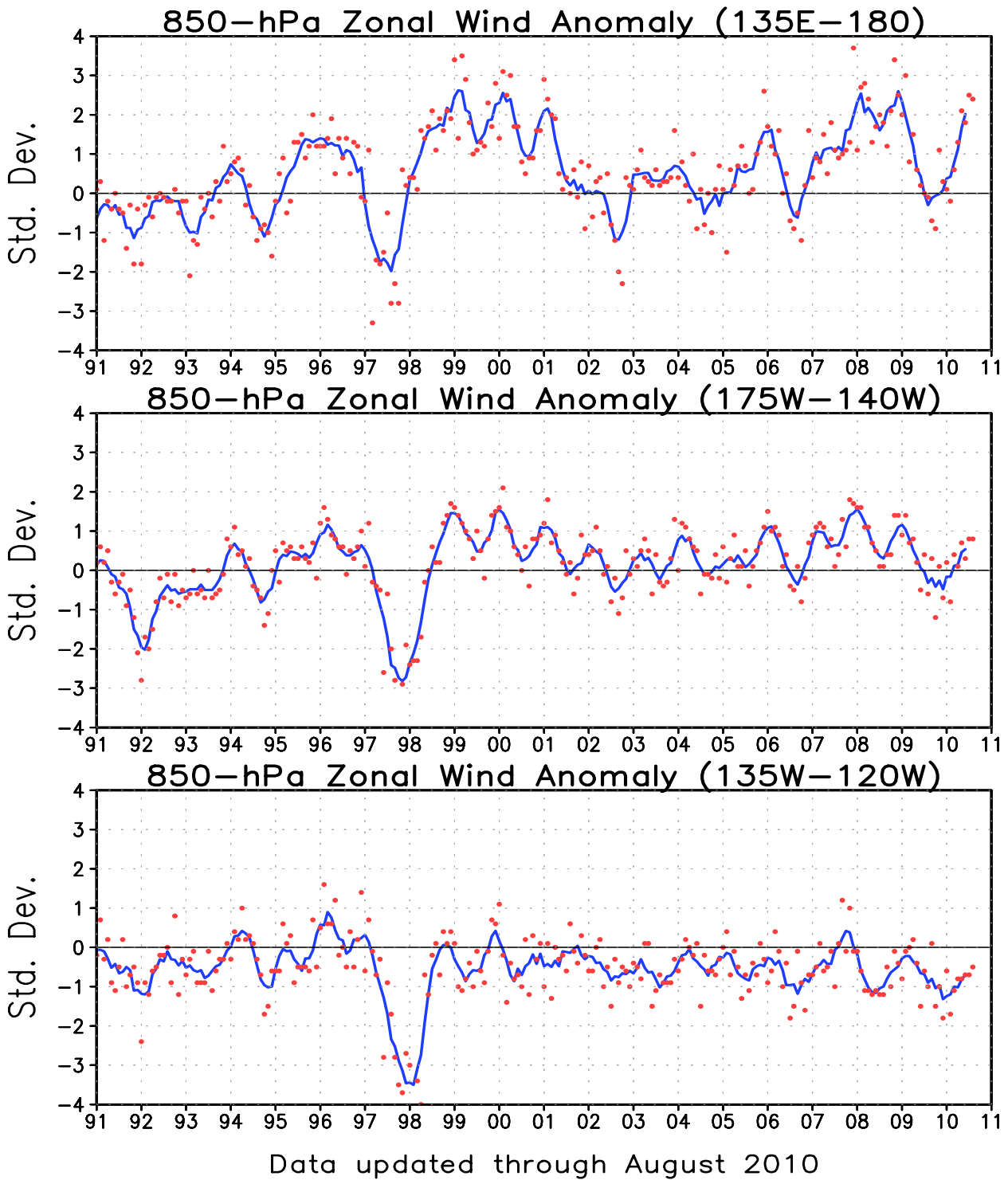


FIGURE T4. Five-month running mean (solid line) and individual monthly mean (dots) of the standardized 850-hPa zonal wind anomaly index in the latitude belt 5N-5S for 135E-180 (top), 175W-140W (middle) and 135W-120W (bottom). Anomalies are departures from the 1979-1995 base period means and are normalized by the mean annual standard deviation. The x-axis labels are centered on January. Positive (negative) values indicate easterly (westerly) anomalies.

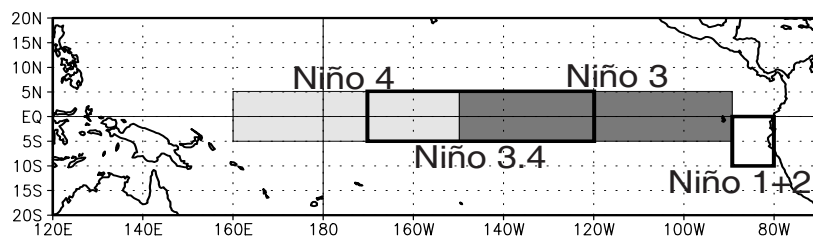
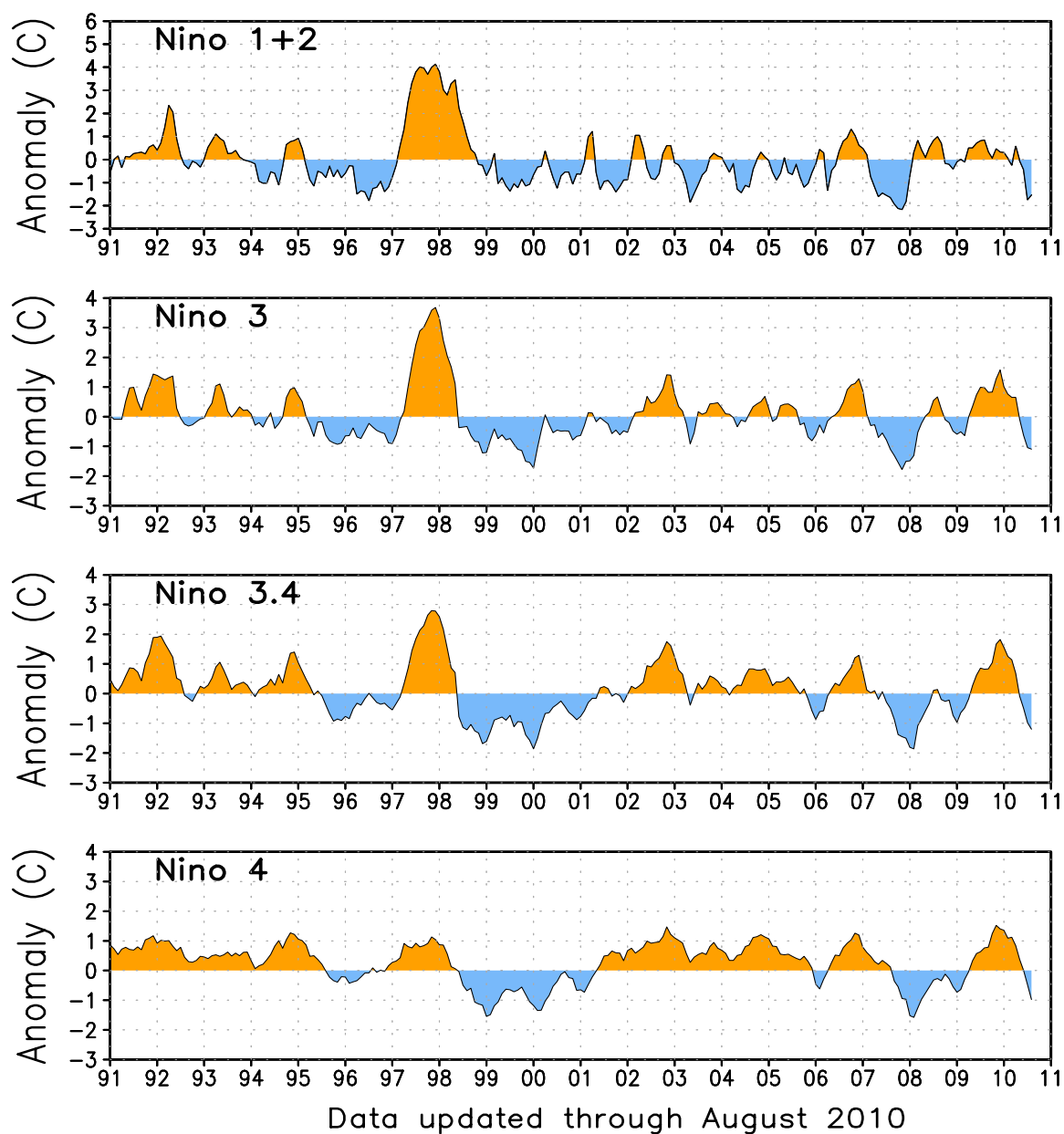


FIGURE T5. Niño region indices, calculated as the area-averaged sea surface temperature anomalies (C) for the specified region. The Niño 1+2 region (top) covers the extreme eastern equatorial Pacific between 0-10S, 90W-80W. The Niño-3 region (2nd from top) spans the eastern equatorial Pacific between 5N-5S, 150W-90W. The Niño 3.4 region (3rd from top) spans the east-central equatorial Pacific between 5N-5S, 170W-120W. The Niño 4 region (bottom) spans the date line and covers the area 5N-5S, 160E-150W. Anomalies are departures from the 1971-2000 base period monthly means (*Smith and Reynolds 1998, J. Climate, 11, 3320-3323*). Monthly values of each index are also displayed in [Table 2](#).

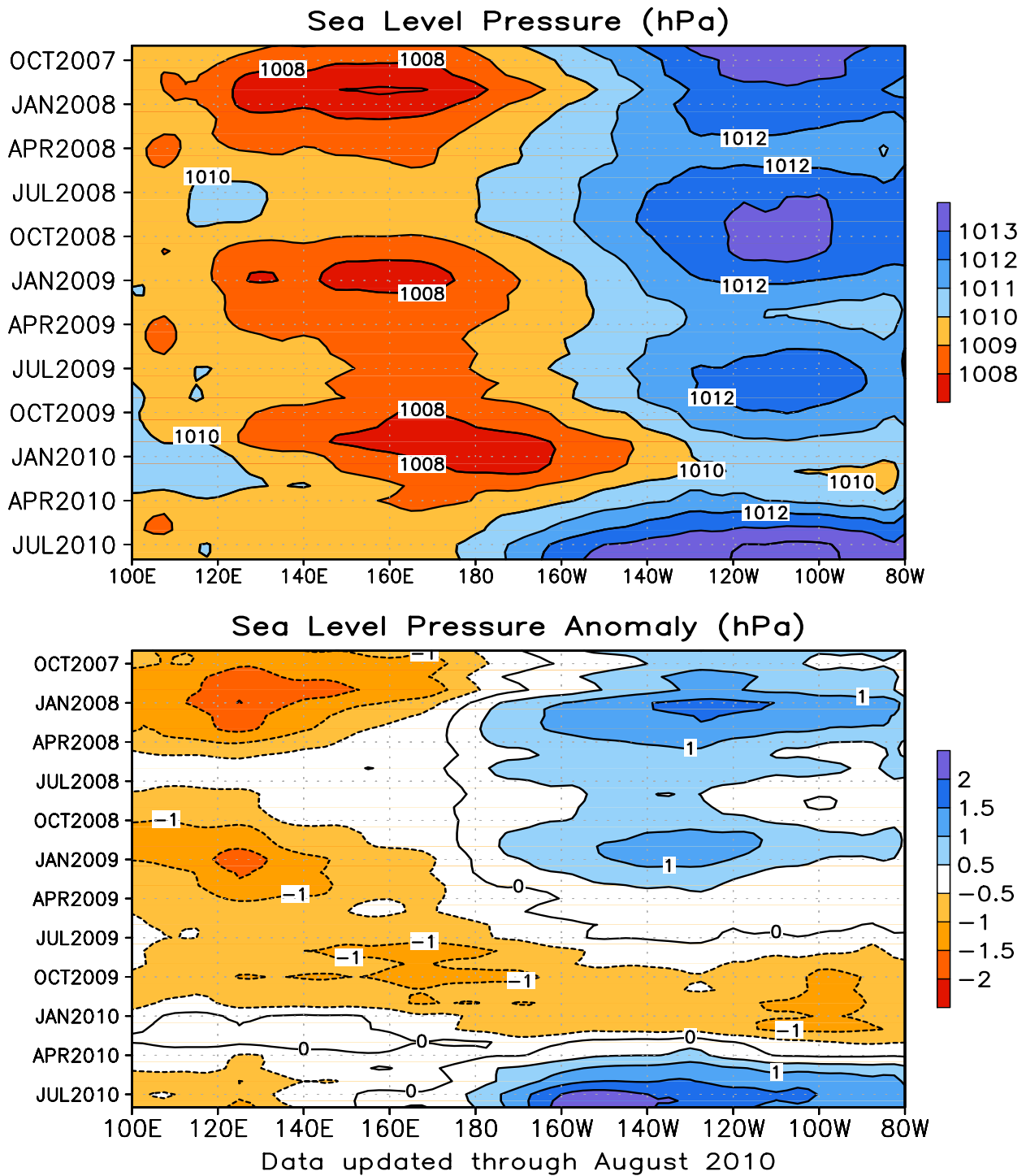


FIGURE T6. Time-longitude section of mean (top) and anomalous (bottom) sea level pressure (SLP) averaged between 5N-5S (CDAS/Reanalysis). Contour interval is 1.0 hPa (top) and 0.5 hPa (bottom). Dashed contours in bottom panel indicate negative anomalies. Anomalies are departures from the 1979-1995 base period monthly means. The data are smoothed temporally using a 3-month running average.

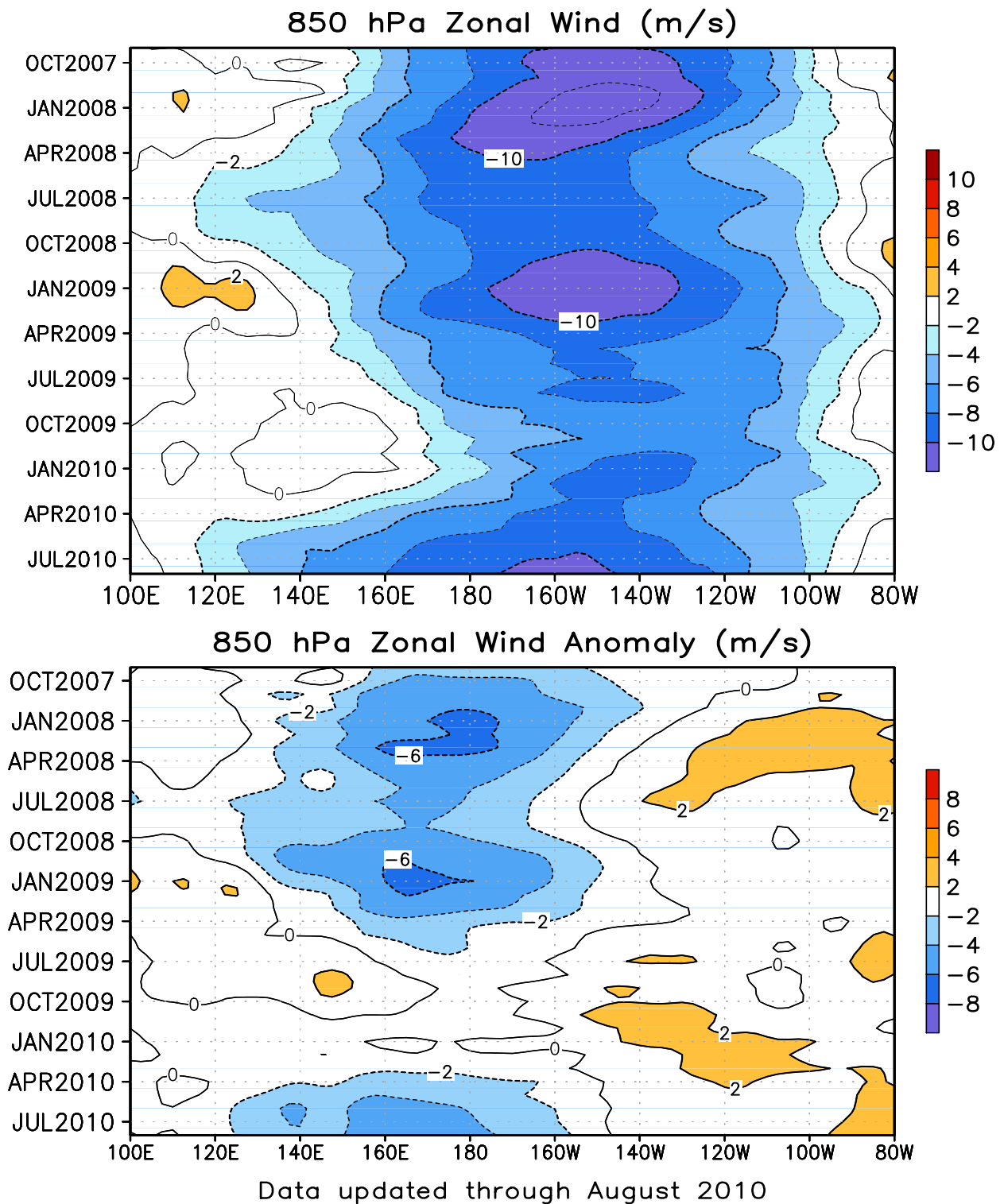


FIGURE T7. Time-longitude section of mean (top) and anomalous (bottom) 850-hPa zonal wind averaged between 5N-5S (CDAS/Reanalysis). Contour interval is 2 ms^{-1} . Blue shading and dashed contours indicate easterlies (top) and easterly anomalies (bottom). Anomalies are departures from the 1979-1995 base period monthly means. The data are smoothed temporally using a 3-month running average.

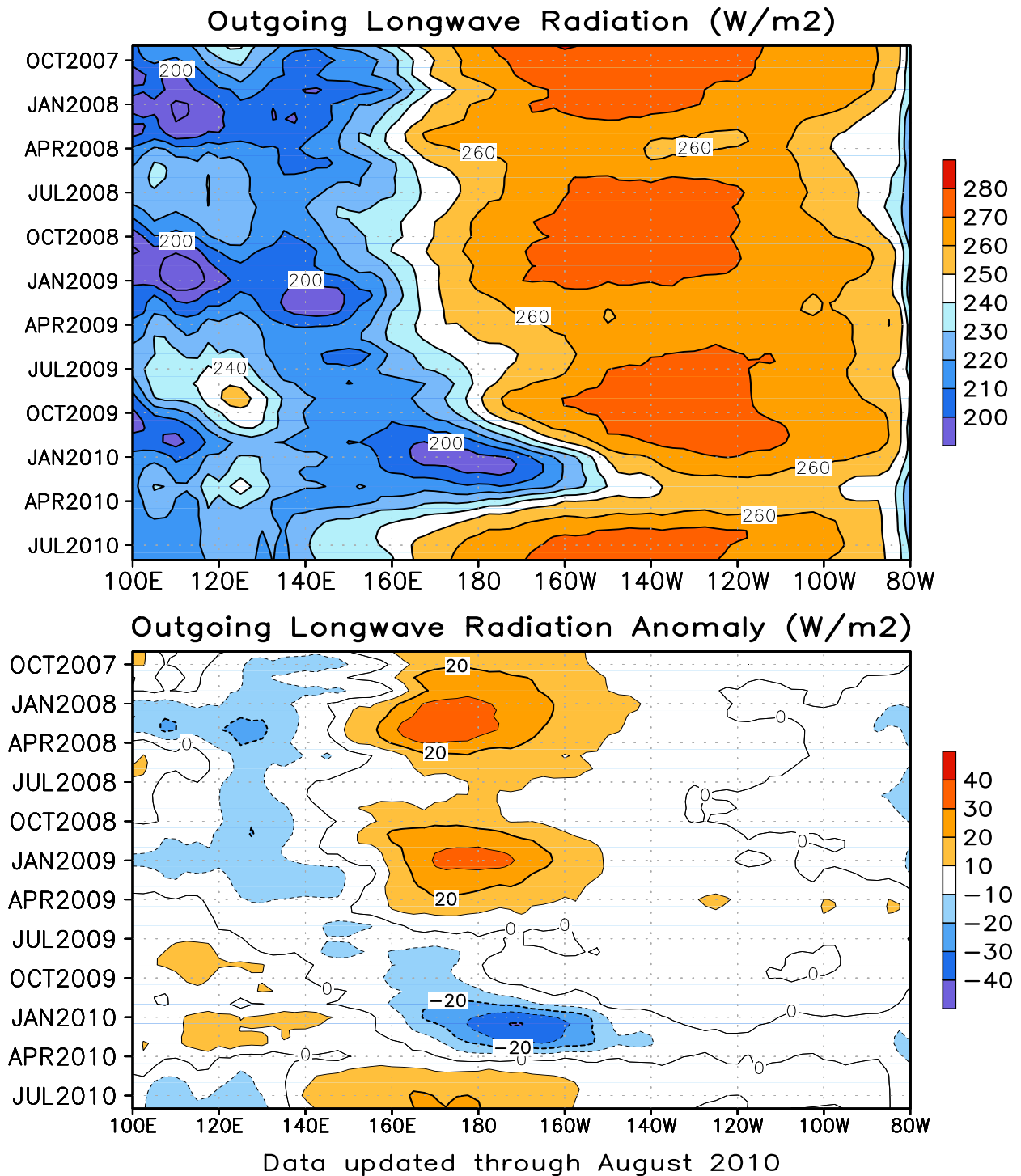


FIGURE T8. Time-longitude section of mean (top) and anomalous (bottom) outgoing longwave radiation (OLR) averaged between 5N-5S. Contour interval is 10 Wm⁻². Dashed contours in bottom panel indicate negative OLR anomalies. Anomalies are departures from the 1979-1995 base period monthly means. The data are smoothed temporally using a 3-month running average.

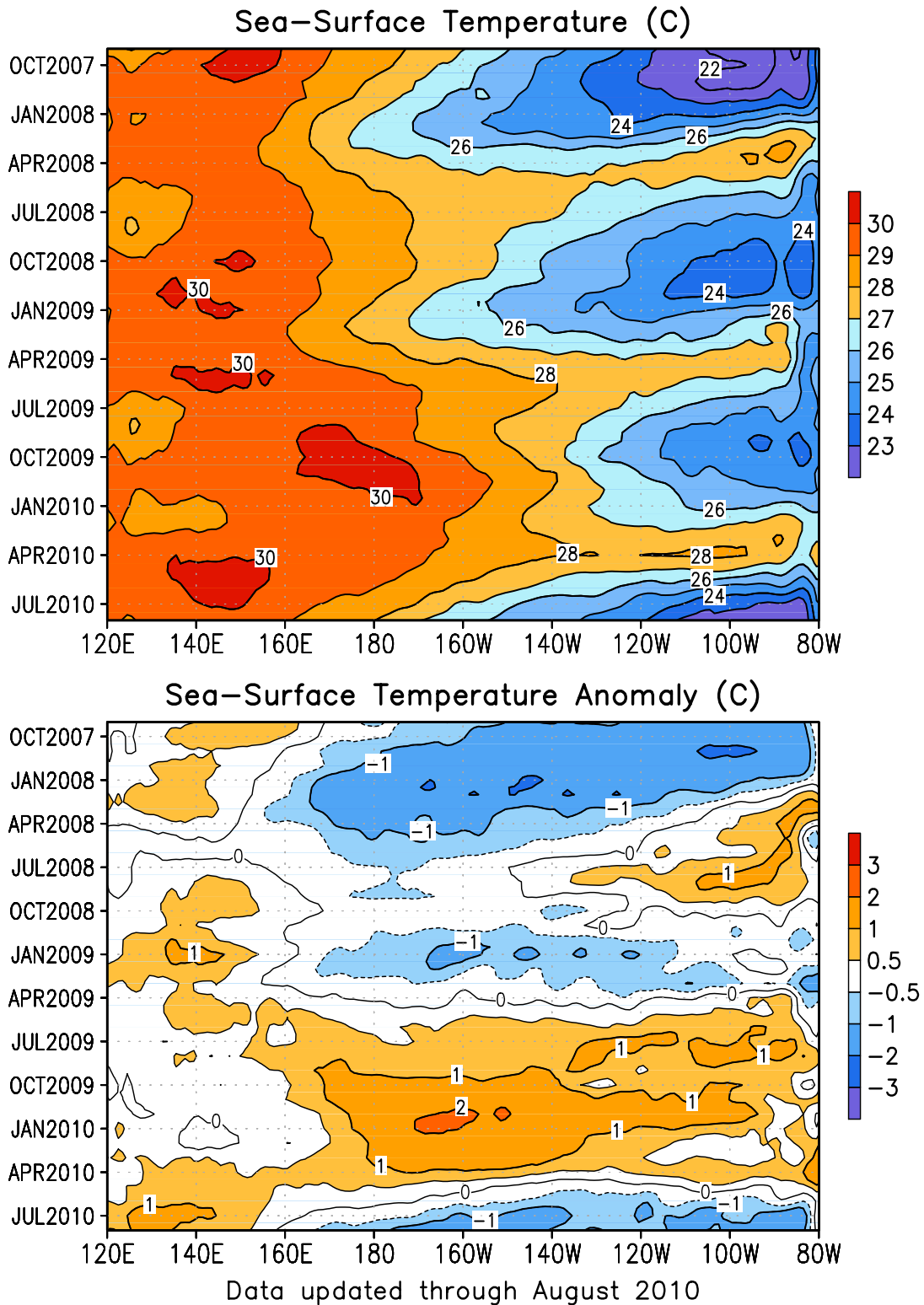


FIGURE T9. Time-longitude section of monthly mean (top) and anomalous (bottom) sea surface temperature (SST) averaged between 5N-5S. Contour interval is 1C (top) and 0.5C (bottom). Dashed contours in bottom panel indicate negative anomalies. Anomalies are departures from the 1971-2000 base period means (Smith and Reynolds 1998, *J. Climate*, **11**, 3320-3323).

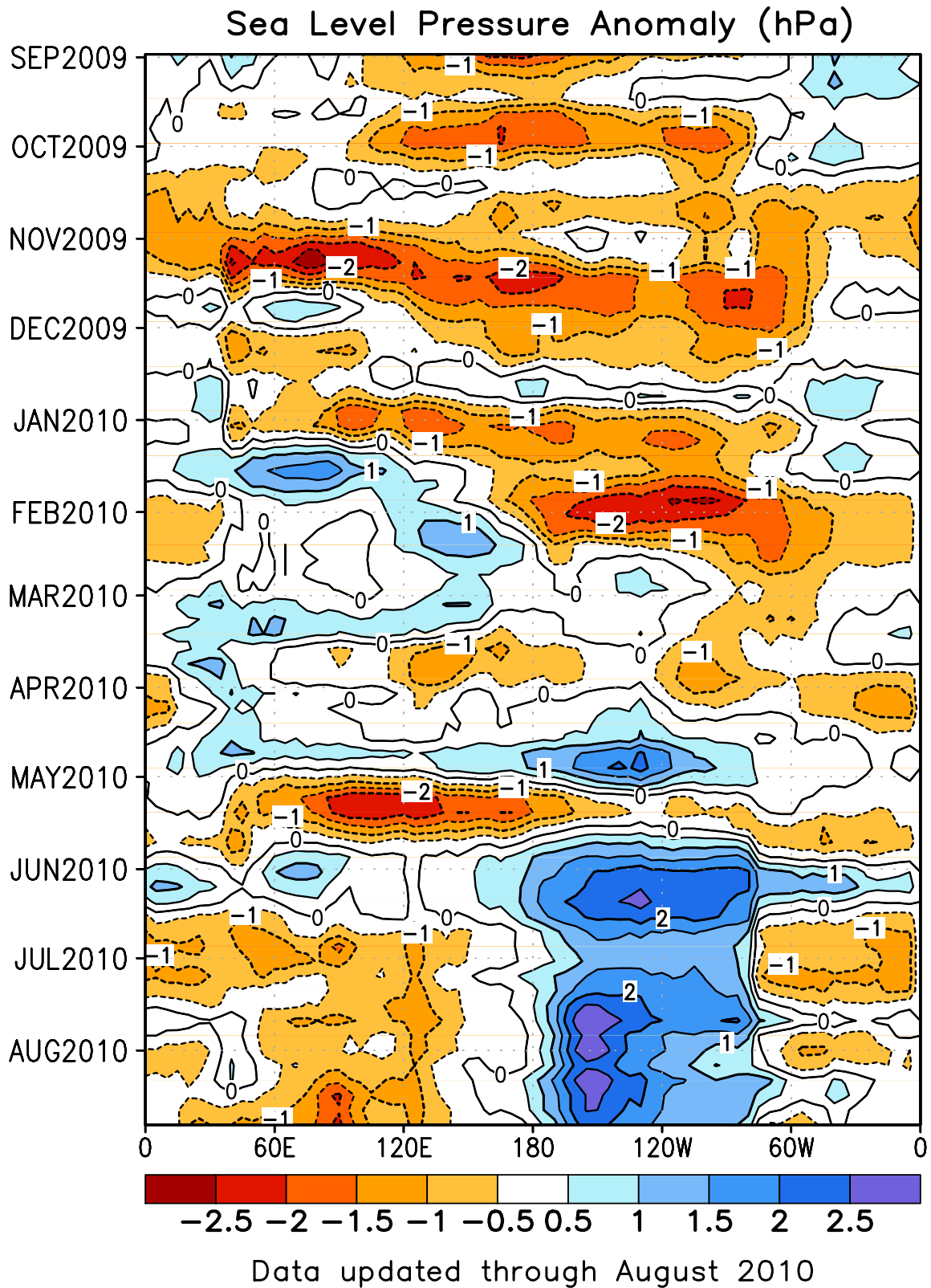


FIGURE T10. Time-longitude section of anomalous sea level pressure (hPa) averaged between 5N-5S (CDAS/Reanalysis). Contour interval is 1 hPa. Dashed contours indicate negative anomalies. Anomalies are departures from the 1979-1995 base period pentad means. The data are smoothed temporally using a 3-point running average.

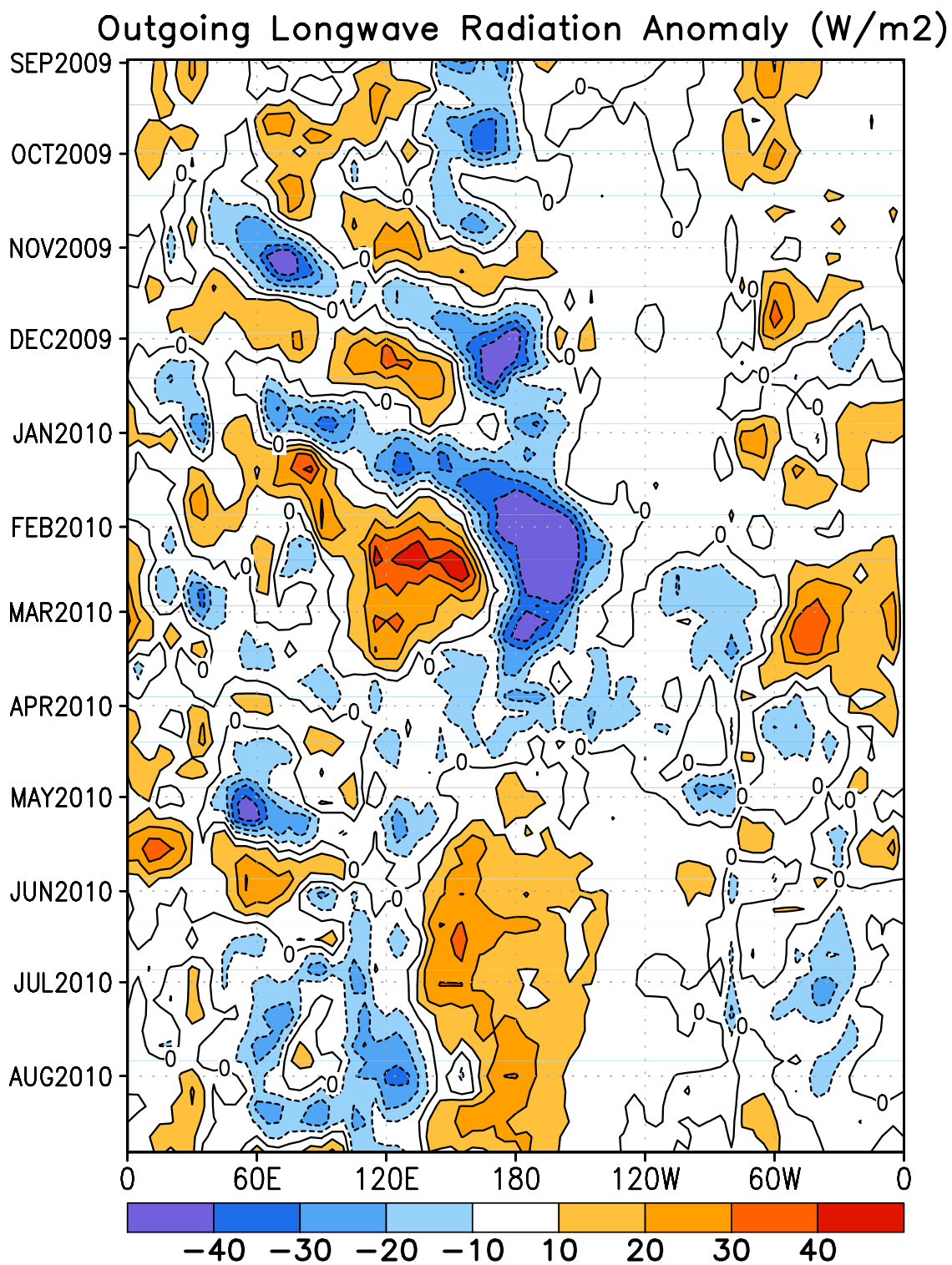


FIGURE T11. Time-longitude section of anomalous outgoing longwave radiation averaged between 5N-5S. Contour interval is 15 Wm⁻². Dashed contours indicate negative anomalies. Anomalies are departures from the 1979-1995 base period pentad means. The data are smoothed temporally using a 3-point running average.

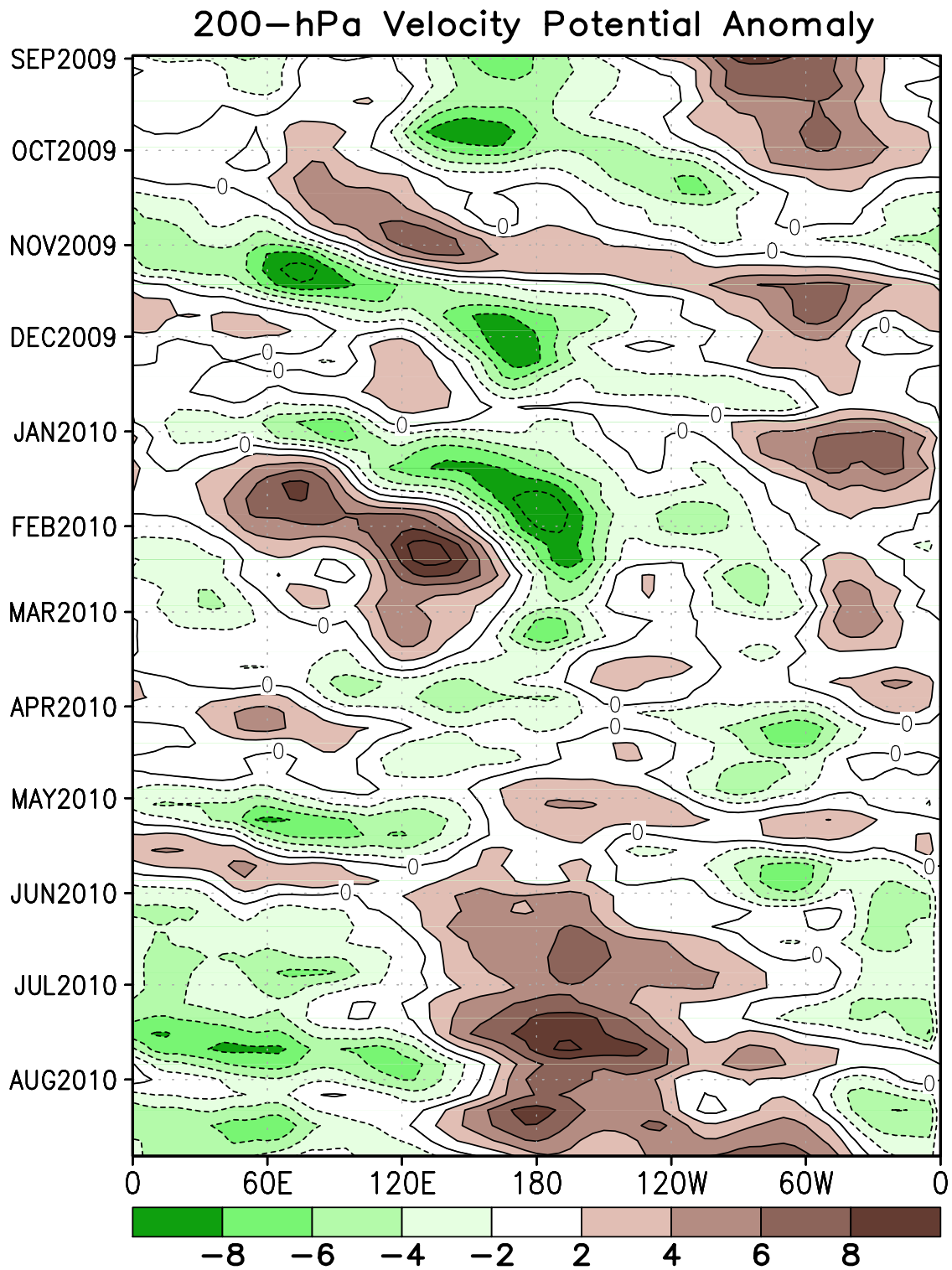


FIGURE T12. Time-longitude section of anomalous 200-hPa velocity potential averaged between 5N-5S (CDAS/Re-analysis). Contour interval is $3 \times 10^6 \text{ m}^2\text{s}^{-1}$. Dashed contours indicate negative anomalies. Anomalies are departures from the 1979-1995 base period pentad means. The data are smoothed temporally using a 3-point running average.

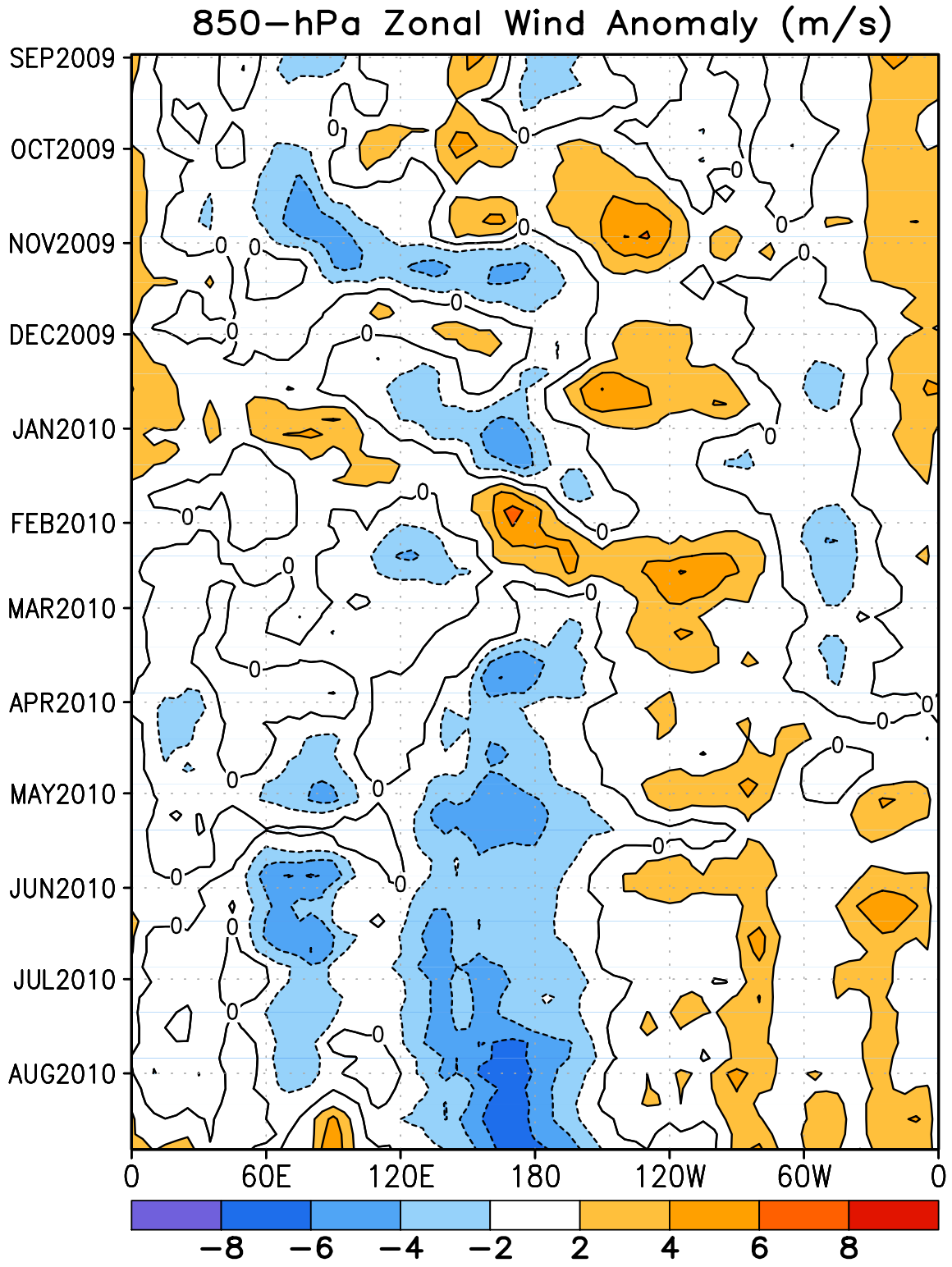


FIGURE T13. Time-longitude section of anomalous 850-hPa zonal wind averaged between 5N-5S (CDAS/Reanalysis). Contour interval is 2 ms^{-1} . Dashed contours indicate negative anomalies. Anomalies are departures from the 1979-1995 base period pentad means. The data are smoothed temporally by using a 3-point running average.

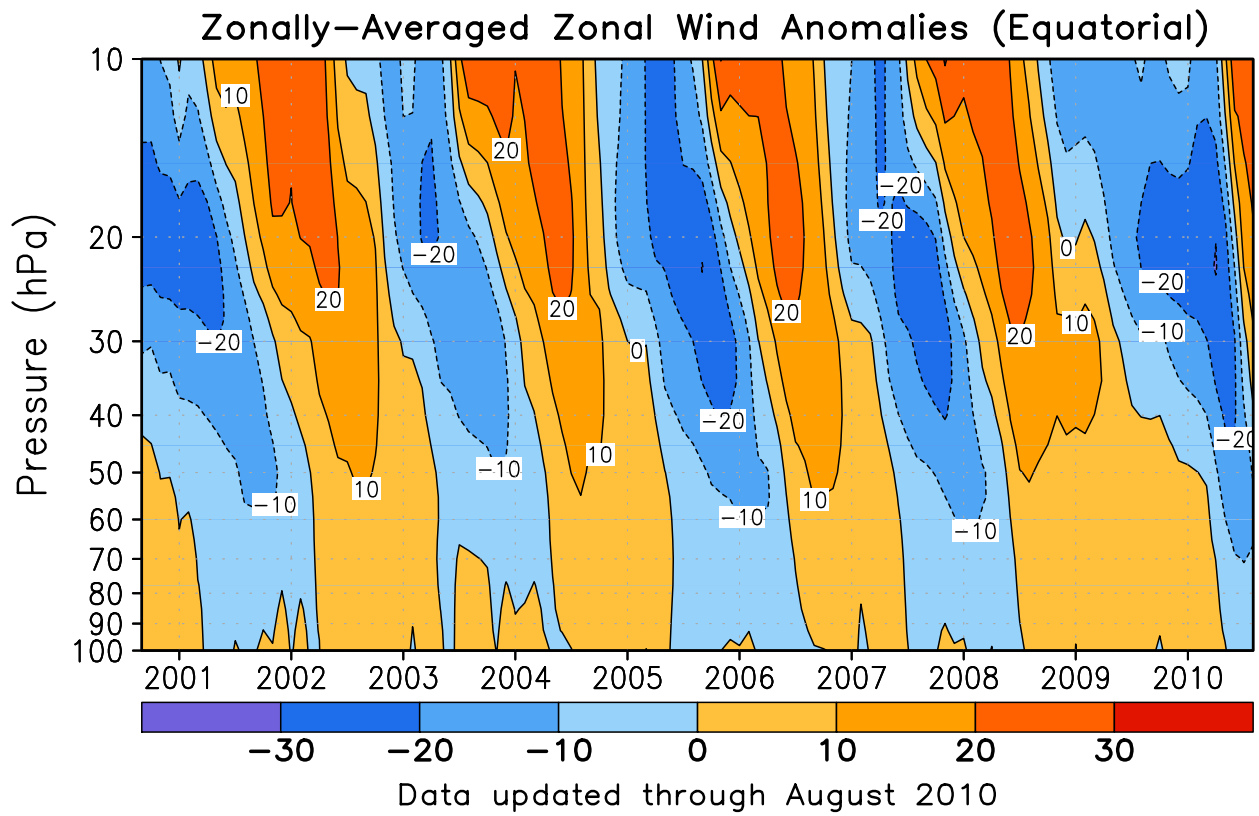


FIGURE T14. Equatorial time-height section of anomalous zonally-averaged zonal wind (m s^{-1}) (CDAS/Reanalysis). Contour interval is 10 m s^{-1} . Anomalies are departures from the 1979-1995 base period monthly means.

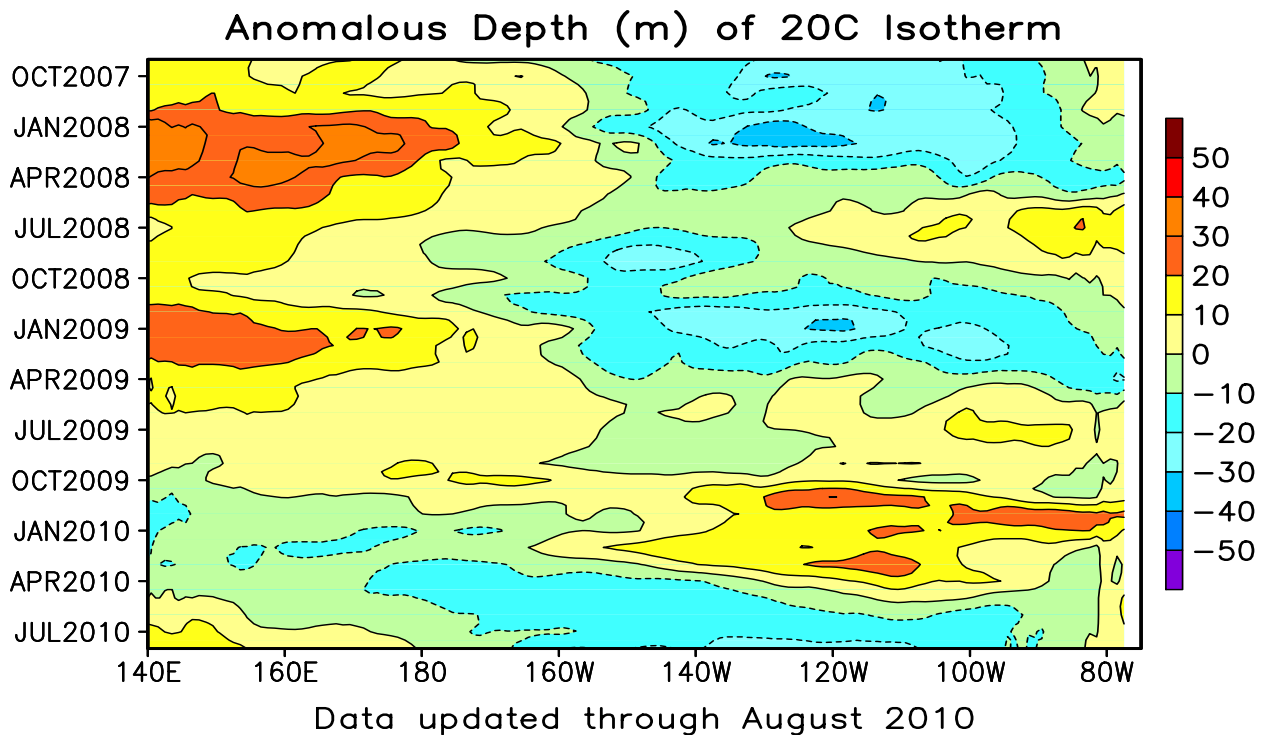
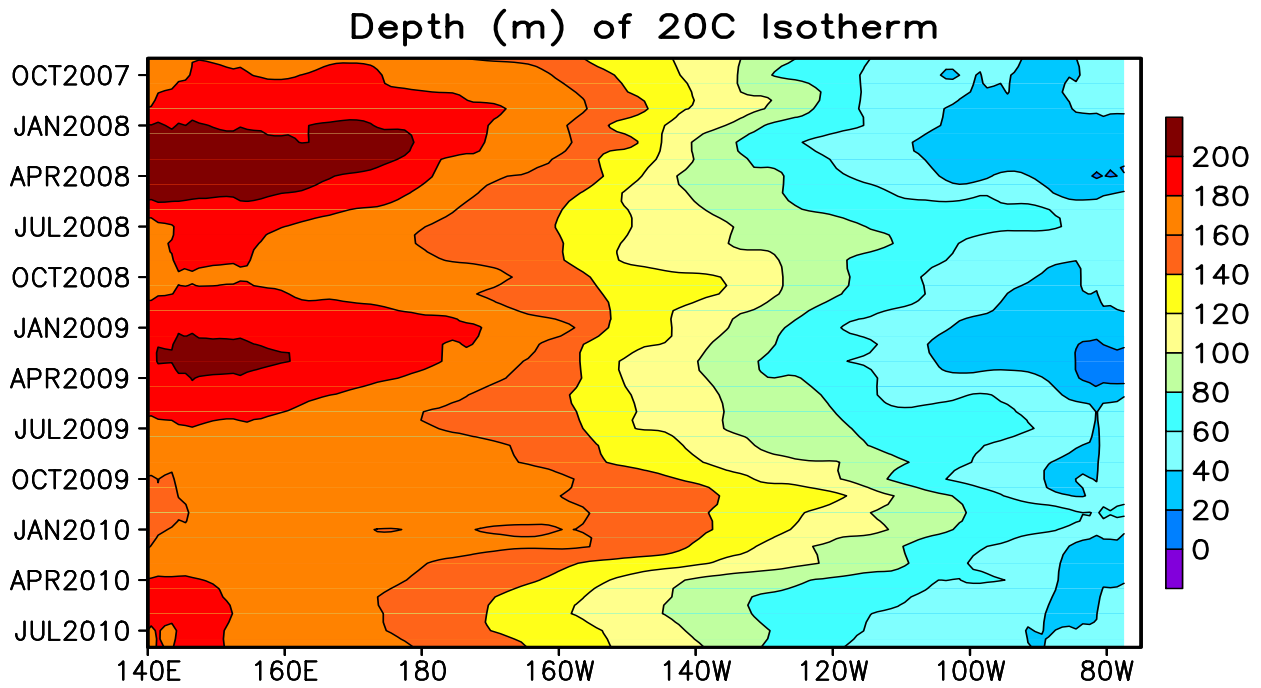


FIGURE T15. Mean (top) and anomalous (bottom) depth of the 20C isotherm averaged between 5N-5S in the Pacific Ocean. Data are derived from the NCEP's global ocean data assimilation system which assimilates oceanic observations into an oceanic GCM (Behringer, D. W., and Y. Xue, 2004: Evaluation of the global ocean data assimilation system at NCEP: The Pacific Ocean. AMS 84th Annual Meeting, Seattle, Washington, 11-15). The contour interval is 10 m. Dashed contours in bottom panel indicate negative anomalies. Anomalies are departures from the 1982-2004 base period means.

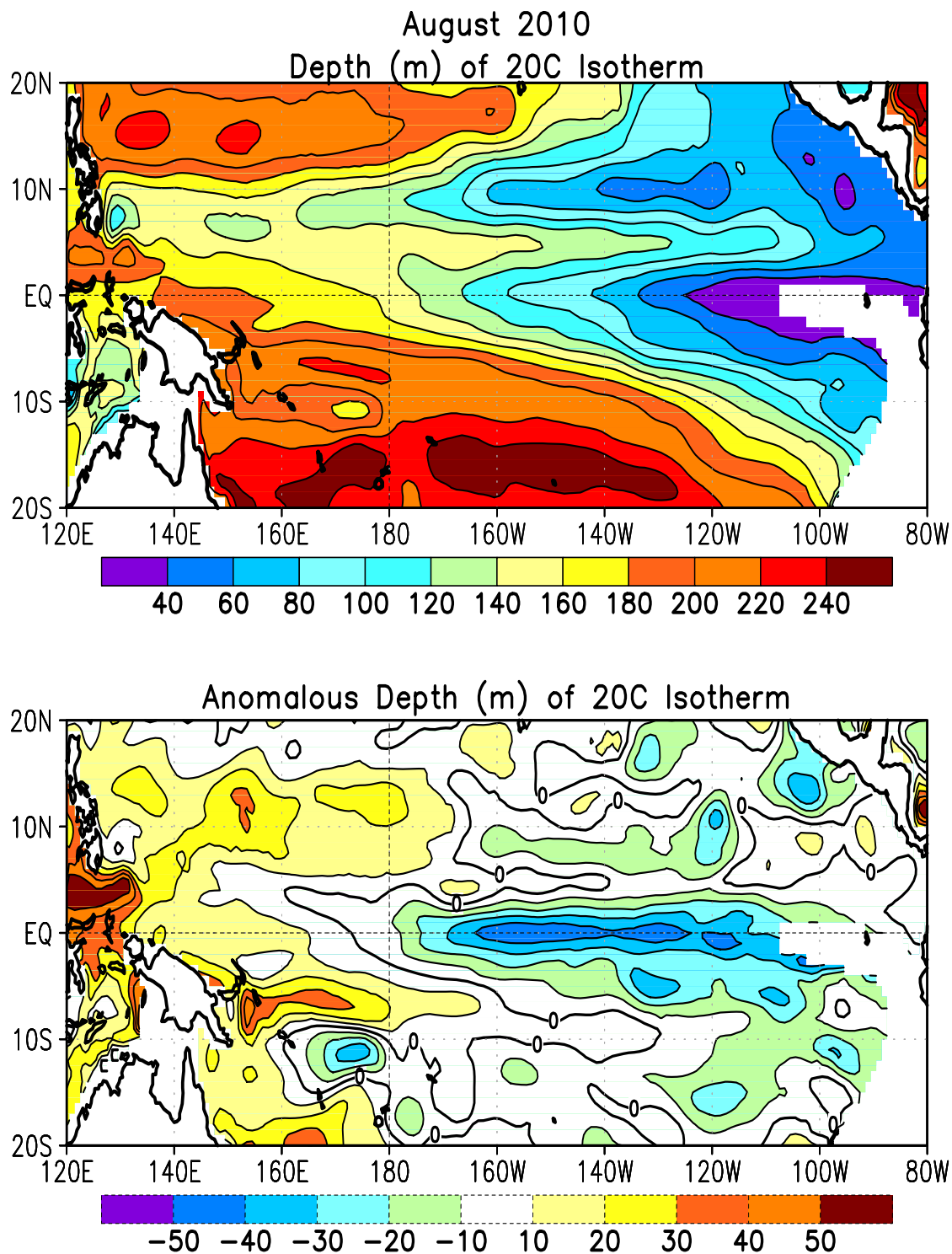
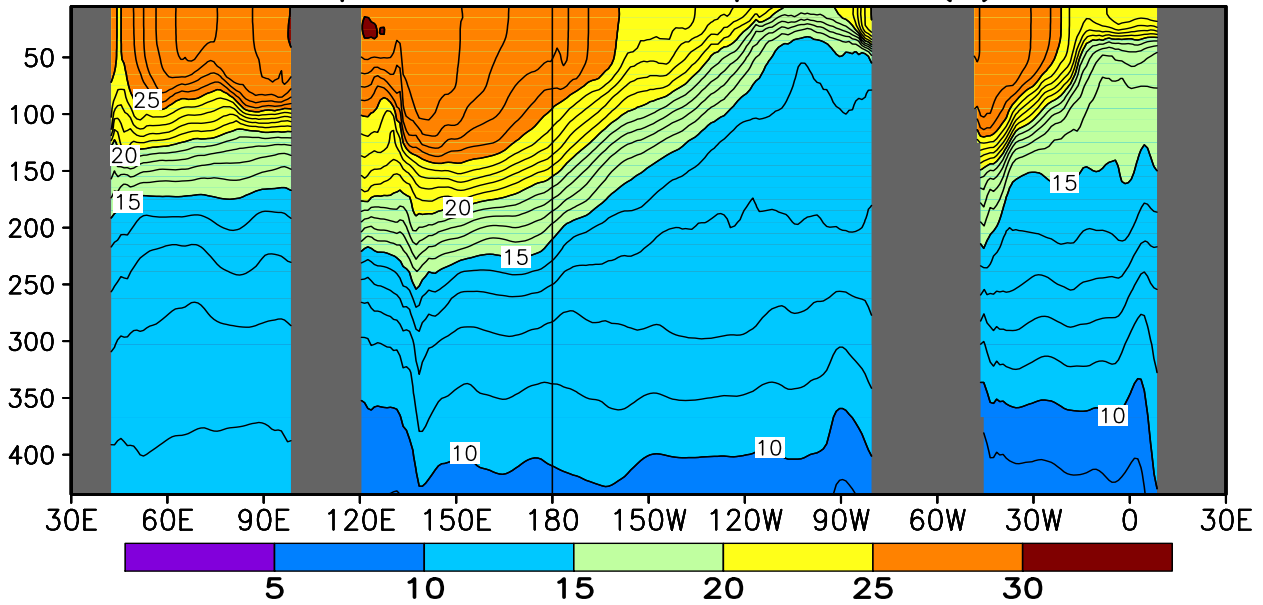


FIGURE T16. Mean (top) and anomalous (bottom) depth of the 20°C isotherm for AUG 2010. Contour interval is 40 m (top) and 10 m (bottom). Dashed contours in bottom panel indicate negative anomalies. Data are derived from the NCEP's global ocean data assimilation system version 2 which assimilates oceanic observations into an oceanic GCM (Xue, Y. and Behringer, D.W., 2006: Operational global ocean data assimilation system at NCEP, to be submitted to BAMS). Anomalies are departures from the 1982–2004 base period means.

August 2010: Depth–Longitude Section Equatorial Ocean Temperatures (C)



Equatorial Ocean Temperature Anomalies (C)

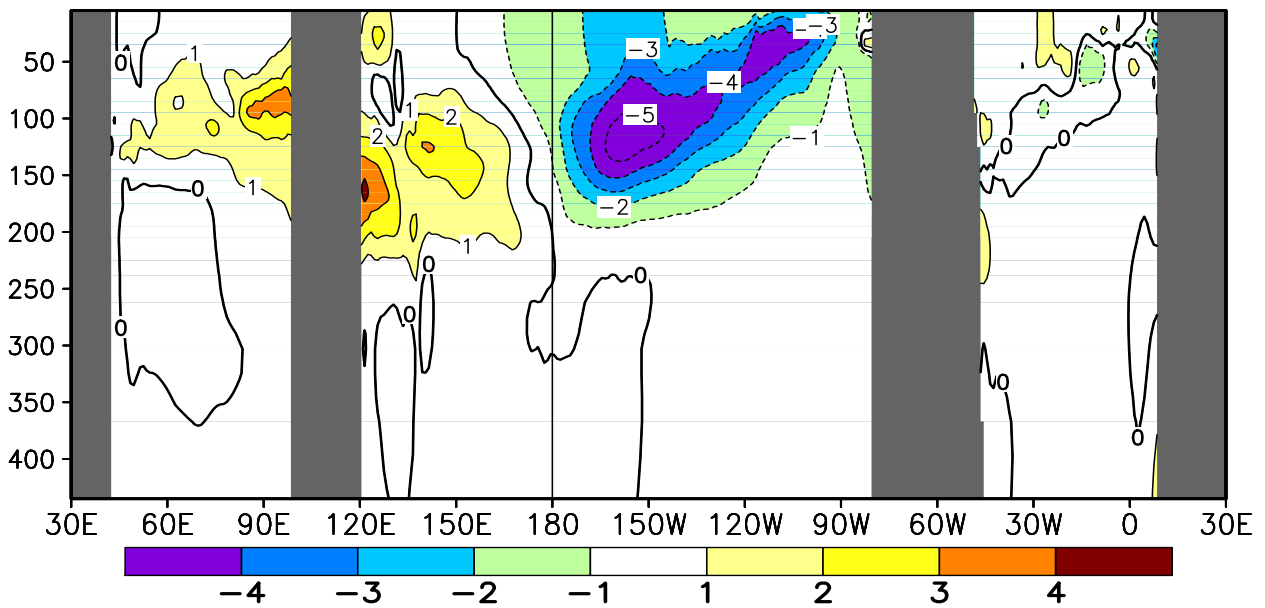


FIGURE T17. Equatorial depth–longitude section of ocean temperature (top) and ocean temperature anomalies (bottom) for AUG 2010. Contour interval is 1°C. Dashed contours in bottom panel indicate negative anomalies. Data are derived from the NCEP’s global ocean data assimilation system version 2 which assimilates oceanic observations into an oceanic GCM (Xue, Y. and Behringer, D.W., 2006: Operational global ocean data assimilation system at NCEP, to be submitted to BAMS). Anomalies are departures from the 1982–2004 base period means.

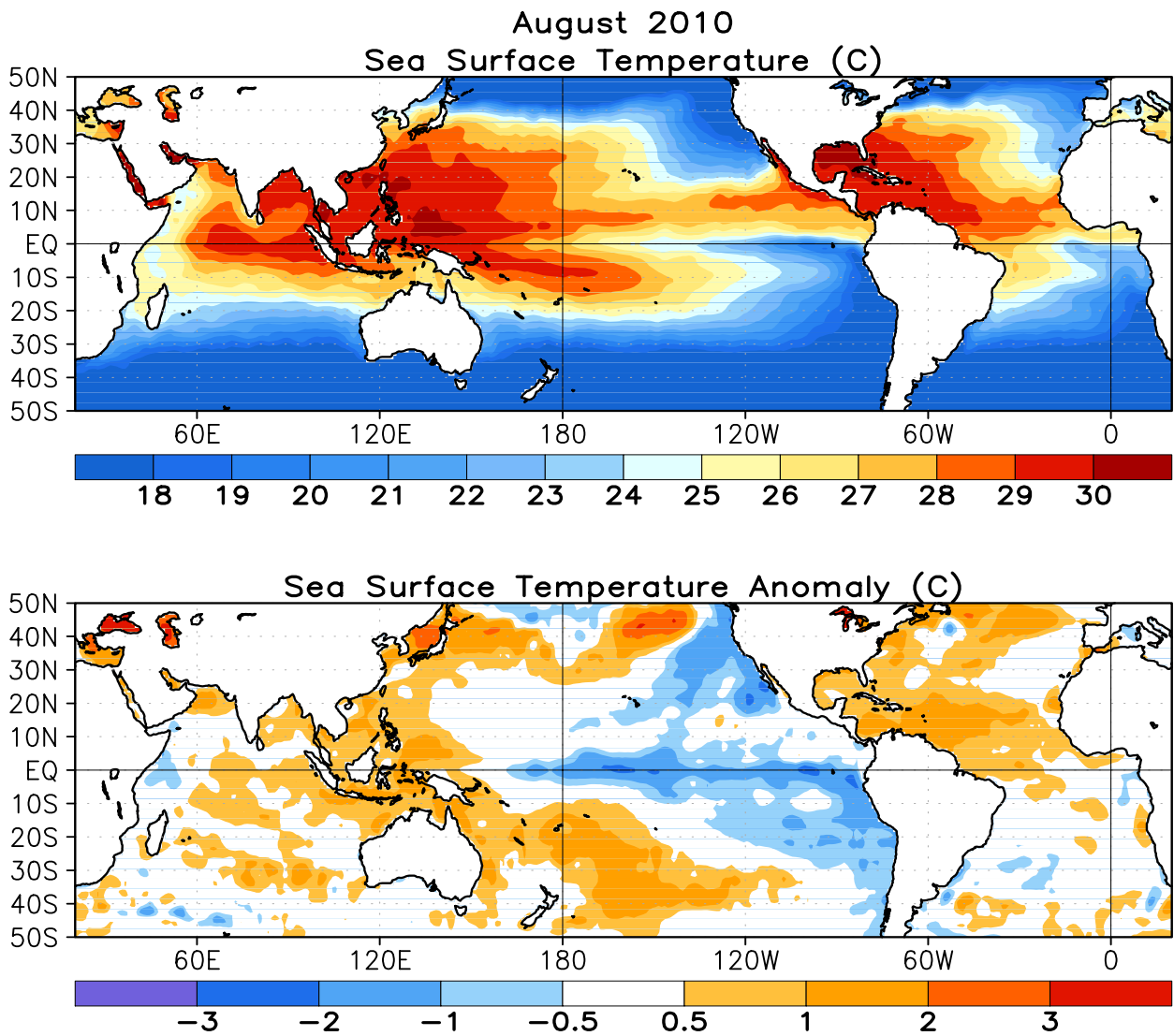


FIGURE T18. Mean (top) and anomalous (bottom) sea surface temperature (SST). Anomalies are departures from the 1971-2000 base period monthly means (Smith and Reynolds 1998, *J. Climate*, **11**, 3320-3323).

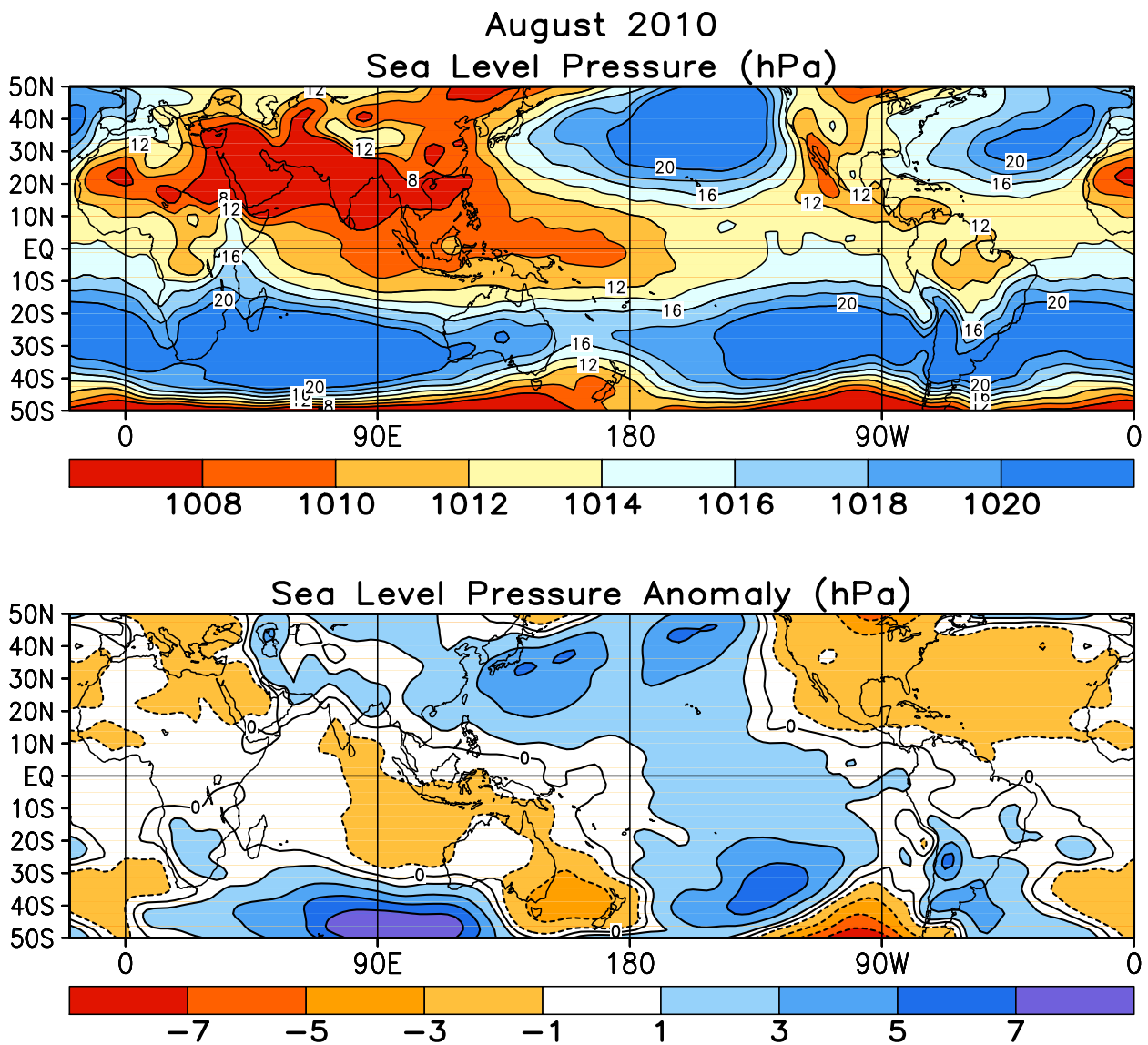


FIGURE T19. Mean (top) and anomalous (bottom) sea level pressure (SLP) (CDAS/Reanalysis). In top panel, 1000 hPa has been subtracted from contour labels, contour interval is 2 hPa, and values below 1000 hPa are indicated by dashed contours. In bottom panel, anomaly contour interval is 1 hPa and negative anomalies are indicated by dashed contours. Anomalies are departures from the 1979-1995 base period monthly means.

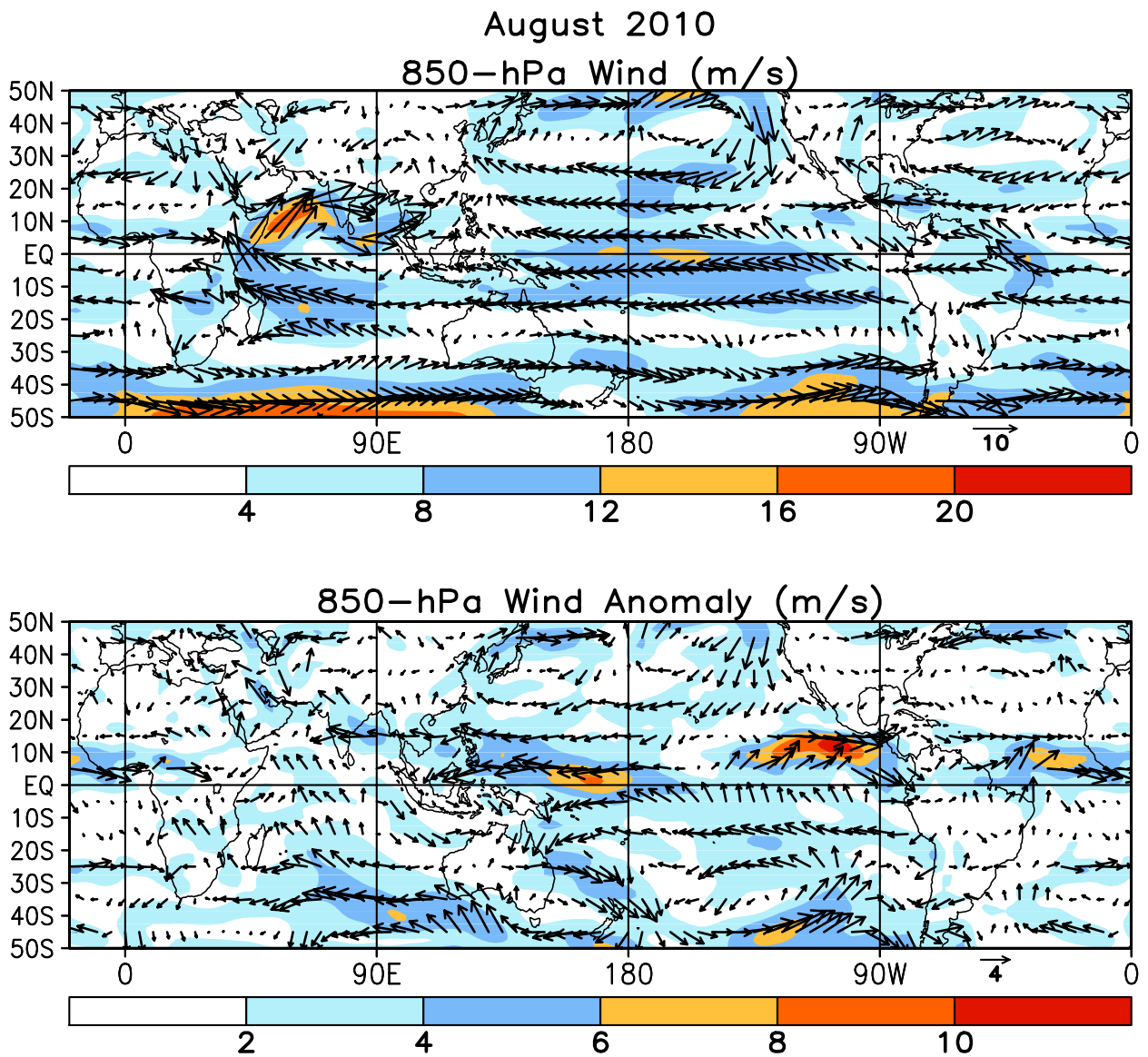


FIGURE T20. Mean (top) and anomalous (bottom) 850-hPa vector wind (CDAS/Reanalysis) for AUG 2010. Contour interval for isotachs is 4 ms^{-1} (top) and 2 ms^{-1} (bottom). Anomalies are departures from the 1979–95 base period monthly means.

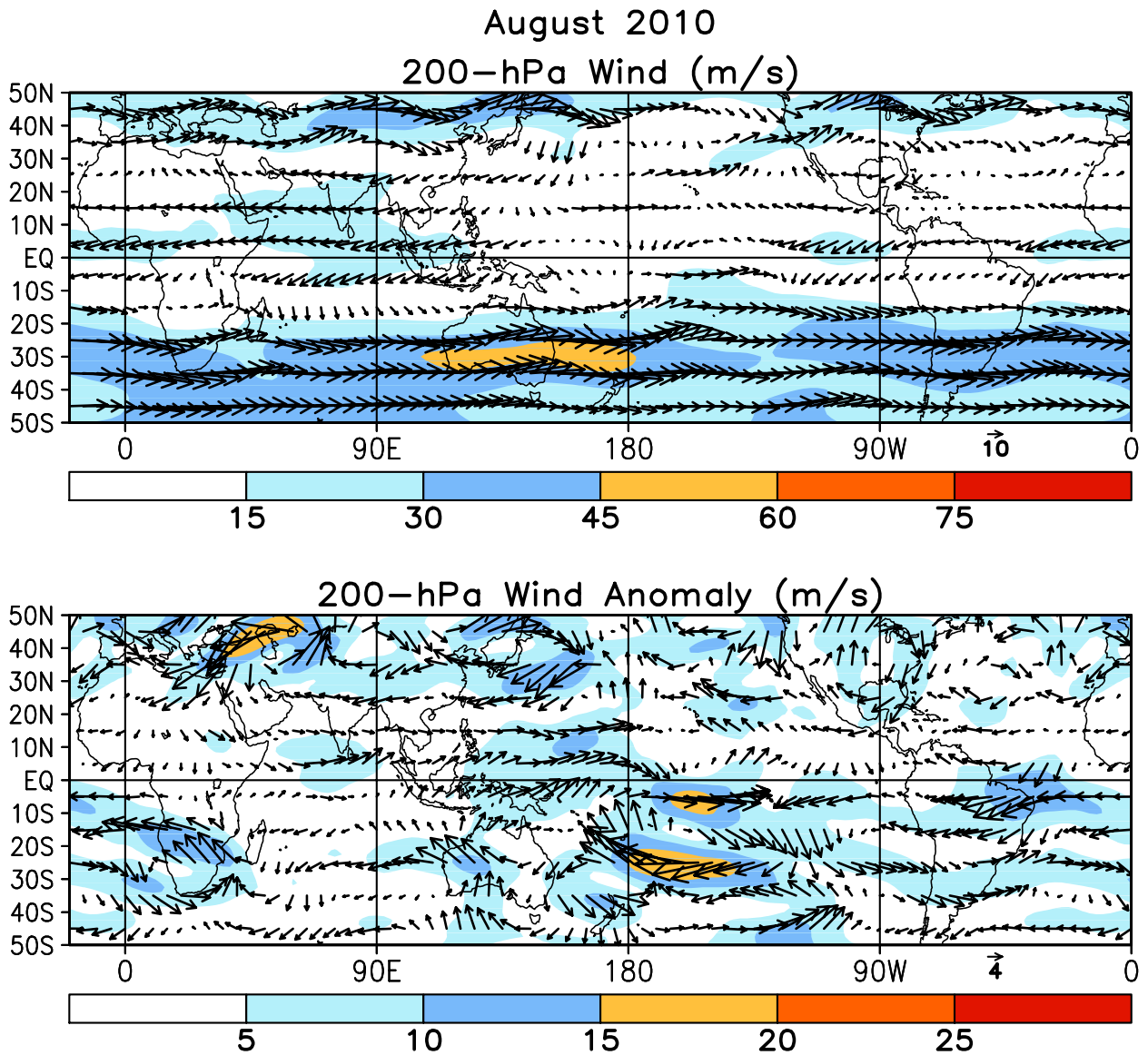


FIGURE T21. Mean (top) and anomalous (bottom) 200-hPa vector wind (CDAS/Reanalysis) for AUG 2010. Contour interval for isotachs is 15 ms^{-1} (top) and 5 ms^{-1} (bottom). Anomalies are departures from 1979–95 base period monthly means.

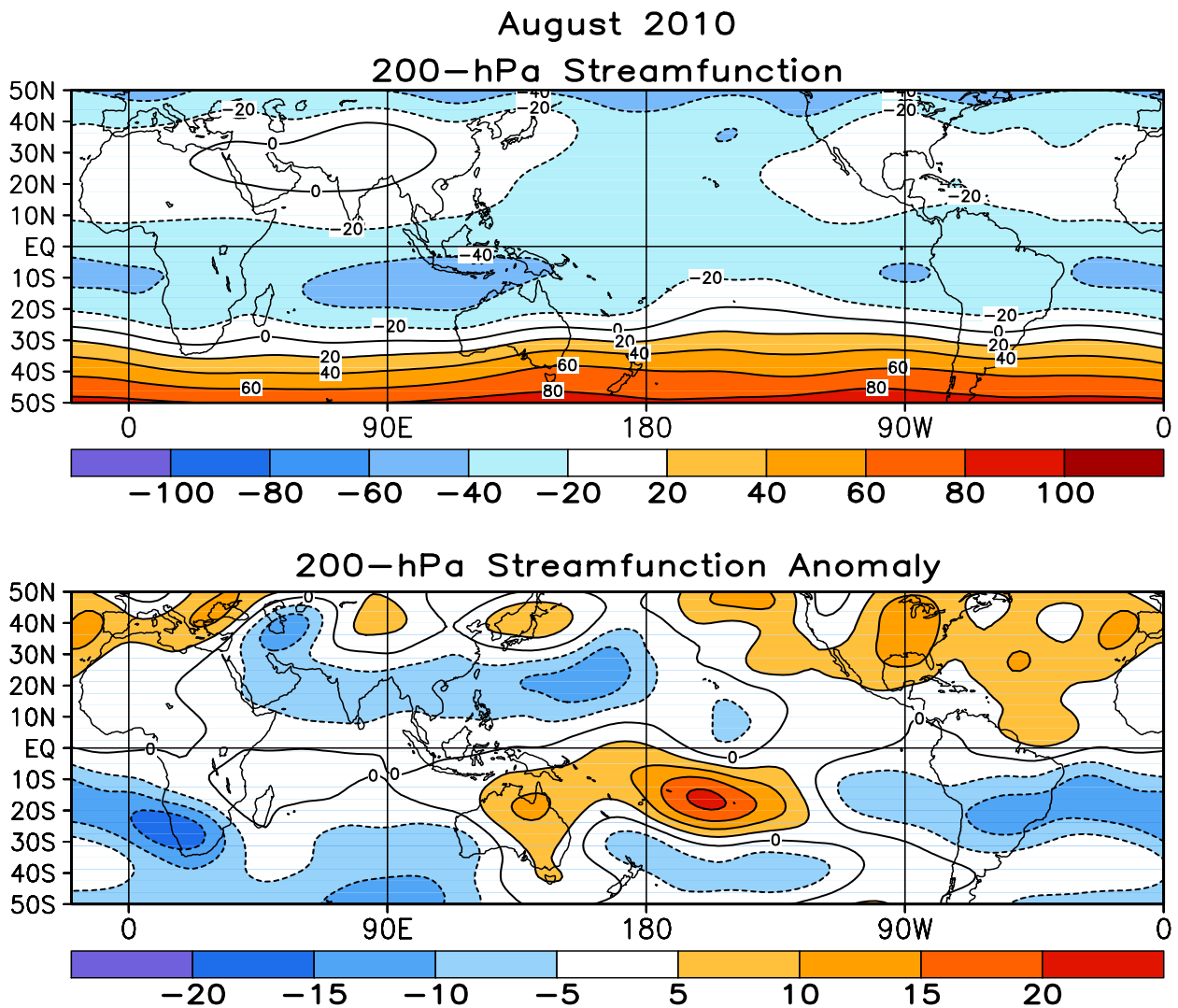


FIGURE T22. Mean (top) and anomalous (bottom) 200-hPa streamfunction (CDAS/Reanalysis). Contour interval is $20 \times 10^6 \text{ m}^2\text{s}^{-1}$ (top) and $5 \times 10^6 \text{ m}^2\text{s}^{-1}$ (bottom). Negative (positive) values are indicated by dashed (solid) lines. The non-divergent component of the flow is directed along the contours with speed proportional to the gradient. Thus, high (low) stream function corresponds to high (low) geopotential height in the Northern Hemisphere and to low (high) geopotential height in the Southern Hemisphere. Anomalies are departures from the 1979-1995 base period monthly means.

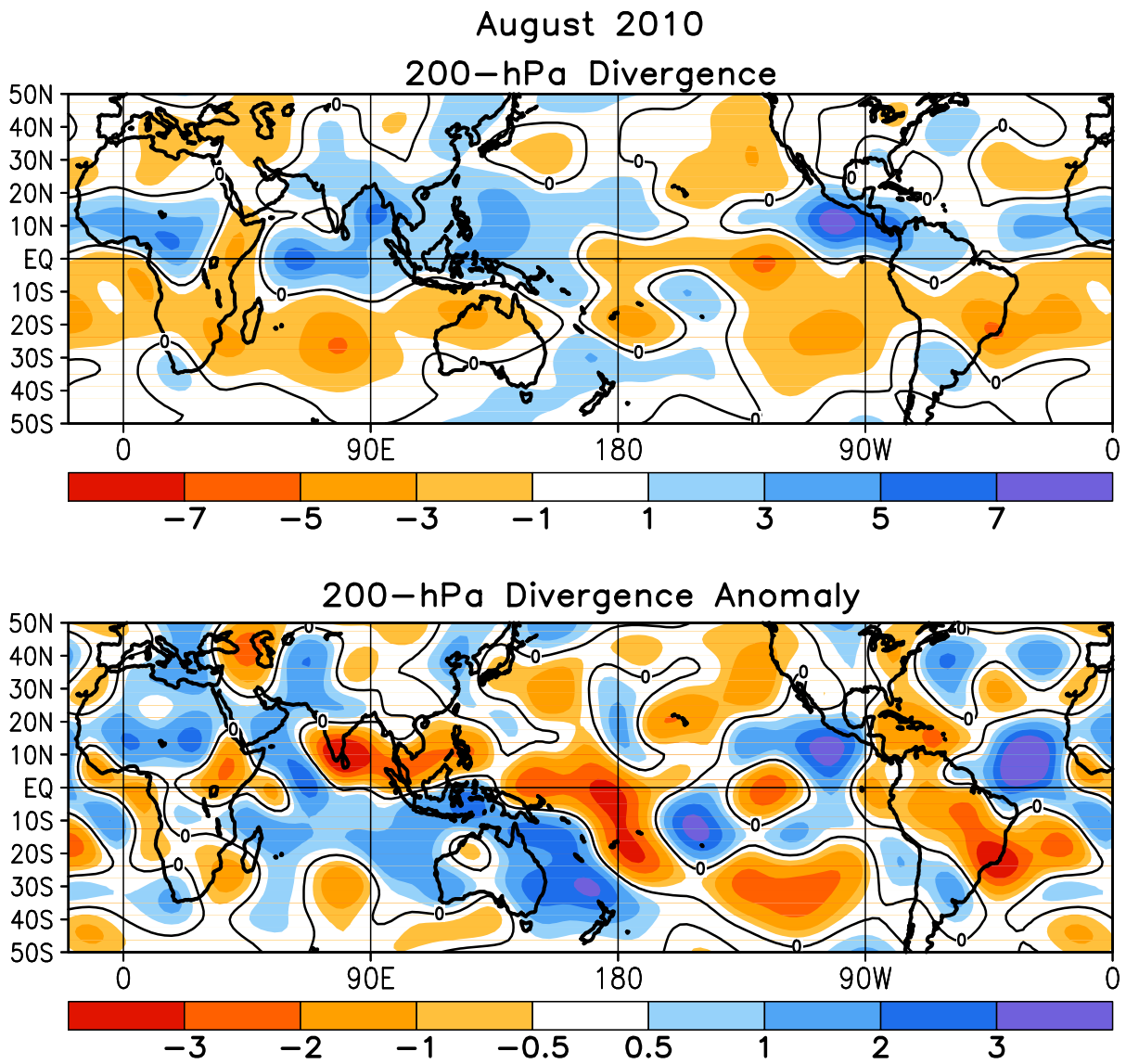


FIGURE T23. Mean (top) and anomalous (bottom) 200-hPa divergence (CDAS/Reanalysis). Divergence and anomalous divergence are shaded blue. Convergence and anomalous convergence are shaded orange. Anomalies are departures from the 1979-1995 base period monthly means.

August 2010

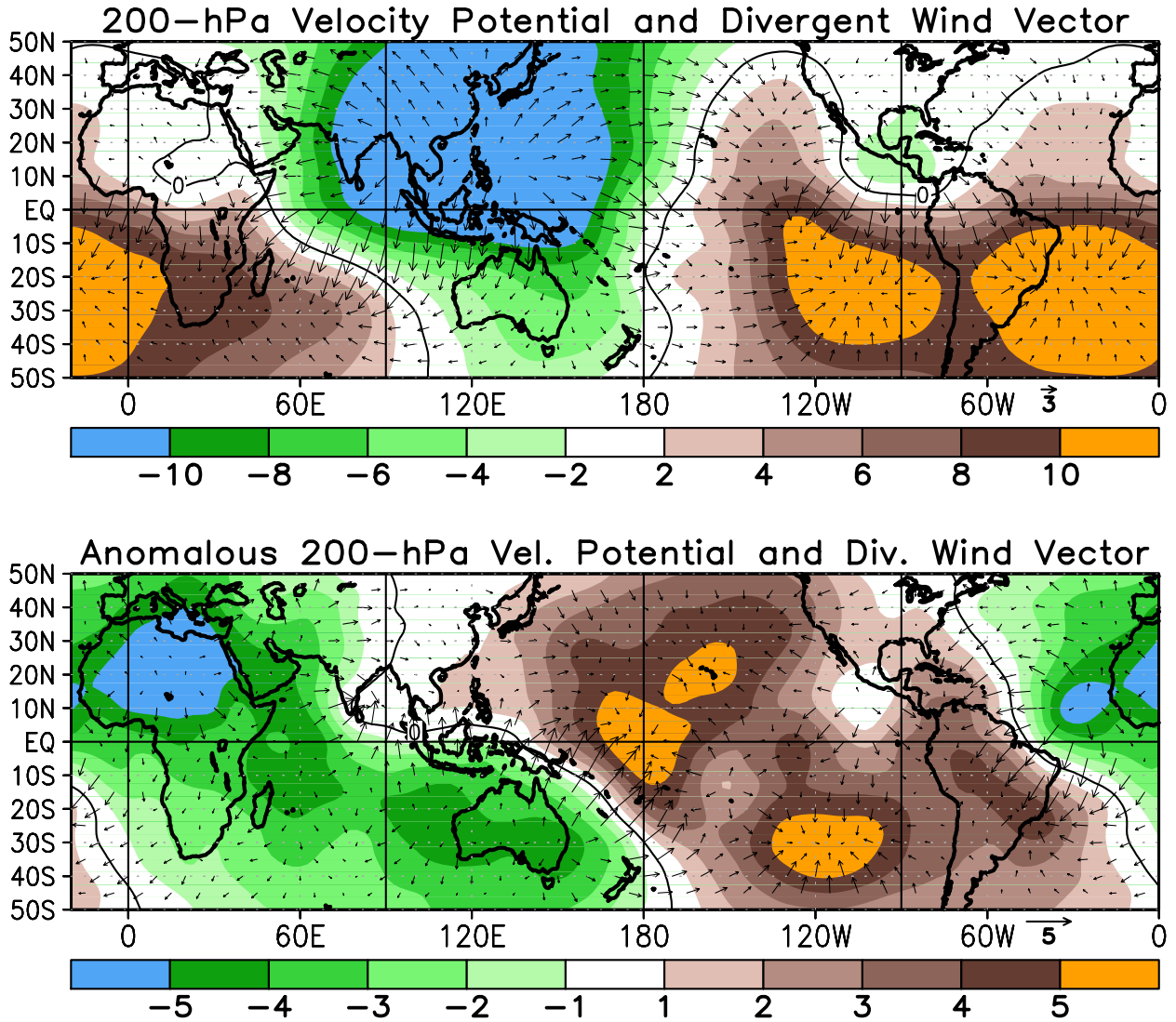


FIGURE T24. Mean (top) and anomalous (bottom) 200-hPa velocity potential ($10^6\text{m}^2\text{s}$) and divergent wind (CDAS/ Reanalysis). Anomalies are departures from the 1979-1995 base period monthly means.

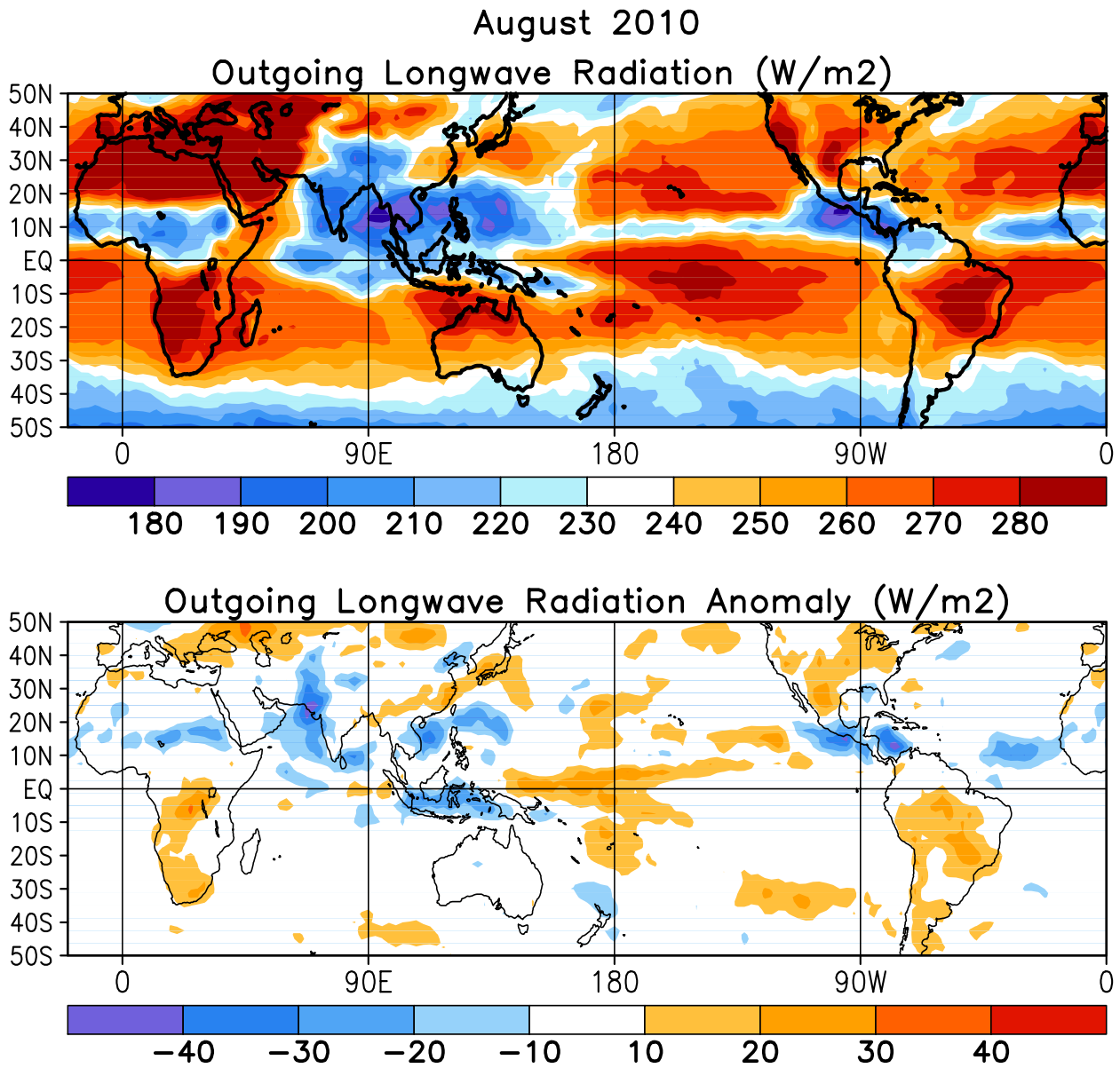


FIGURE T25. Mean (top) and anomalous (bottom) outgoing longwave radiation for AUG 2010 (NOAA 18 AVHRR IR window channel measurements by NESDIS/ORA). OLR contour interval is $20 Wm^{-2}$ with values greater than $280 Wm^{-2}$ indicated by dashed contours. Anomaly contour interval is $15 Wm^{-2}$ with positive values indicated by dashed contours and light shading. Anomalies are departures from the 1979–95 base period monthly means.

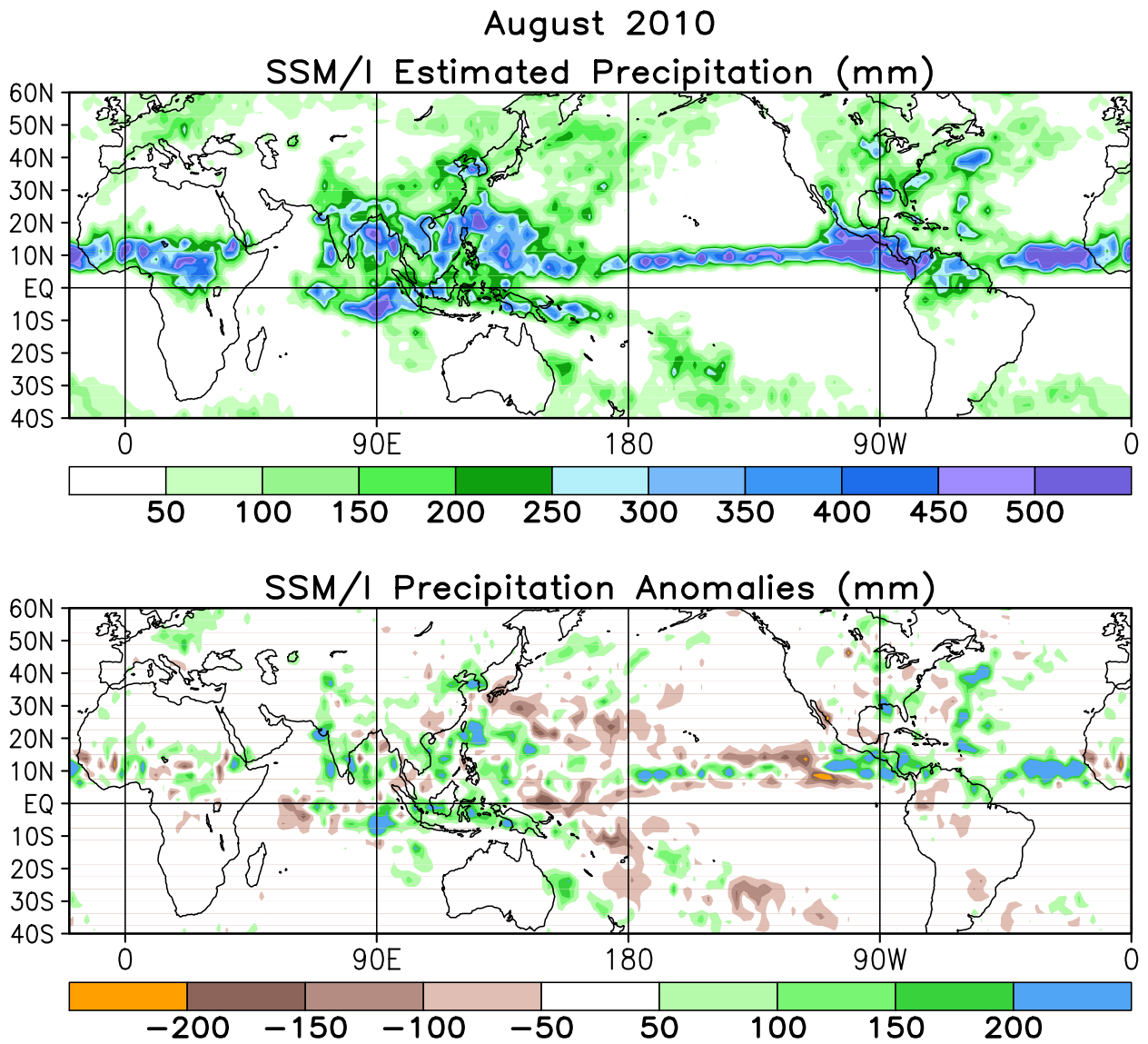


FIGURE T26. Estimated total (top) and anomalous (bottom) rainfall (mm) based on the Special Sensor Microwave/Imager (SSM/S) precipitation index (Ferraro 1997, *J. Geophys. Res.*, **102**, 16715-16735). Anomalies are computed from the SSM/I 1987-2006 base period monthly means. Anomalies have been smoothed for display purposes.

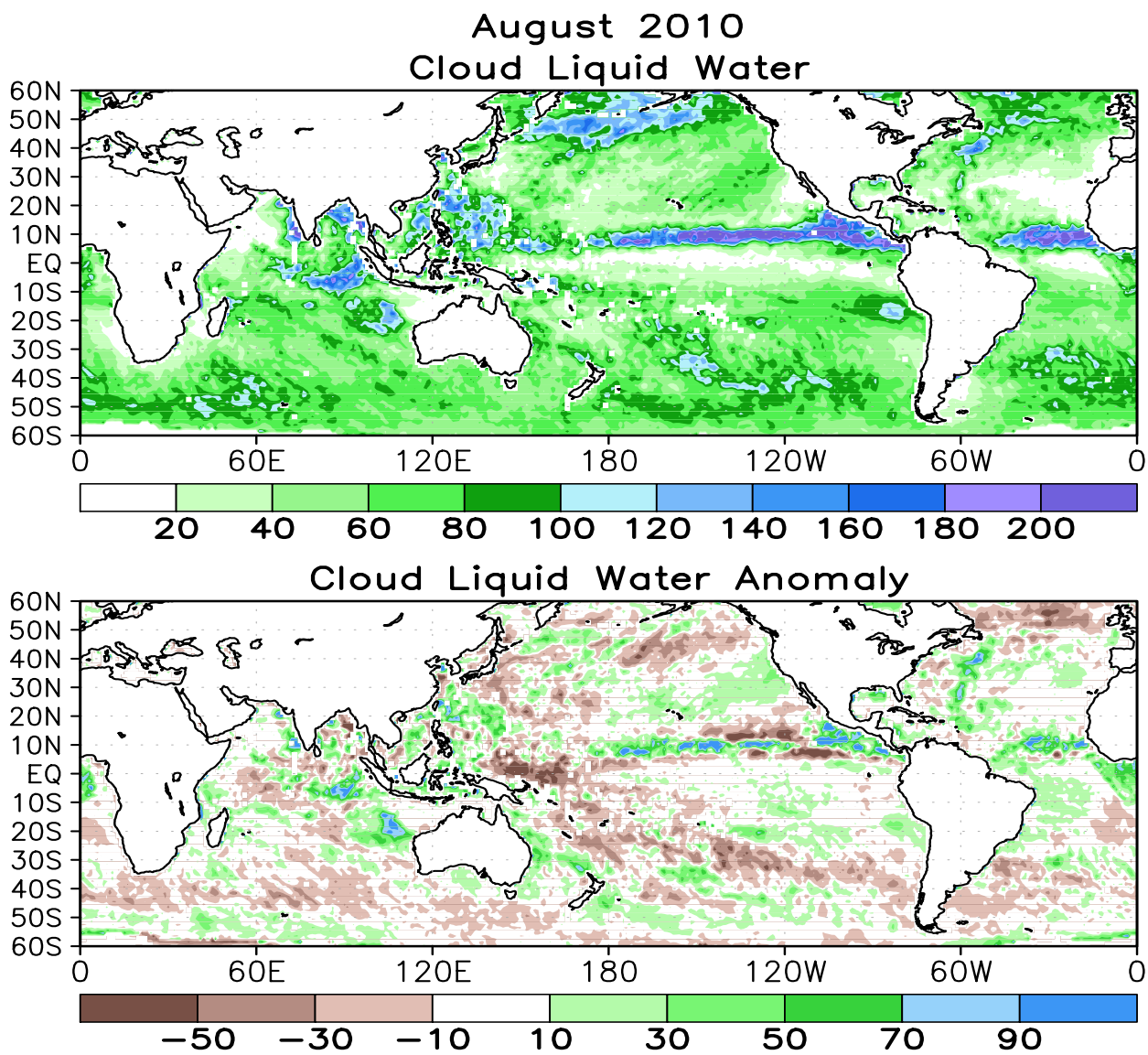


FIGURE T27. Mean (top) and anomalous (bottom) cloud liquid water (g m^{-2}) based on the Special Sensor Microwave/Imager (SSM/I) (Weng et al 1997: *J. Climate*, **10**, 1086-1098). Anomalies are calculated from the 1987-2006 base period means.

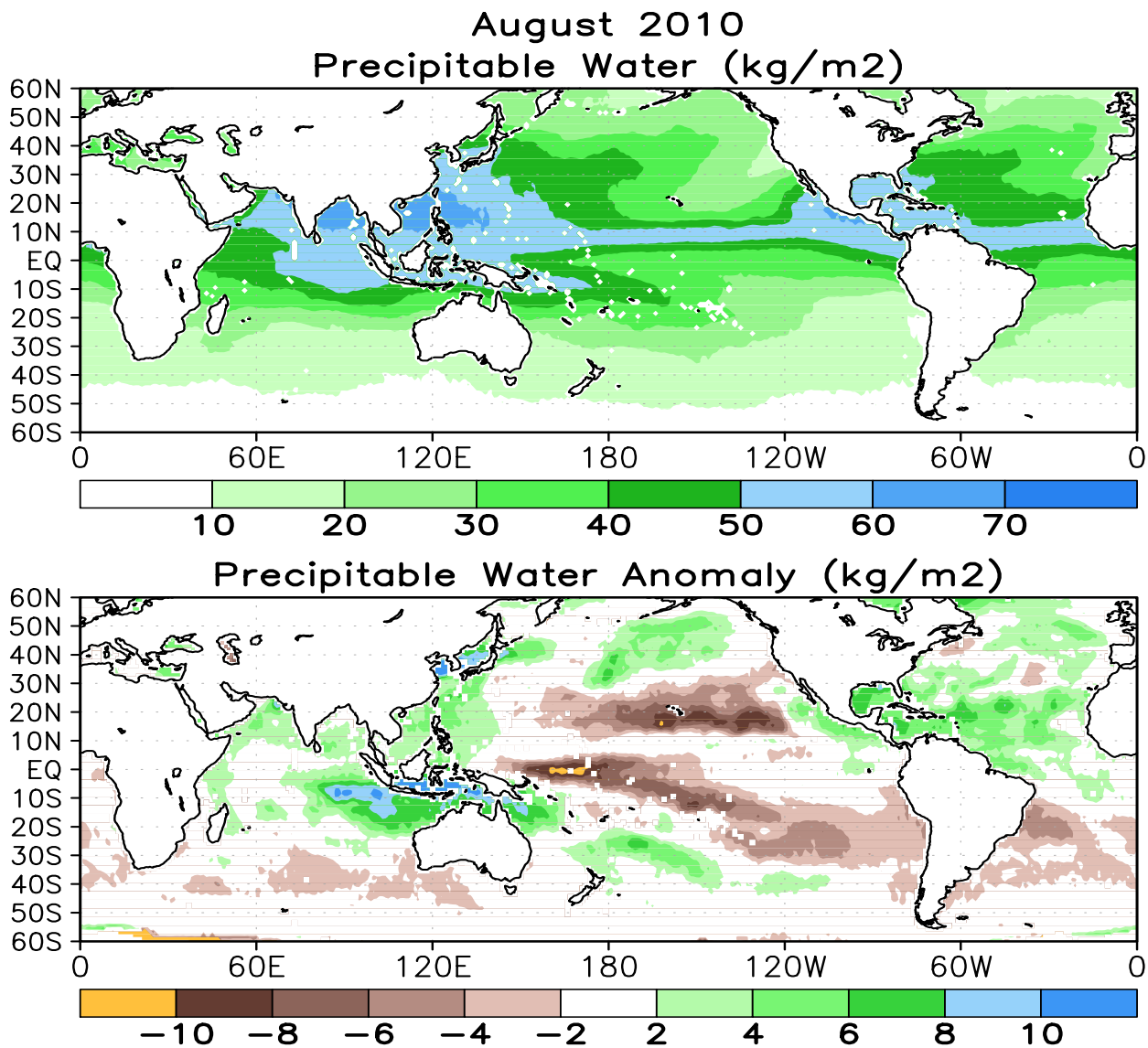


FIGURE T28. Mean (top) and anomalous (bottom) vertically integrated water vapor or precipitable water (kg m^{-2}) based on the Special Sensor Microwave/Imager (SSM/I) (Ferraro et. al, 1996: *Bull. Amer. Meteor. Soc.*, **77**, 891-905). Anomalies are calculated from the 1987-2006 base period means.

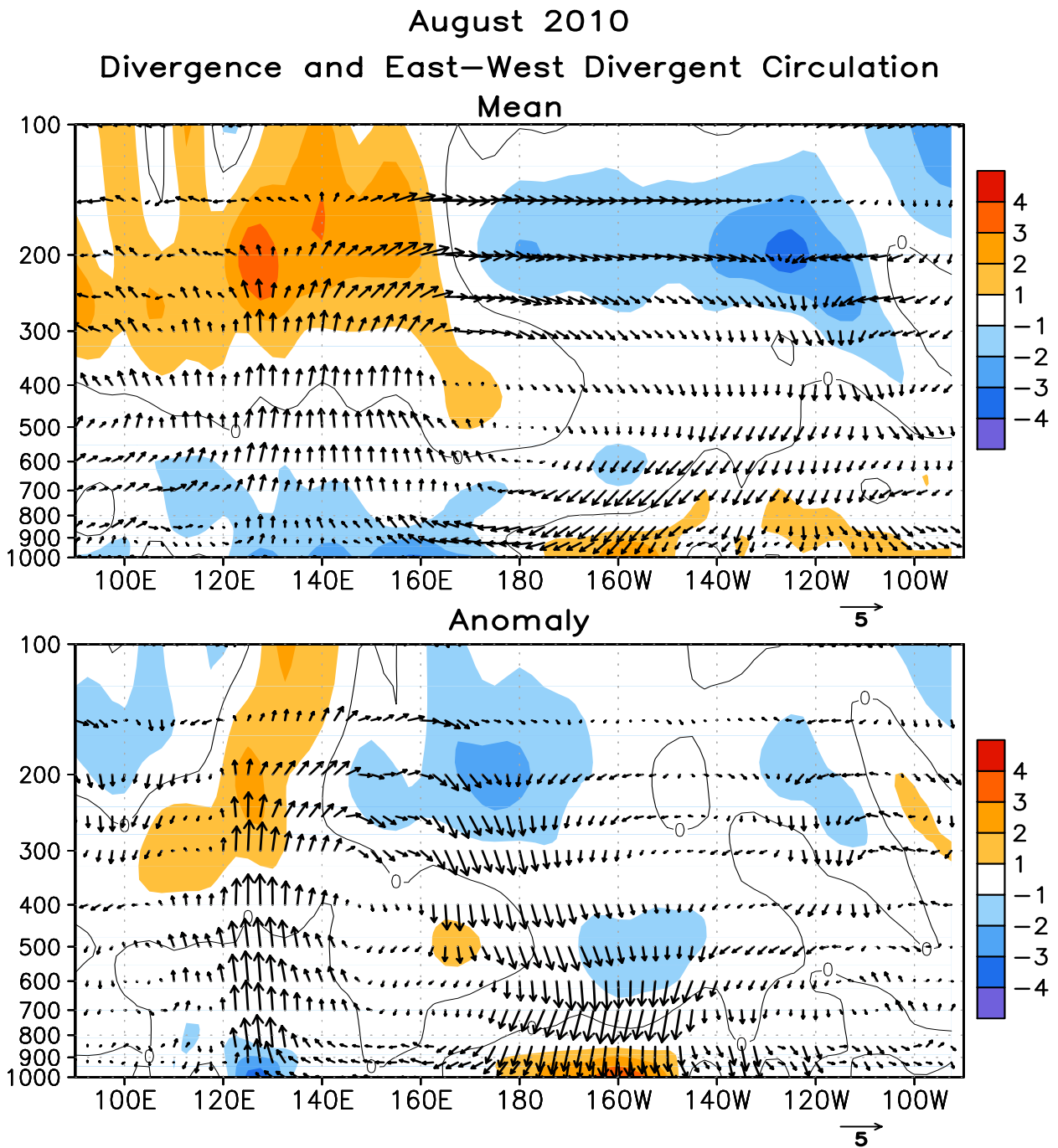


FIGURE T29. Pressure-longitude section (100E–80W) of the mean (top) and anomalous (bottom) divergence (contour interval is $1 \times 10^{-6} \text{ s}^{-1}$) and divergent circulation averaged between 5N–5S. The divergent circulation is represented by vectors of combined pressure vertical velocity and the divergent component of the zonal wind. Red shading and solid contours denote divergence (top) and anomalous divergence (bottom). Blue shading and dashed contours denote convergence (top) and anomalous convergence (bottom). Anomalies are departures from the 1979–1995 base period monthly means.

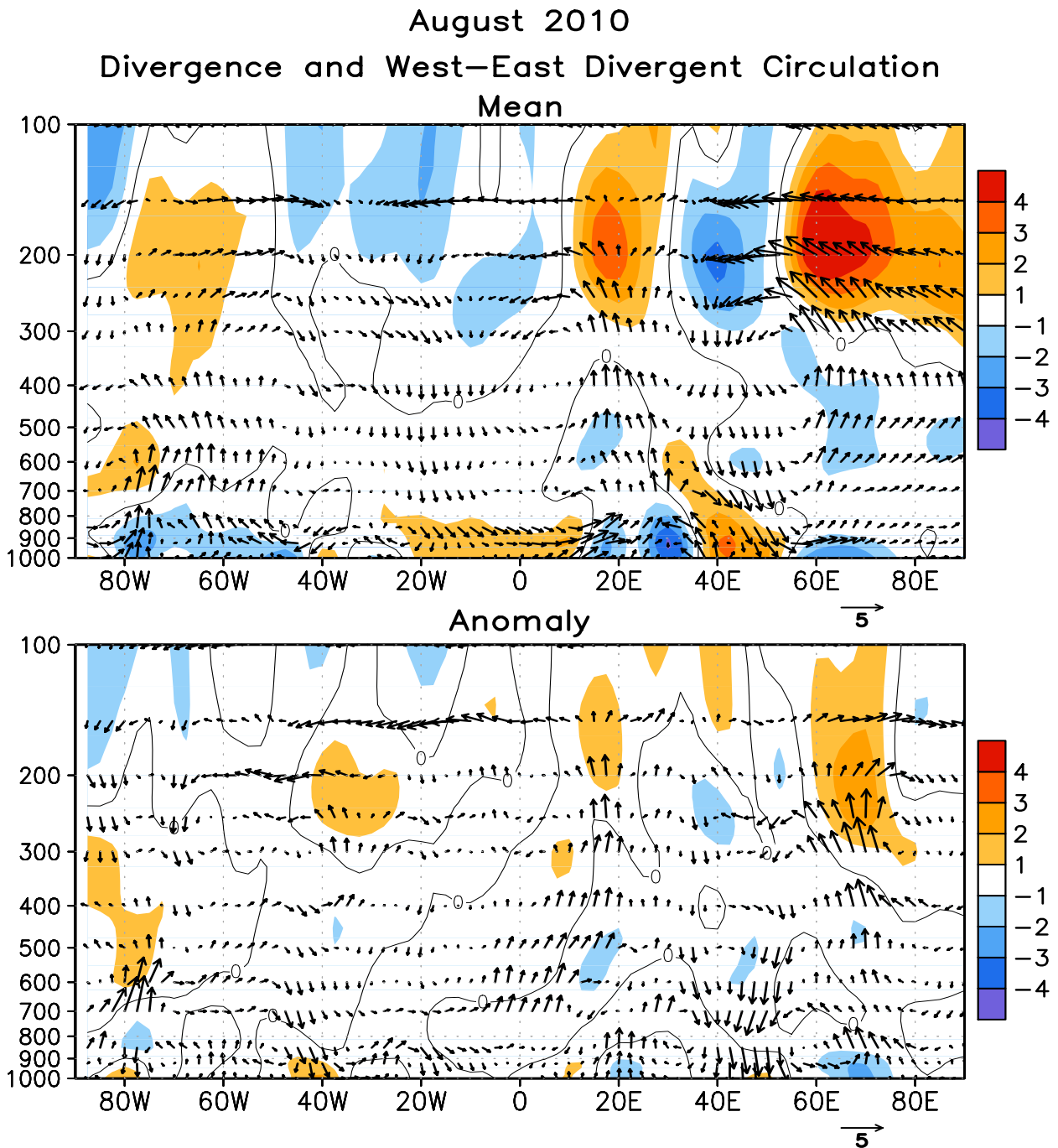


FIGURE T30. Pressure-longitude section (80W-100E) of the mean (top) and anomalous (bottom) divergence (contour interval is $1 \times 10^{-6} \text{ s}^{-1}$) and divergent circulation averaged between 5N-5S. The divergent circulation is represented by vectors of combined pressure vertical velocity and the divergent component of the zonal wind. Red shading and solid contours denote divergence (top) and anomalous divergence (bottom). Blue shading and dashed contours denote convergence (top) and anomalous convergence (bottom). Anomalies are departures from the 1979-1995 base period monthly means.

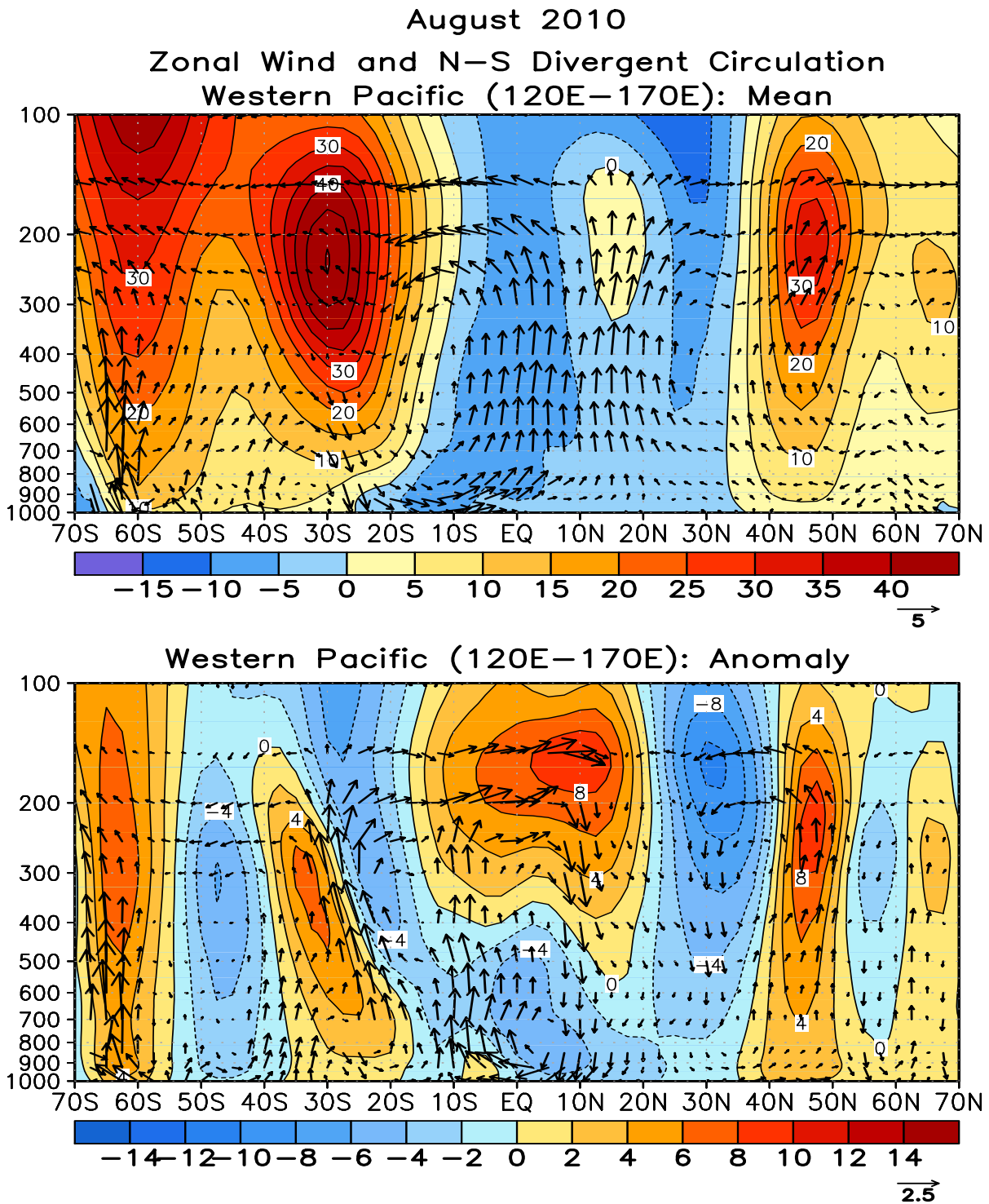


FIGURE T31. Pressure-latitude section of the mean (top) and anomalous (bottom) zonal wind (m s^{-1}) and divergent circulation averaged over the west Pacific sector (120E-170E). The divergent circulation is represented by vectors of combined pressure vertical velocity and the divergent component of the meridional wind. Red shading and solid contours denote a westerly (top) or anomalous westerly (bottom) zonal wind. Blue shading and dashed contours denote an easterly (top) or anomalous easterly (bottom) zonal wind. Anomalies are departures from the 1979-1995 base period monthly means.

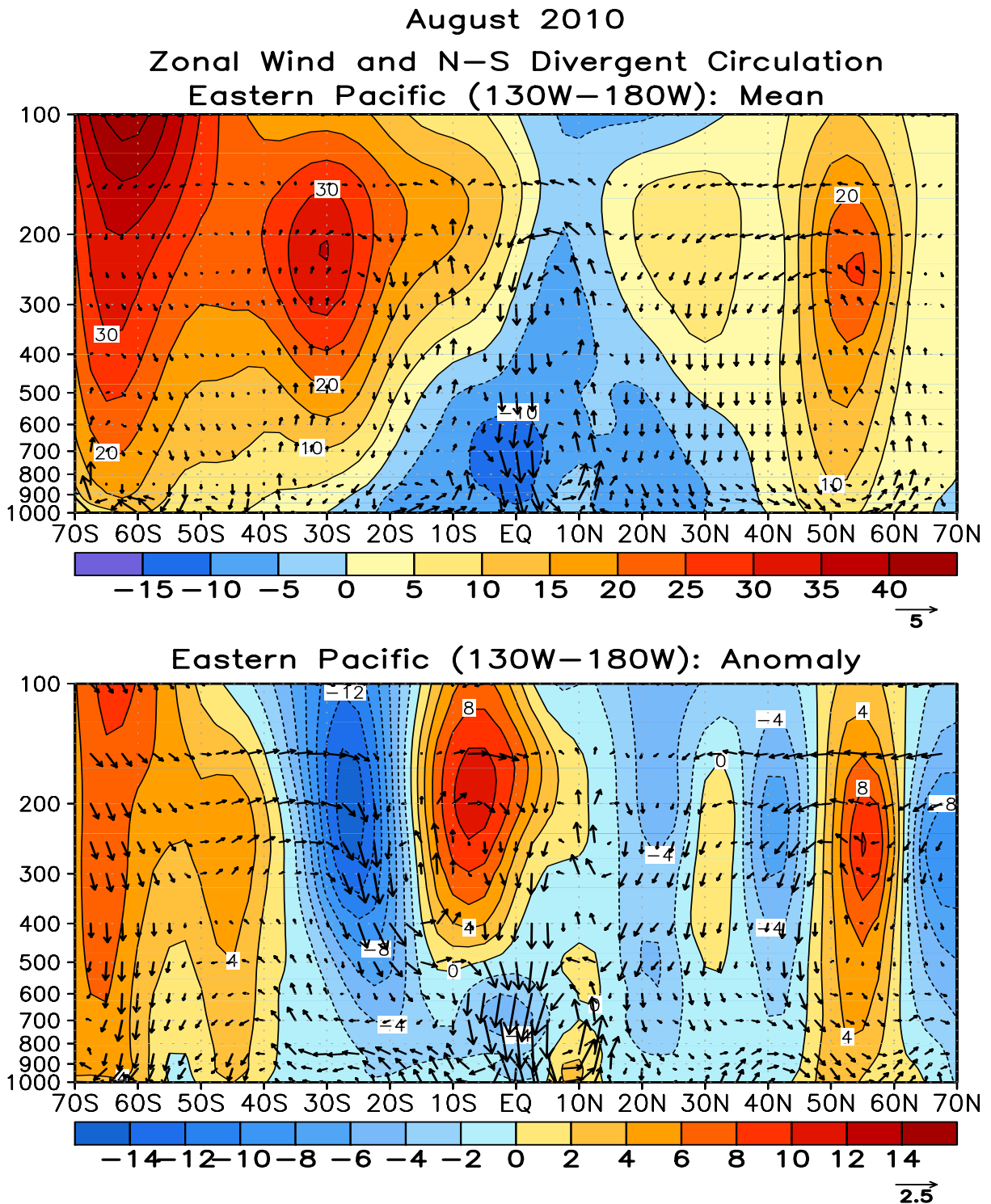


FIGURE T32. Pressure-latitude section of the mean (top) and anomalous (bottom) zonal wind (m s^{-1}) and divergent circulation averaged over the central Pacific sector (130W-180W). The divergent circulation is represented by vectors of combined pressure vertical velocity and the divergent component of the meridional wind. Red shading and solid contours denote a westerly (top) or anomalous westerly (bottom) zonal wind. Blue shading and dashed contours denote an easterly (top) or anomalous easterly (bottom) zonal wind. Anomalies are departures from the 1979-1995 base period monthly means.

During August 2010, 453 satellite-tracked surface drifting buoys, 71% with subsurface drogues attached for measuring mixed layer currents, were reporting from the tropical Pacific. As seen in the last two months, dramatic 50 cm/s westward anomalies were measured by many near-equatorial drifters, although this was primarily seen at longitudes of 140-180W. In July, this pattern was present across the basin. These westward anomalies are an intensification of the pattern seen since March. Equatorial drifters in the center of the basin measured cold SST anomalies of -1 to -3C. Off-equatorial drifters measured SSTs at or slightly above normal July values west of 160-170W, and at or slightly below normal east of this.

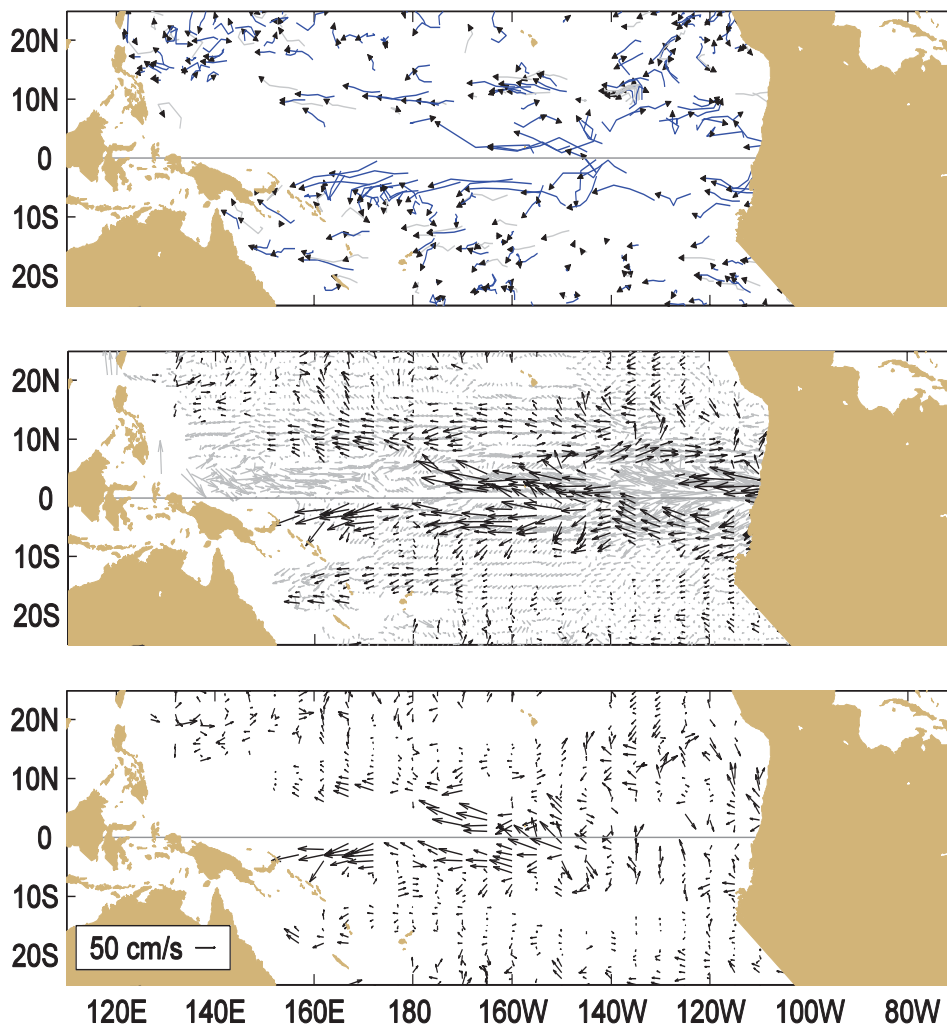


Figure A1.1 Top: Movements of drifting buoys in the tropical Pacific Ocean during August 2010. The linear segments of each trajectory represent a one week displacement. Trajectories of buoys which have lost their subsurface drogues are gray; those with drogues are black.

Middle: Monthly mean currents calculated from all buoys 1993-2002 (gray), and currents measured by the drogued buoys this month (black) smoothed by an optimal filter.

Bottom: Anomalies from the climatological monthly mean currents for this month.

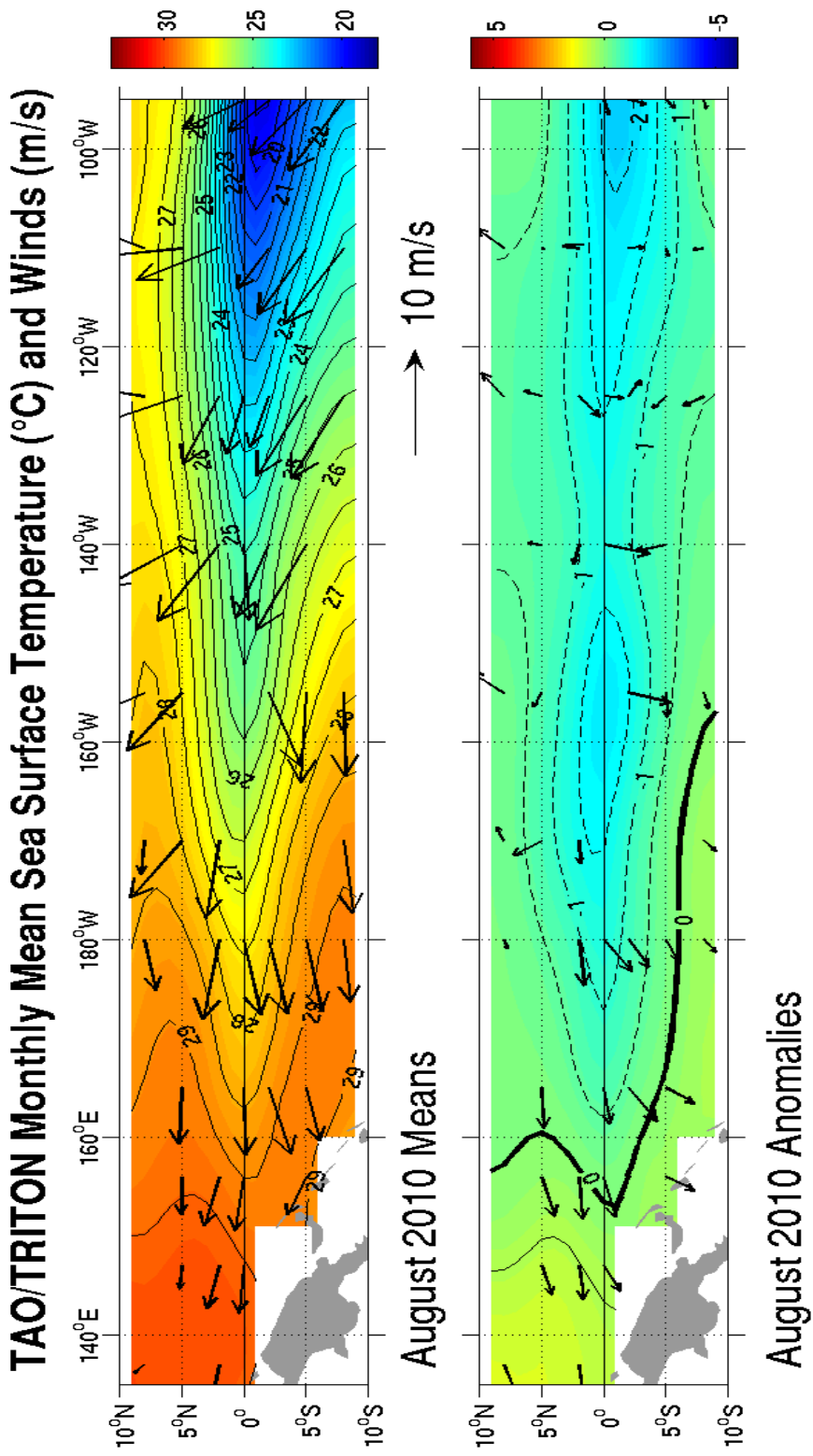


FIGURE A1.2. Wind Vectors and sea surface temperature (SSTs) from the TAO/TRITON mooring array. Top panel shows monthly means; bottom panel shows monthly anomalies from the COADS wind climatology and Reynolds SST climatology (1971-2000). The TAO/TRITON array is presently supported by the United States (NOAA), Japan (STA), and France (IRD). Further information is available from Richard L. Crout (NOAA/NDBC).

Five Day Zonal Wind, SST, and 20°C Isotherm Depth 2°S to 2°N Average

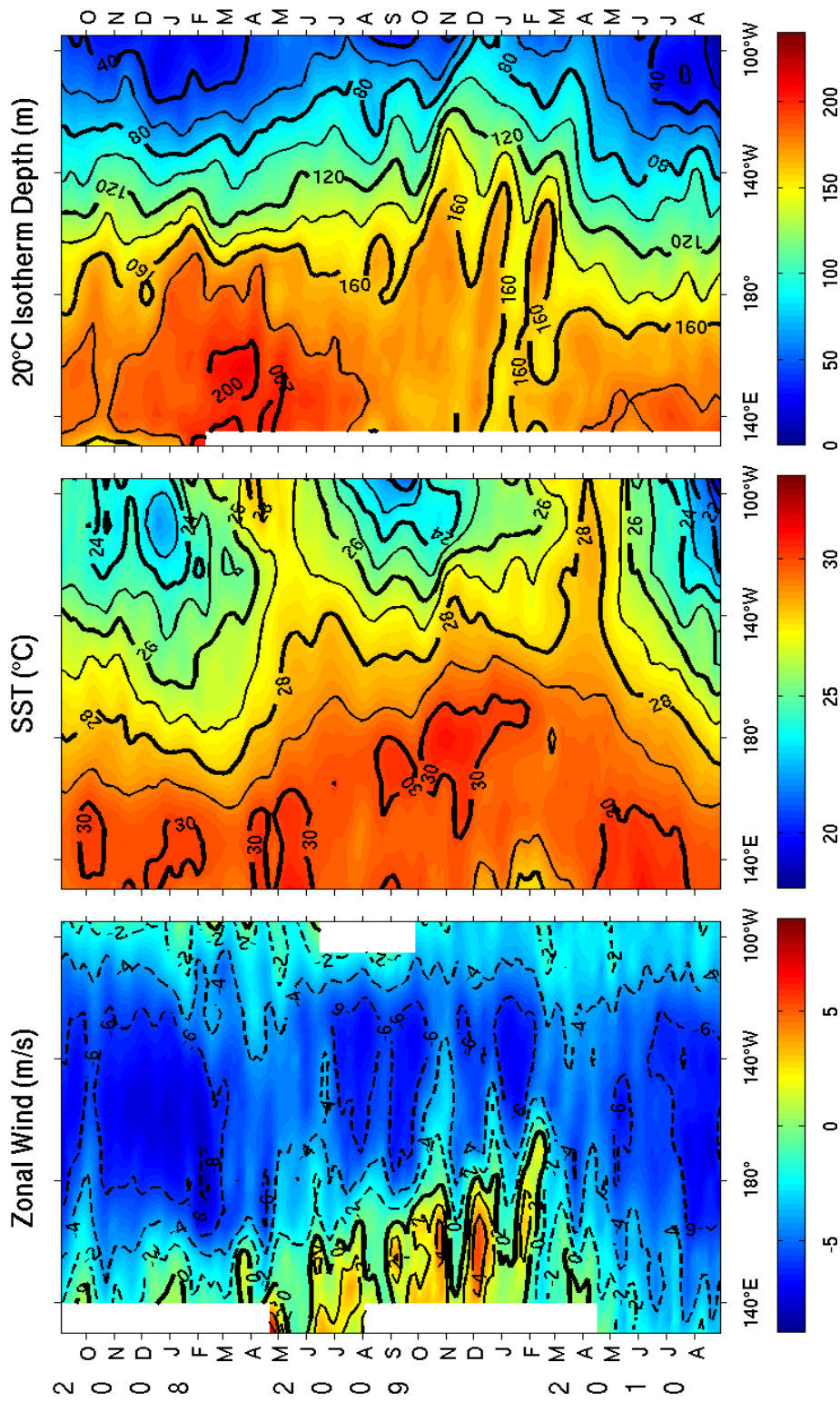


FIGURE A1.3. Time-longitude sections of surface zonal winds (m s^{-1}), sea surface temperature (C) and 20C isotherm depth (m) for the past 24 months. Analysis is based on 5-day averages of moored time series data from the TAO/TRITON array. Positive winds are westerly. Squares on the abscissas indicate longitude where data were available at the start of the time series (top) and end of the time series (bottom). The TAO/TRITON array is presently supported by the United States (NOAA), Japan (STA), and France (IRD). Further information is available from Richard L. Crout (NOAA/NDBC)

Five Day Zonal Wind, SST, and 20°C Isotherm Depth Anomalies 2°S to 2°N Average

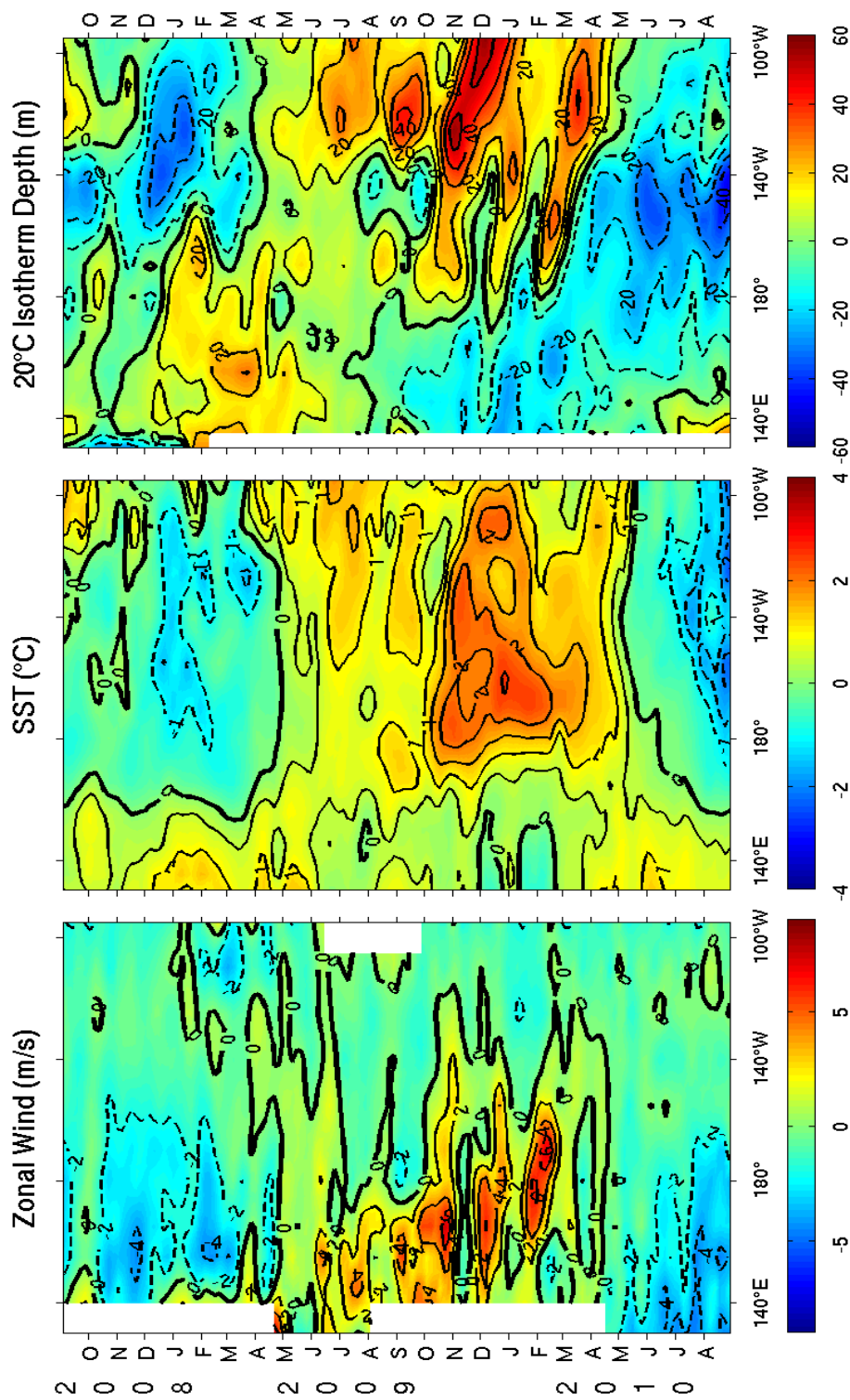
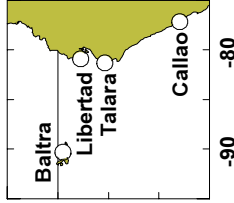


FIGURE A1.4. Time-longitude sections of surface zonal winds ($m s^{-1}$), sea surface temperature (C) and 20C isotherm depth (m) for the past 24 months. Analysis is based on 5-day averages of moored time series data from the TAO/TRITON array. Anomalies are relative to monthly climatologic cubic spline fitted to 5-day intervals (COADS winds, Reynolds SST, CTD/XBT 20C depth). Positive winds are westerly. Squares on the abscissas indicate longitude where data were available at the start of the time series (top) and end of the time series (bottom). The TAO/TRITON array is presently supported by the United States (NOAA), Japan (STA), and France (IRD). Further information is available from Richard L. Crout (NOAA/

Sea Surface Temperature and Sea Level From Eastern Pacific GOES Stations

David B. Enfield, NOAA/AOML, 4301 Rickenbacker Cswy, Miami FL 33149, USA
 Instituto Oceanográfico de la Armada, Guayaquil, ECUADOR
 Dirección de Hidrografía y Navegación de la Marina, Callao, PERU



In cooperation with institutions in Peru and Ecuador, NOAA-AOML maintained a network coastal stations reporting SST and sea level in real time (via satellite downlink) during the TOGA program, from 1985 to 1995. The South American partners took over full operational responsibility thereafter while NOAA-AOML assumed a data management role, continuing publication of these monthly reports along with their partners. The five-day averages (pentads) at critical stations give us an effective means of monitoring coastal conditions with good time resolution and compact data volume.

The negative SST and sea level anomalies along the South American coast are persisting and becoming more intense. Intraseasonal modulations are weak and the evolution is consistent with a strong La Nina event.

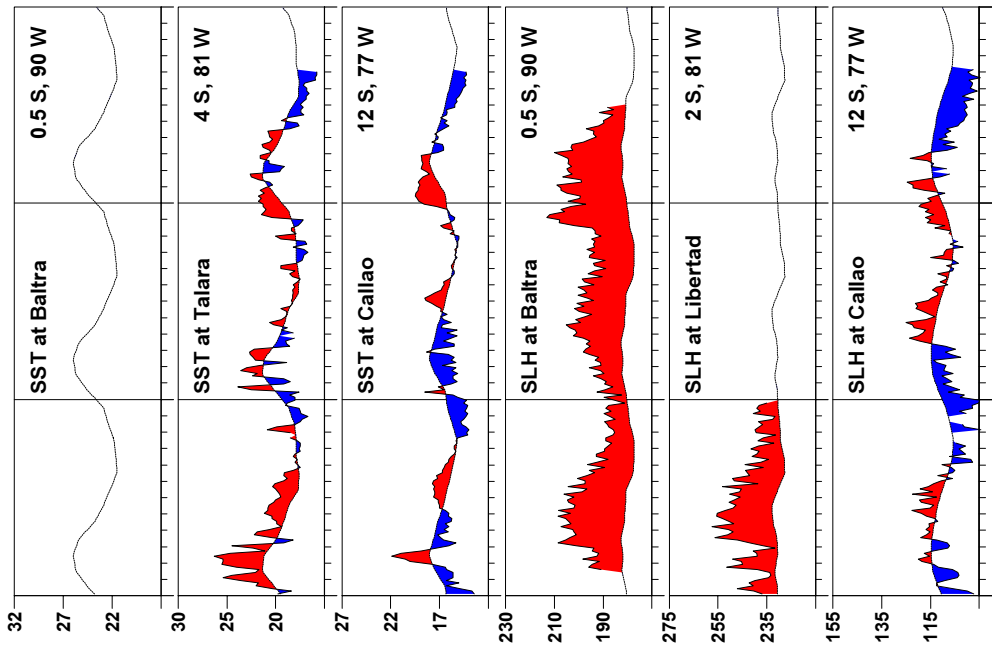
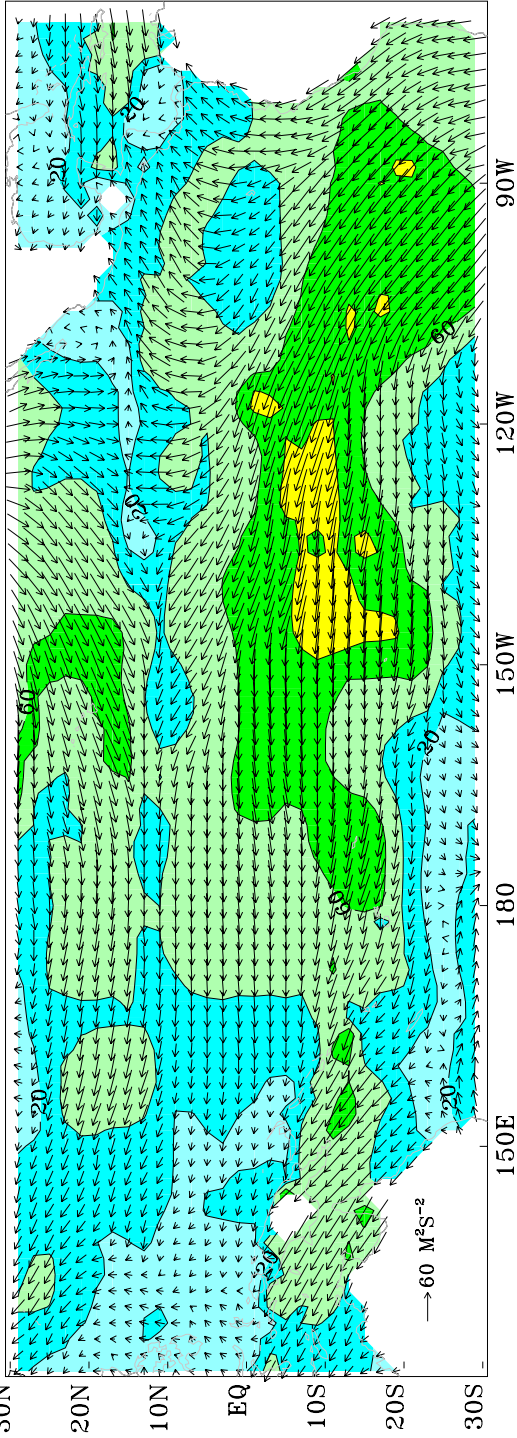


FIGURE A1.5. Five-day averages of sea surface temperature (SST, °C) and sea level height (SLH_{cm}) from GOES receiving stations in Ecuador & Peru. Dashed line and shading show climatology, departures.

| | | Sea Sfc Temperature | | | Sea Level Height | | |
|-----------|----|---------------------|--------|--------|------------------|----------|--------|
| AUG | | Baltra | Talara | Callao | Baltra | Libertad | Callao |
| 1 | ** | 16.8 | 14.6 | 14.6 | ** | ** | 98.0 |
| 6 | ** | 17.2 | 14.3 | 14.3 | ** | ** | 97.7 |
| 11 | ** | 17.0 | 14.4 | 14.4 | ** | ** | 99.2 |
| 16 | ** | 15.9 | 14.3 | 14.3 | ** | ** | 94.6 |
| 21 | ** | 16.0 | 14.5 | 14.5 | ** | ** | 98.2 |
| 26 | ** | 15.8 | 14.2 | 14.2 | ** | ** | 99.6 |
| 31 | ** | 15.8 | 14.3 | 14.3 | ** | ** | 97.5 |
| Anomalies | | | | | | | |
| AUG | | Baltra | Talara | Callao | Baltra | Libertad | Callao |
| 1 | ** | -0.8 | -1.4 | -1.4 | ** | ** | -10.4 |
| 6 | ** | -0.4 | -1.6 | -1.6 | ** | ** | -10.3 |
| 11 | ** | -0.6 | -1.5 | -1.5 | ** | ** | -8.4 |
| 16 | ** | -1.7 | -1.5 | -1.5 | ** | ** | -12.7 |
| 21 | ** | -1.6 | -1.2 | -1.2 | ** | ** | -8.9 |
| 26 | ** | -1.9 | -1.5 | -1.5 | ** | ** | -7.2 |
| 31 | ** | -1.9 | -1.3 | -1.3 | ** | ** | -9.0 |

Email: David.Enfield@noaa.gov; Phone: (305) 361-4351; Fax: (305) 361-4392
 ** - Data missing due to hardware failure

Near-real-time Objective FSU Pseudo-stress Magnitude and Vectors (10m) August 2010



Near-real-time Objective FSU Pseudo-stress Anomalies (10m) August 2010

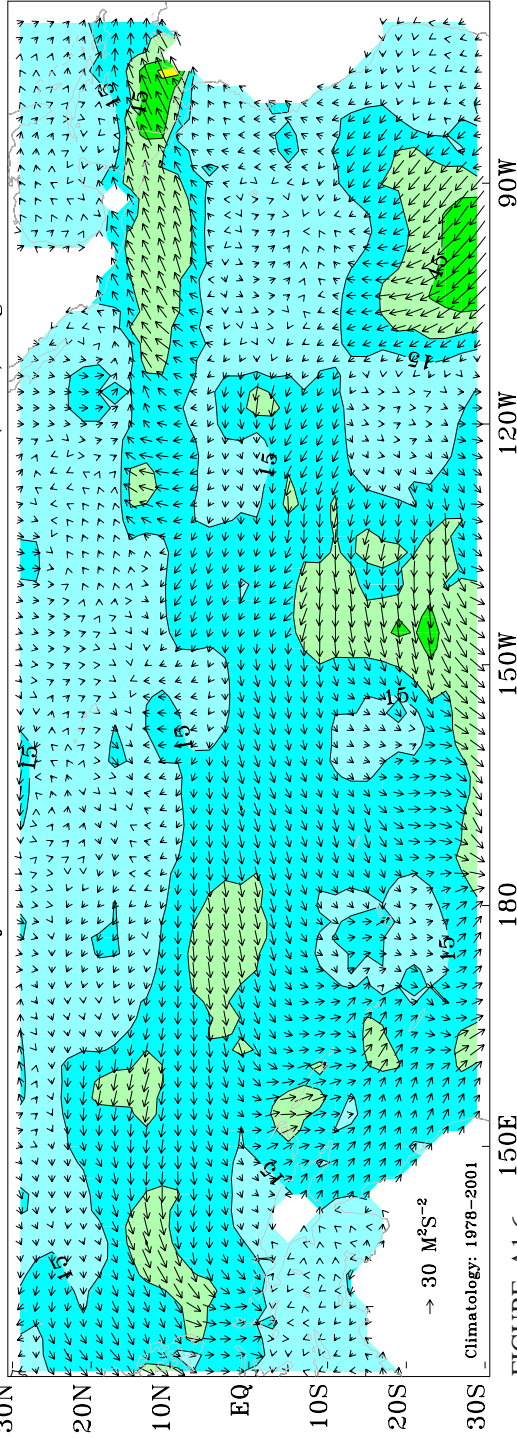


FIGURE A1.6.

FSU SURFACE PSEUDO-STRESS VECTORS AND ANOMALIES: August 2010. Pseudo-stress vectors (top) are objectively analyzed from ship and buoy winds on a 2° grid. Ship and buoy data are independently weighted and the background field is created from the data. Contour interval of the vector magnitudes is $20 \text{ M}^2\text{S}^{-2}$. Anomalies (bottom) are departures from 1978-2001 mean. The contour interval is $15 \text{ M}^2\text{S}^{-2}$. For more information, please visit our web site at <http://www.coaps.fsu.edu/RVSMDC/html/winds.shtml>. Produced by Jeremy Rolph, Mark A. Bourassa, and Shawn R. Smith, Center for Ocean-Atmospheric Prediction Studies, Florida State University, Tallahassee, FL 32306-2840, USA.

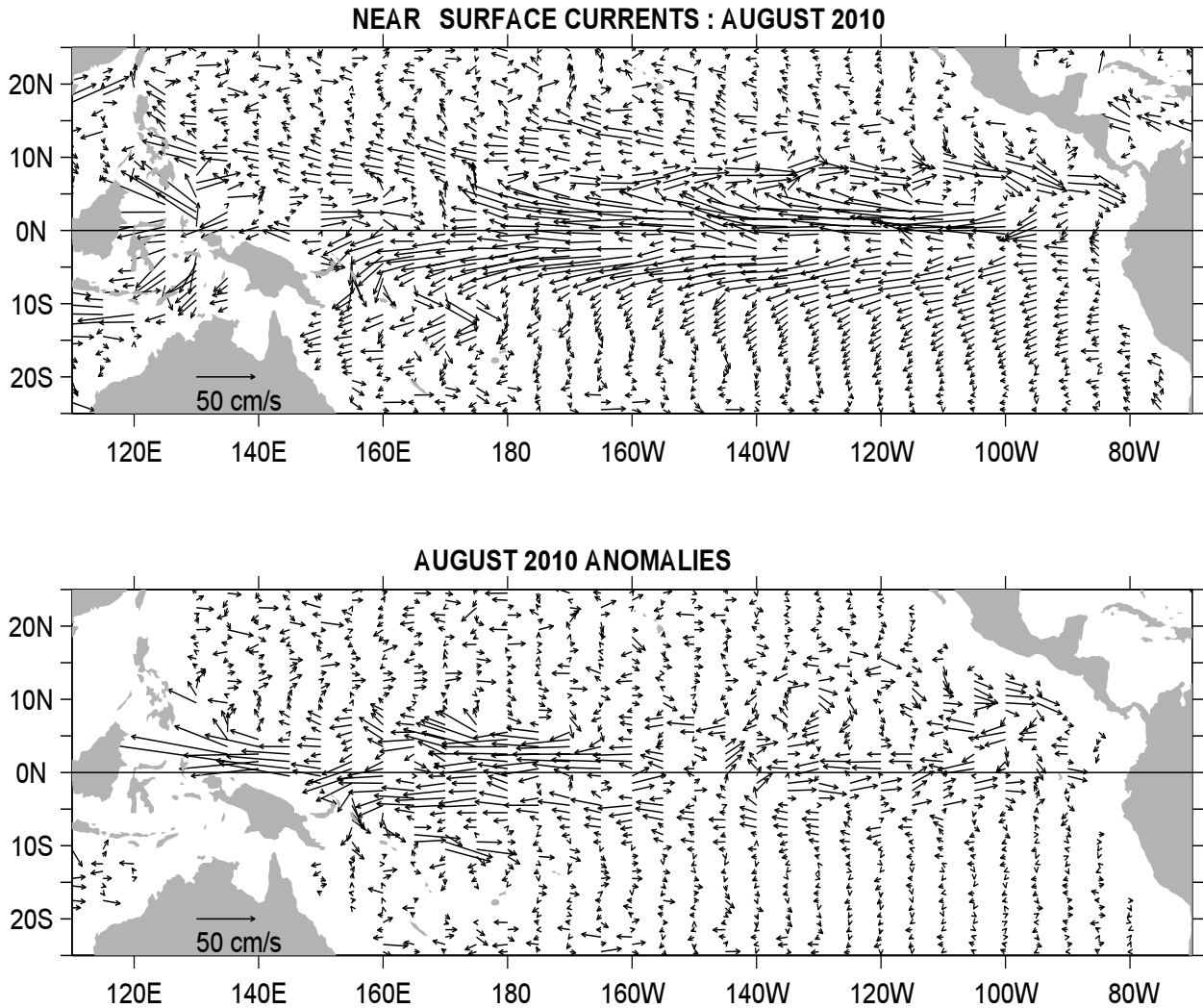


FIGURE A1.7. Ocean Surface Current Analysis-Real-time (OSCAR) for AUG 2010 (Bonjean and Lagerloef 2002, *J. Phys. Oceanogr.*, Vol. 32, No. 10, 2938-2954; Lagerloef et al. 1999, *JGR-Oceans*, 104, 23313-23326). (top) Total velocity. Surface currents are calculated from satellite data including Jason sea level anomalies and NCEP winds. (bottom) Velocity anomalies. The subtracted climatology was based on SSM/I and QuickScat winds and Topex/Poseidon and Jason from 1993-2003. See also <http://www.oscar.noaa.gov>.

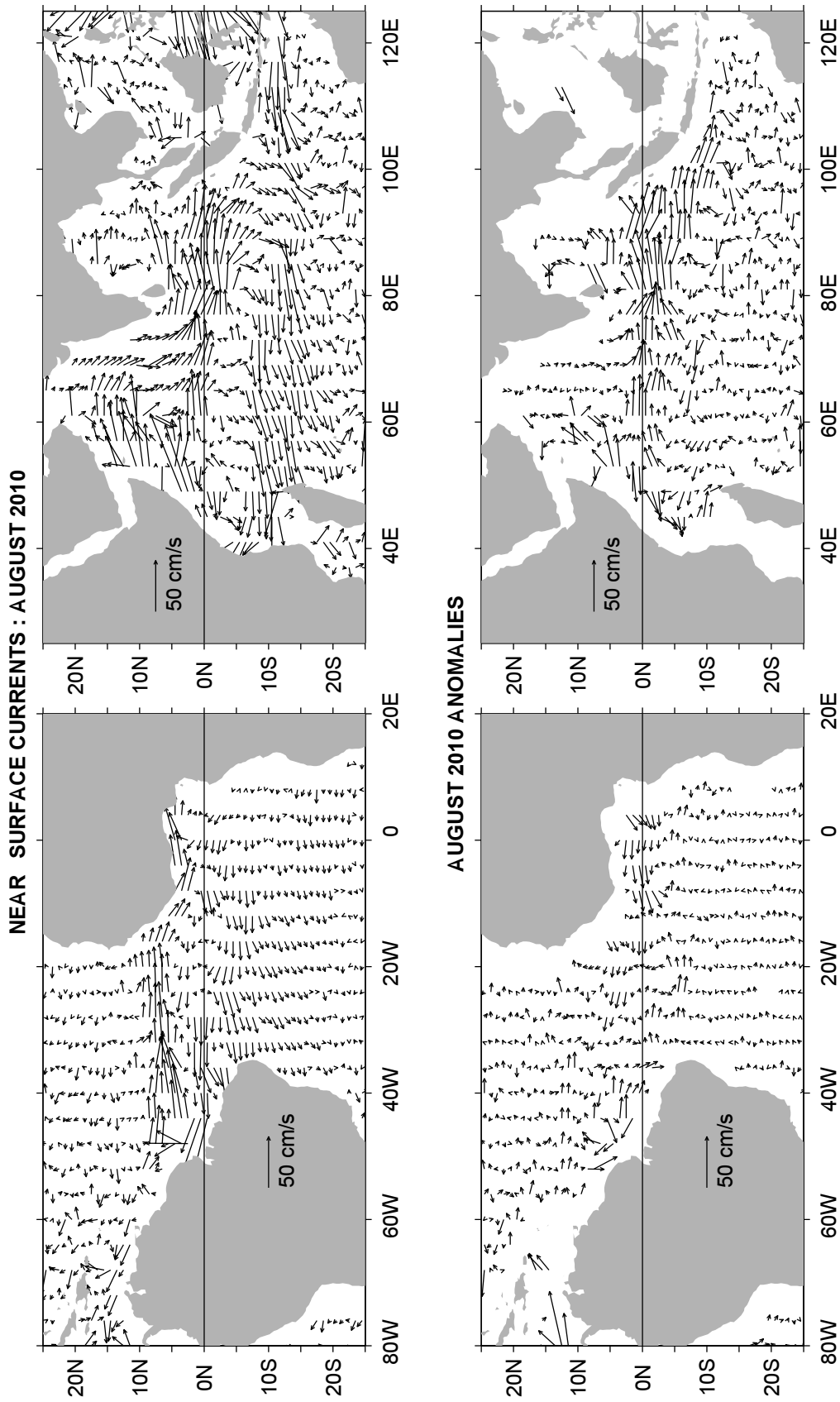


FIGURE A1.8. Ocean Surface Current Analysis-Real-time (OSCAR) for AUG 2010 (Bonjean and Lagerloef 2002, J. Phys. Oceanogr., Vol. 32, No. 10, 2938-2954; Lagerloef et al. 1999, JGR-Oceans, 104, 23313-23326). (top) Total velocity. Surface currents are calculated from satellite data including Jason sea level anomalies and NCEP winds. (bottom) Velocity anomalies. The subtracted climatology was based on SSM/I and QuickScat winds and Topex/Poseidon and Jason from 1993-2003. See also <http://www.oscar.noaa.gov>.

Forecast Forum

The canonical correlation analysis (CCA) forecast of SST in the central Pacific (Barnett et al. 1988, *Science*, **241**, 192196; Barnston and Ropelewski 1992, *J. Climate*, **5**, 13161345), is shown in **Figs. F1 and F2**. This forecast is produced routinely by the Prediction Branch of the Climate Prediction Center. The predictions from the National Centers for Environmental Prediction (NCEP) Coupled Forecast System Model (CFS03) are presented in **Figs. F3 and F4a, F4b**. Predictions from the Markov model (Xue, et al. 2000: *J. Climate*, **13**, 849871) are shown in **Figs. F5 and F6**. Predictions from the latest version of the LDEO model (Chen et al. 2000: *Geophys. Res. Lett.*, **27**, 25852587) are shown in **Figs. F7 and F8**. Predictions using linear inverse modeling (Penland and Magorian 1993: *J. Climate*, **6**, 10671076) are shown in **Figs. F9 and F10**. Predictions from the Scripps / Max Planck Institute (MPI) hybrid coupled model (Barnett et al. 1993: *J. Climate*, **6**, 15451566) are shown in **Fig. F11**. Predictions from the ENSOCLIPER statistical model (Knaff and Landsea 1997, *Wea. Forecasting*, **12**, 633652) are shown in **Fig. F12**. Niño 3.4 predictions are summarized in **Fig. F13**, provided by the Forecasting and Prediction Research Group of the IRI.

The CPC and the contributors to the **Forecast Forum** caution potential users of this predictive information that they can expect only modest skill.

ENSO Alert System Status

La Niña Advisory

Outlook

La Niña is expected to last at least through the Northern Hemisphere winter 2010-11.

Discussion

La Niña strengthened during August 2010, as negative sea surface temperature (SST) anomalies reached at least -1°C across most of the equatorial Pacific Ocean by the end of the month (**Fig. T18**). All of the Niño indices were between -1°C and -1.5°C for the month of August (**Table T2**). Consistent with this evolution, the subsurface heat content (average temperatures in the upper 300m of the ocean) decreased further, reflecting the additional cooling of sub-surface waters east of the Date Line (**Fig. T17**). Also convection was enhanced over Indonesia, while remaining suppressed over the western and central equatorial Pacific (**Fig. T25**). This pattern was associated with a continuation of enhanced low-level easterly trade winds and anomalous upper-level westerly winds over the western and central equatorial Pacific (**Figs. T20, T21**). Collectively, these oceanic and atmospheric anomalies reflect the strengthening of La Niña.

Nearly all models predict La Niña to continue at least through early 2011 (**Figs. F1-F13**). However, the models continue to disagree on the eventual strength of La Niña. Based on current observations and model guidance, we expect the SST anomalies in the Niño-3.4 region to either persist near the present strength, or to strengthen into the winter as is consistent with the historical evolution of La Niña. Thus, it is likely that the peak strength of this event will be at least moderate (3-month average between -1°C to -1.4°C in Niño-3.4) to strong (3-month average of -1.5°C or less in Niño-3.4).

Weekly updates of oceanic and atmospheric conditions are available on the Climate Prediction Center homepage ([El Niño/La Niña Current Conditions and Expert Discussions](#)).

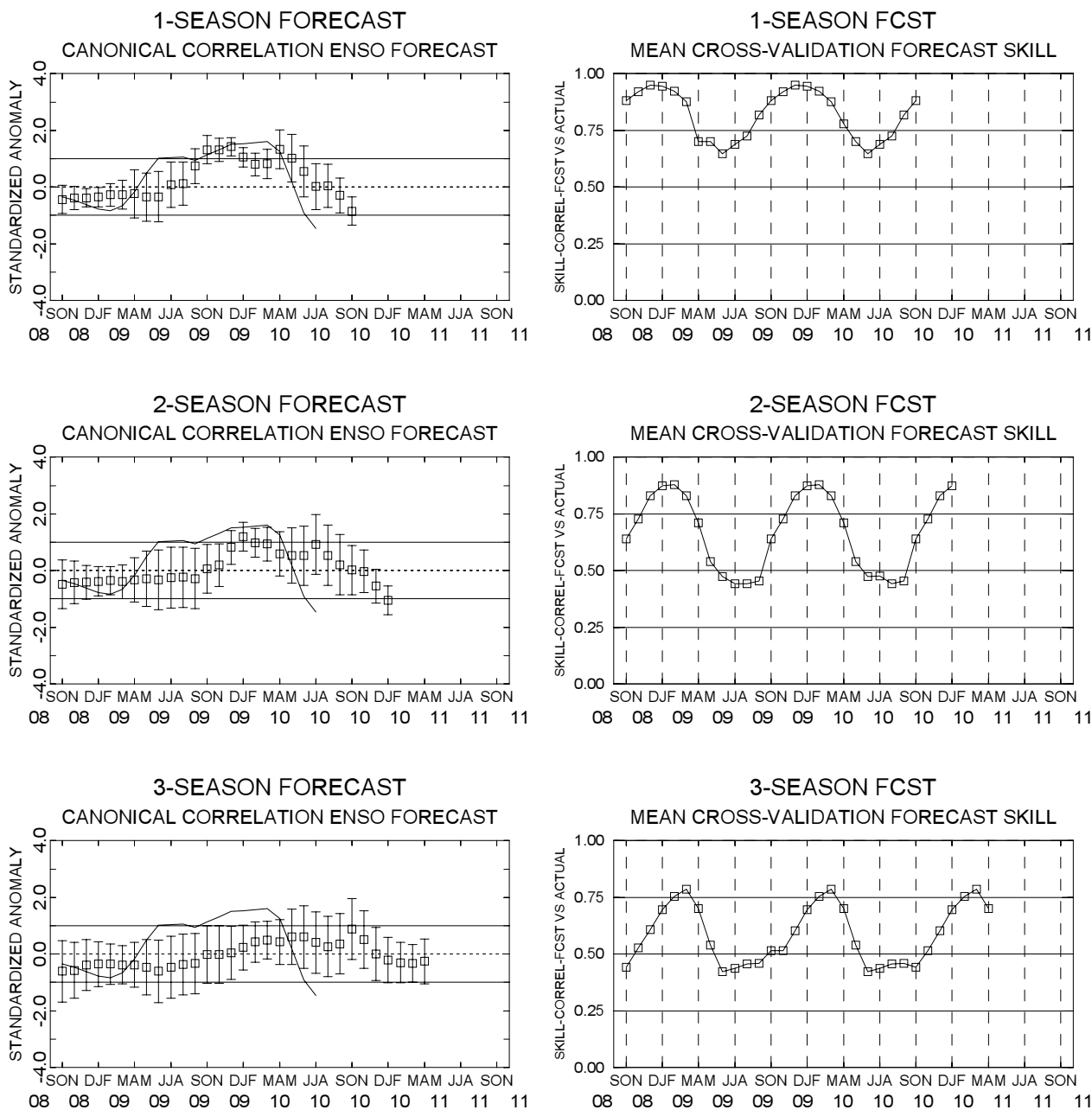


FIGURE F1. Canonical correlation analysis (CCA) sea surface temperature (SST) anomaly prediction for the central Pacific (5°N to 5°S, 120°W to 170°W (Barnston and Ropelewski, 1992, *J. Climate*, **5**, 1316-1345). The three plots on the left hand side are, from top to bottom, the 1-season, 2-season, and 3-season lead forecasts. The solid line in each forecast represents the observed SST standardized anomaly through the latest month. The small squares at the mid-points of the forecast bars represent the real-time CCA predictions based on the anomalies of quasi-global sea level pressure and on the anomalies of tropical Pacific SST, depth of the 20°C isotherm and sea level height over the prior four seasons. The vertical lines represent the one standard deviation error bars for the predictions based on past performance. The three plots on the right side are skills, corresponding to the predicted and observed SST. The skills are derived from cross-correlation tests from 1956 to present. These skills show a clear annual cycle and are inversely proportional to the length of the error bars depicted in the forecast time series.

0-4 SEASON LEAD FORECAST CANONICAL CORRELATION ENSO FORECAST

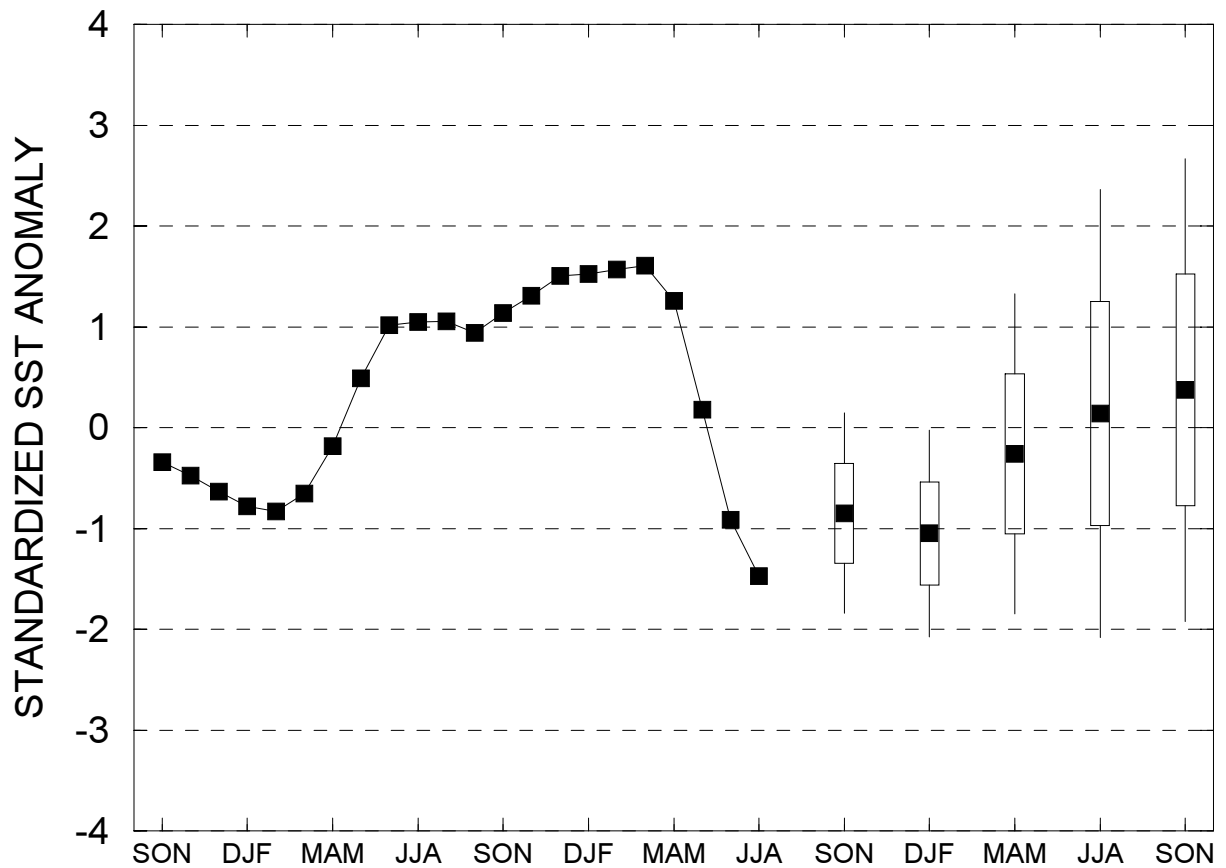


FIGURE F2. Canonical Correlation Analysis (CCA) forecasts of sea-surface temperature anomalies for the Niño 3.4 region (5N-5S, 120W-170W) for the upcoming five consecutive 3-month periods. Forecasts are expressed as standardized SST anomalies. The CCA predictions are based on anomaly patterns of SST, depth of the 20C isotherm, sea level height, and sea level pressure. Small squares at the midpoints of the vertical forecast bars represent the CCA predictions, and the bars show the one (thick) and two (thin) standard deviation errors. The solid continuous line represents the observed standardized three-month mean SST anomaly in the Niño 3.4 region up to the most recently available data.

Last update: Fri Sep 3 2010
Initial conditions: 23Aug2010–01Sep2010

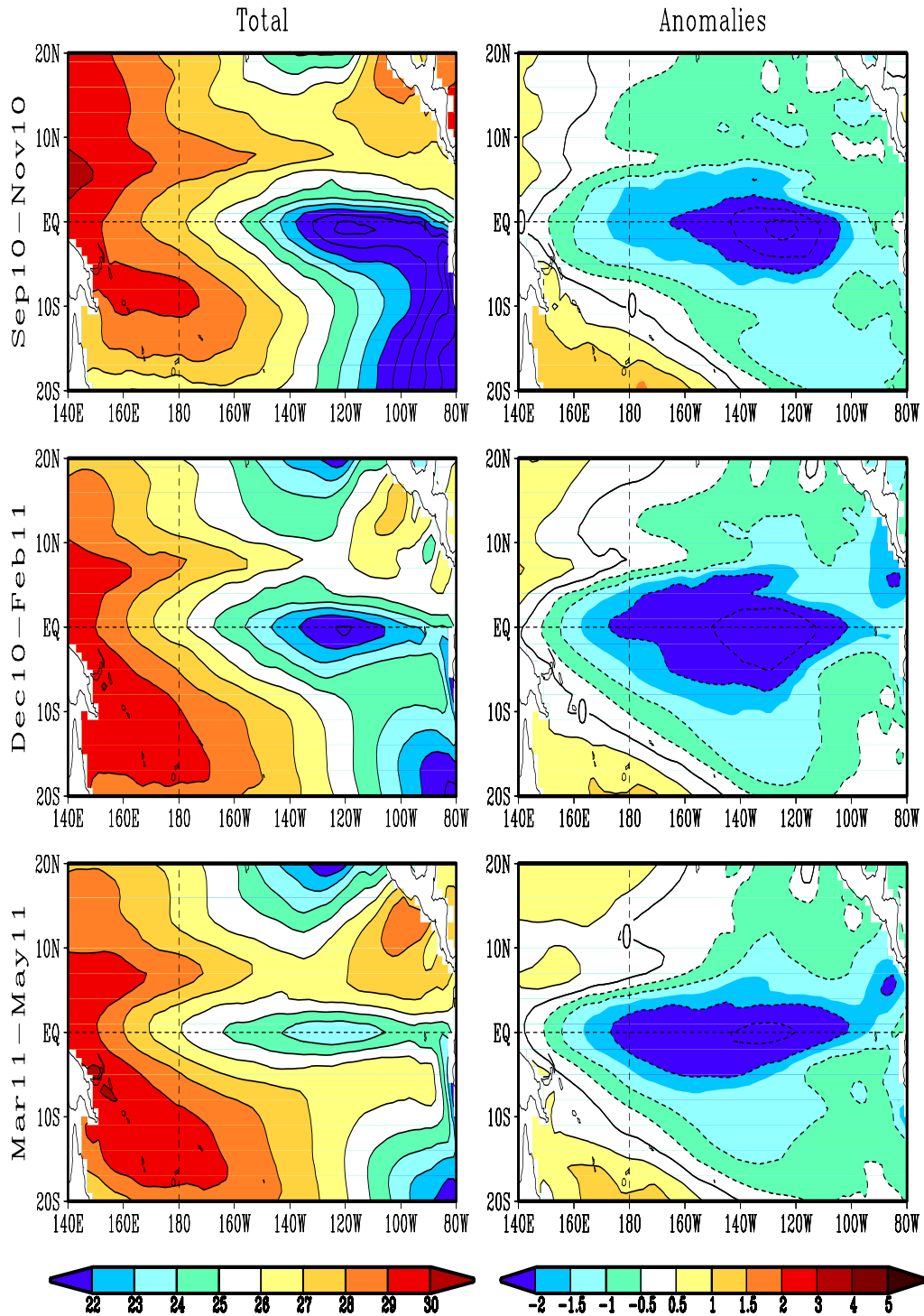


FIGURE F3. Predicted 3-month average sea surface temperature (left) and anomalies (right) from the NCEP Coupled Forecast System Model (CFS03). The forecasts consist of 40 forecast members. Contour interval is 1°C, with additional contours for 0.5°C and -0.5°C. Negative anomalies are indicated by dashed contours.

Last update: Fri Sep 3 2010
Initial conditions: 23Aug2010-01Sep2010

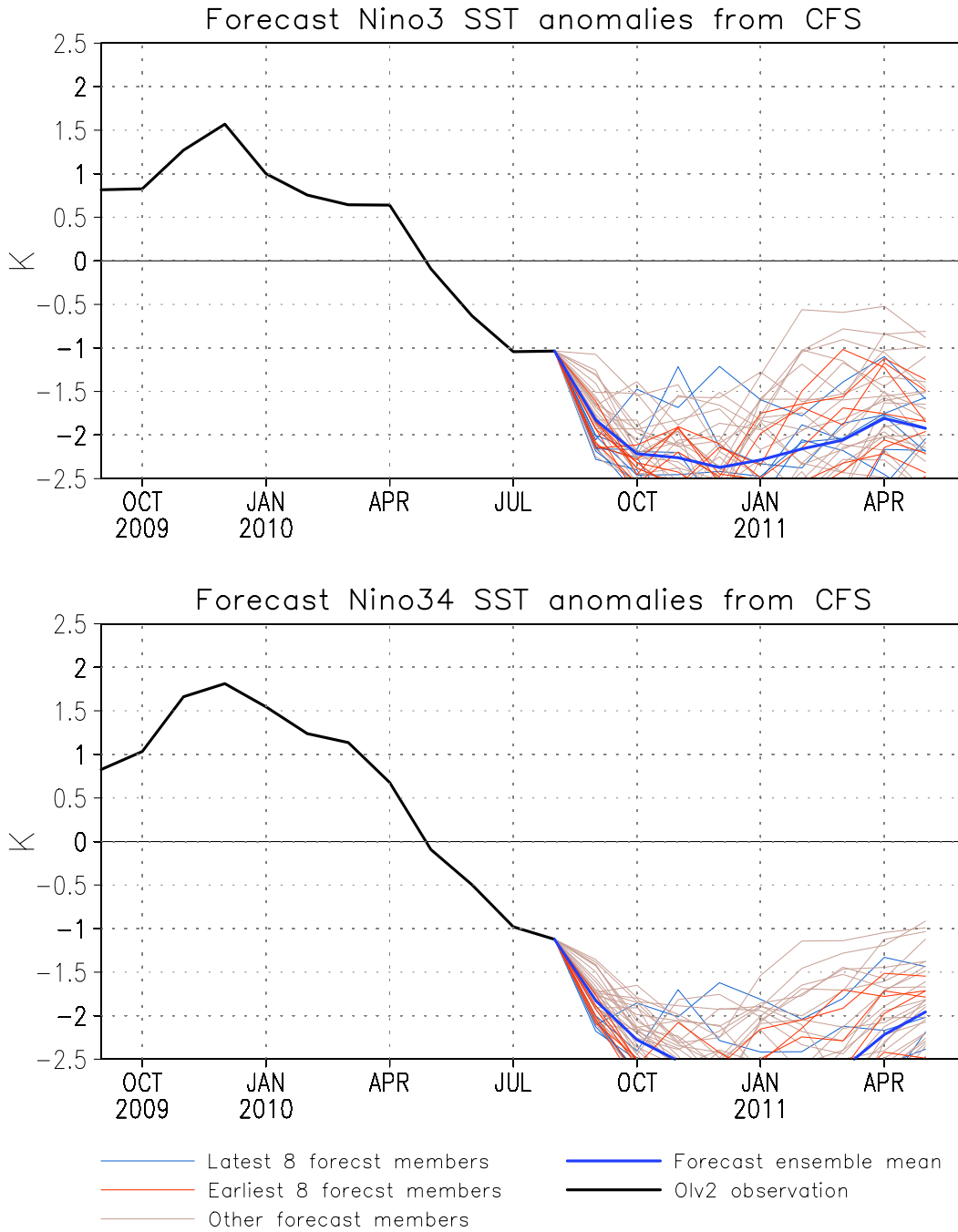


FIGURE F4. Predicted and observed sea surface temperature (SST) anomalies for the Nino 3 (top) and Nino 3.4 (bottom) regions from the NCEP Coupled Forecast System Model (CFS03). The forecasts consist of 40 forecast members. The ensemble mean of all 40 forecast members is shown by the blue line, individual members are shown by thin lines, and the observation is indicated by the black line. The Nino-3 region spans the eastern equatorial Pacific between 5N-5S, 150W-90W. The Nino 3.4 region spans the east-central equatorial Pacific between 5N-5S, 170W-120W.

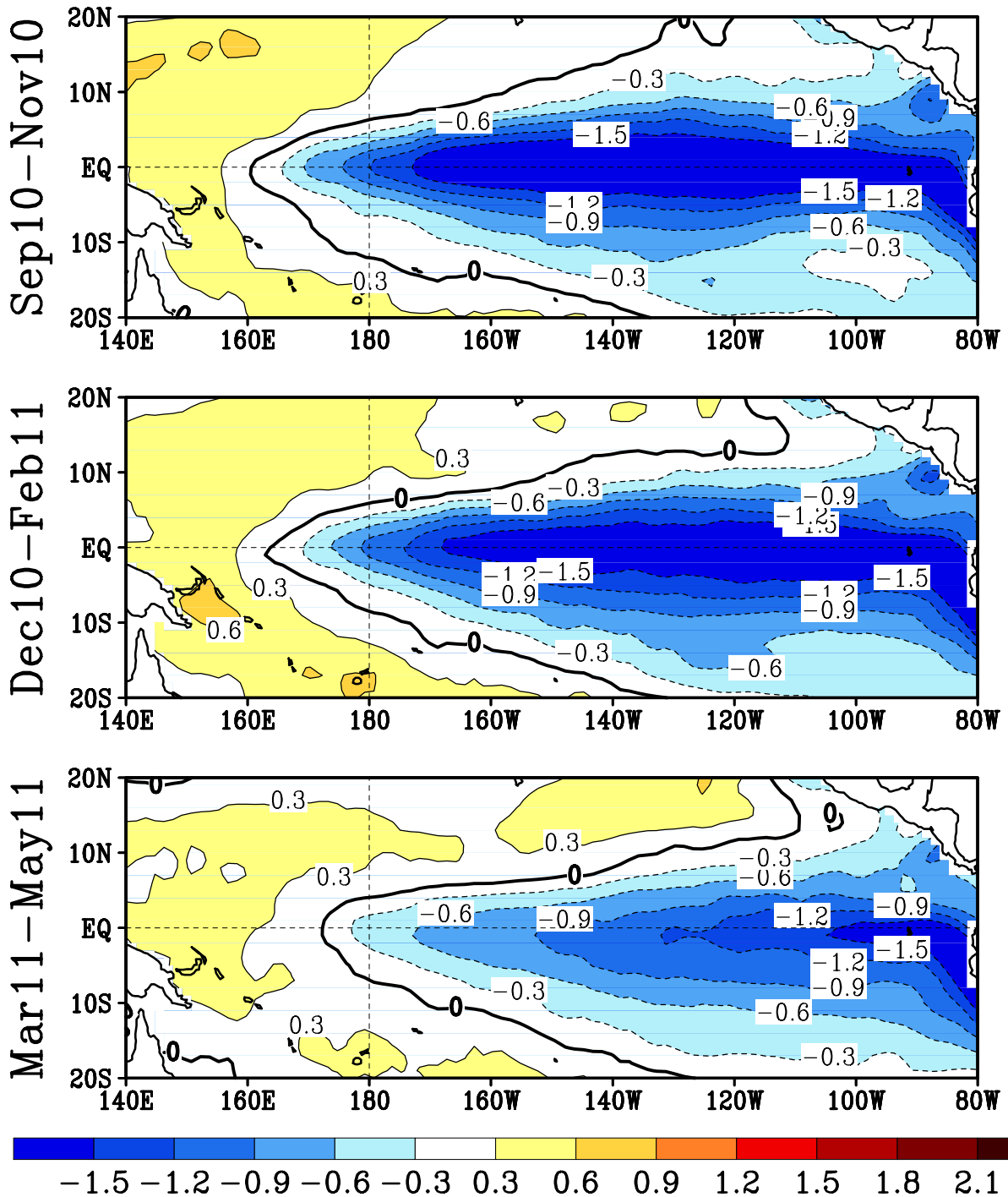


FIGURE F5. Predicted 3-month average sea surface temperature anomalies from the NCEP/CPC Markov model (Xue et al. 2000, *J. Climate*, **13**, 849-871). The forecast is initiated in AUG 2010 . Contour interval is 0.3C and negative anomalies are indicated by dashed contours. Anomalies are calculated relative to the 1971-2000 climatology.

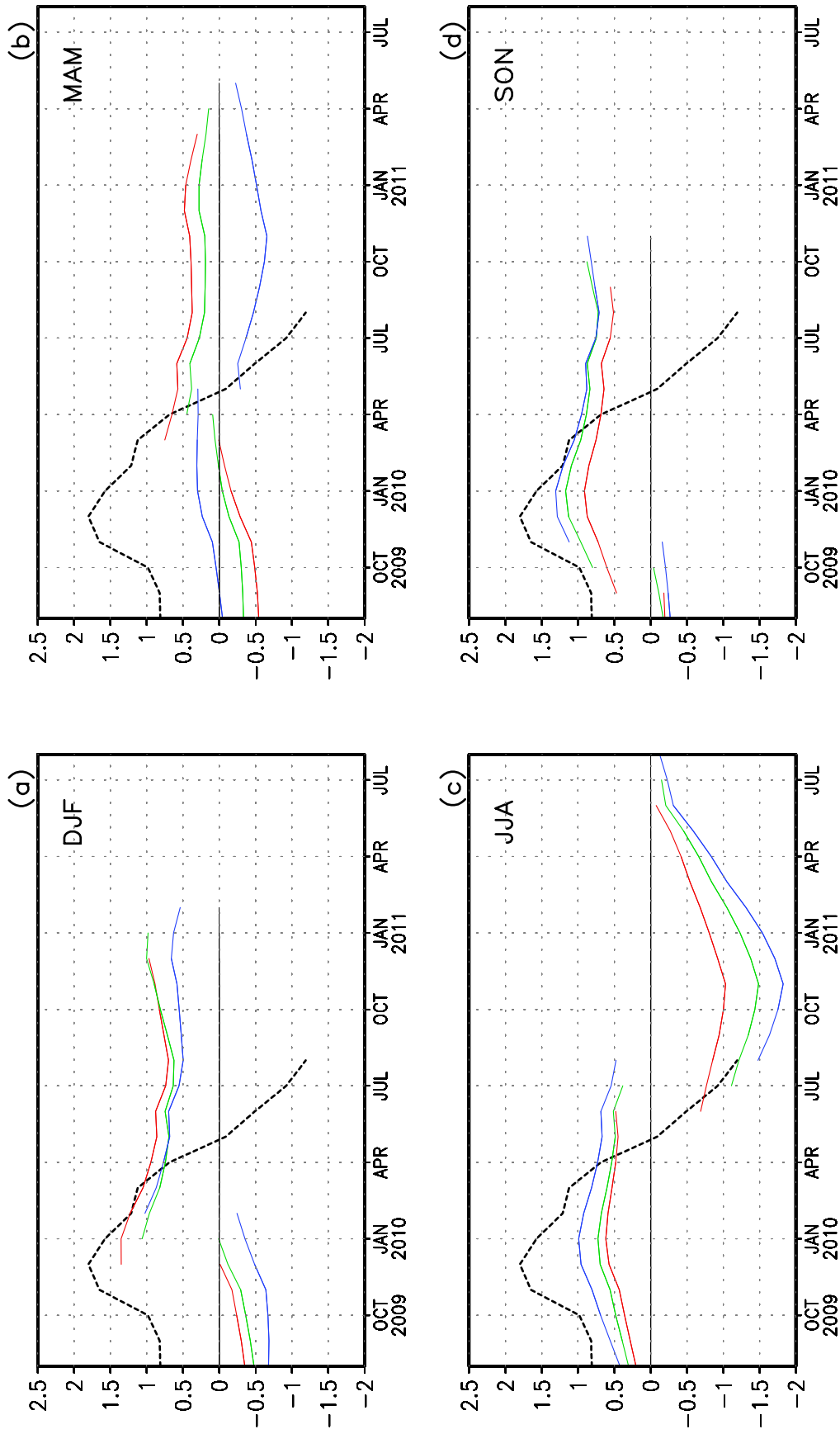


FIGURE F6. Time evolution of observed and predicted SST anomalies in the Niño 3.4 region (up to 12 lead months) by the NCEP/CPC Markov model (Xue et al. 2000, *J. Climate*, **13**, 849-871). Anomalies are calculated relative to the 1971-2000 climatology. Shown in each panel are the forecasts grouped by three consecutive starting months: (a) is for December, January, and February, (b) is for March, April, and May, (c) is for June, July, and August, and (d) is for September, October, and November. The observed Niño 3.4 SST anomalies are indicated by the black dashed lines. The Niño 3.4 region spans the east-central equatorial Pacific between 5N-5S, 170W-120W.

LDEO FORECASTS OF SST AND WIND STRESS ANOMALIES

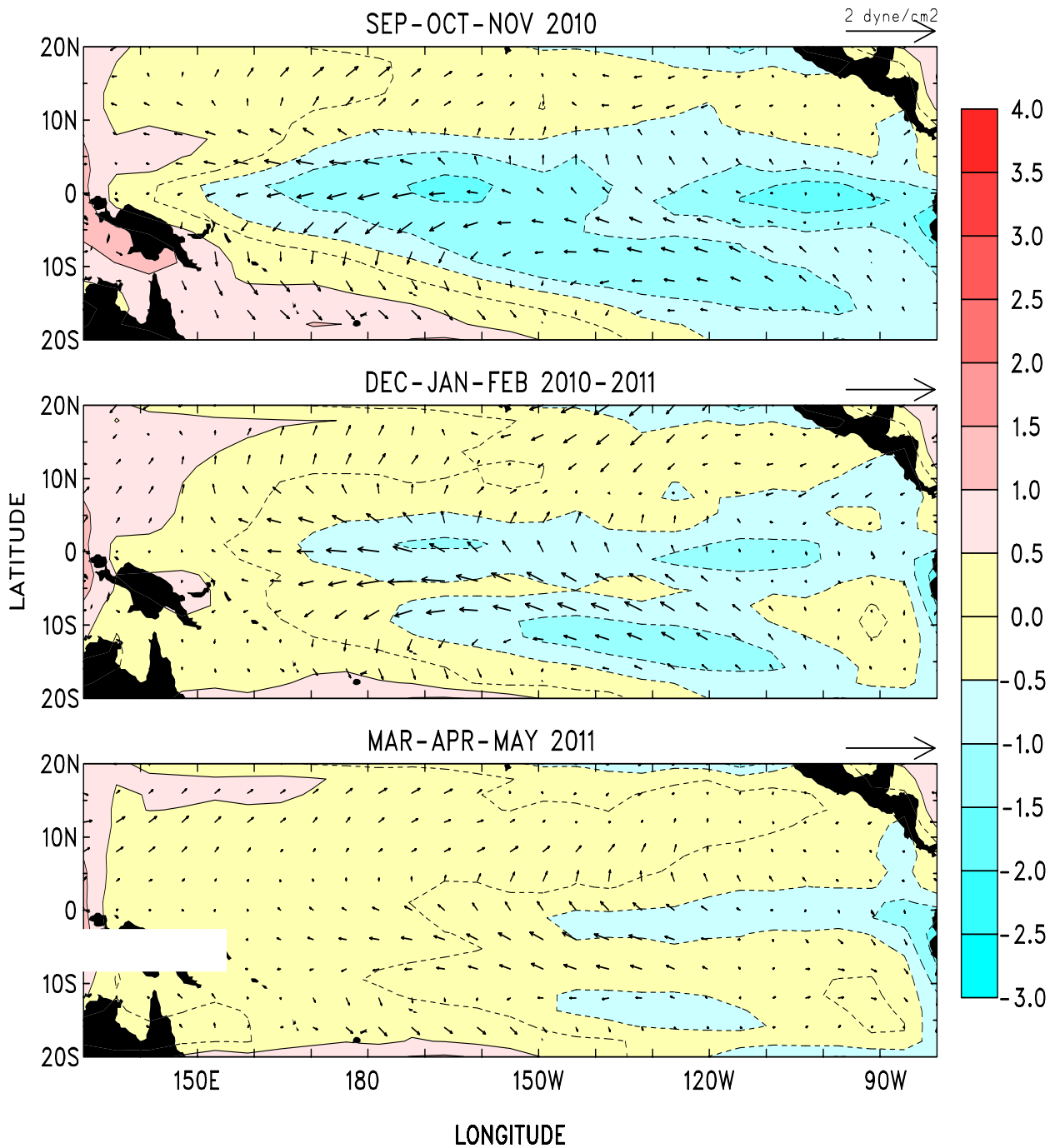


FIGURE F7. Forecasts of the tropical Pacific Predicted SST (shading) and vector wind anomalies for the next 3 seasons based on the LDEO model. Each forecast represents an ensemble average of 3 sets of predictions initialized during the last three consecutive months (see Figure F8).

LDEO FORECASTS OF NINO3

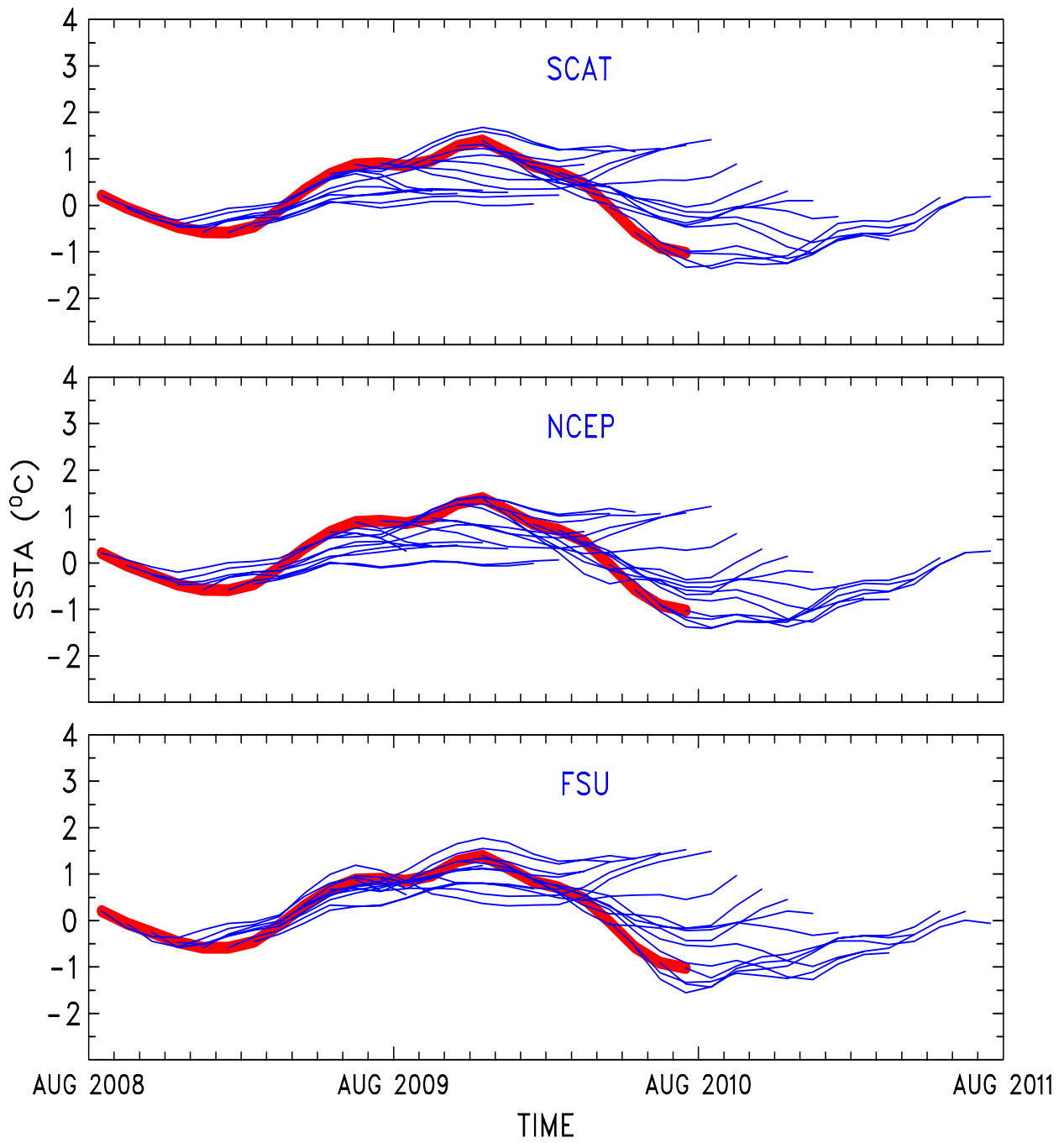


FIGURE F8. LDEO forecasts of SST anomalies for the Niño 3 region using wind stresses obtained from (top) QuikSCAT, (middle) NCEP, and (bottom) Florida State Univ. (FSU), along with SSTs (obtained from NCEP), and sea surface height data (obtained from TOPEX/POSEIDON) data. Each thin blue line represents a 12-month forecast, initialized one month apart for the past 24 months. Observed SST anomalies are indicated by the thick red line. The Niño-3 region spans the eastern equatorial Pacific between 5N-5S, 150W-90W.

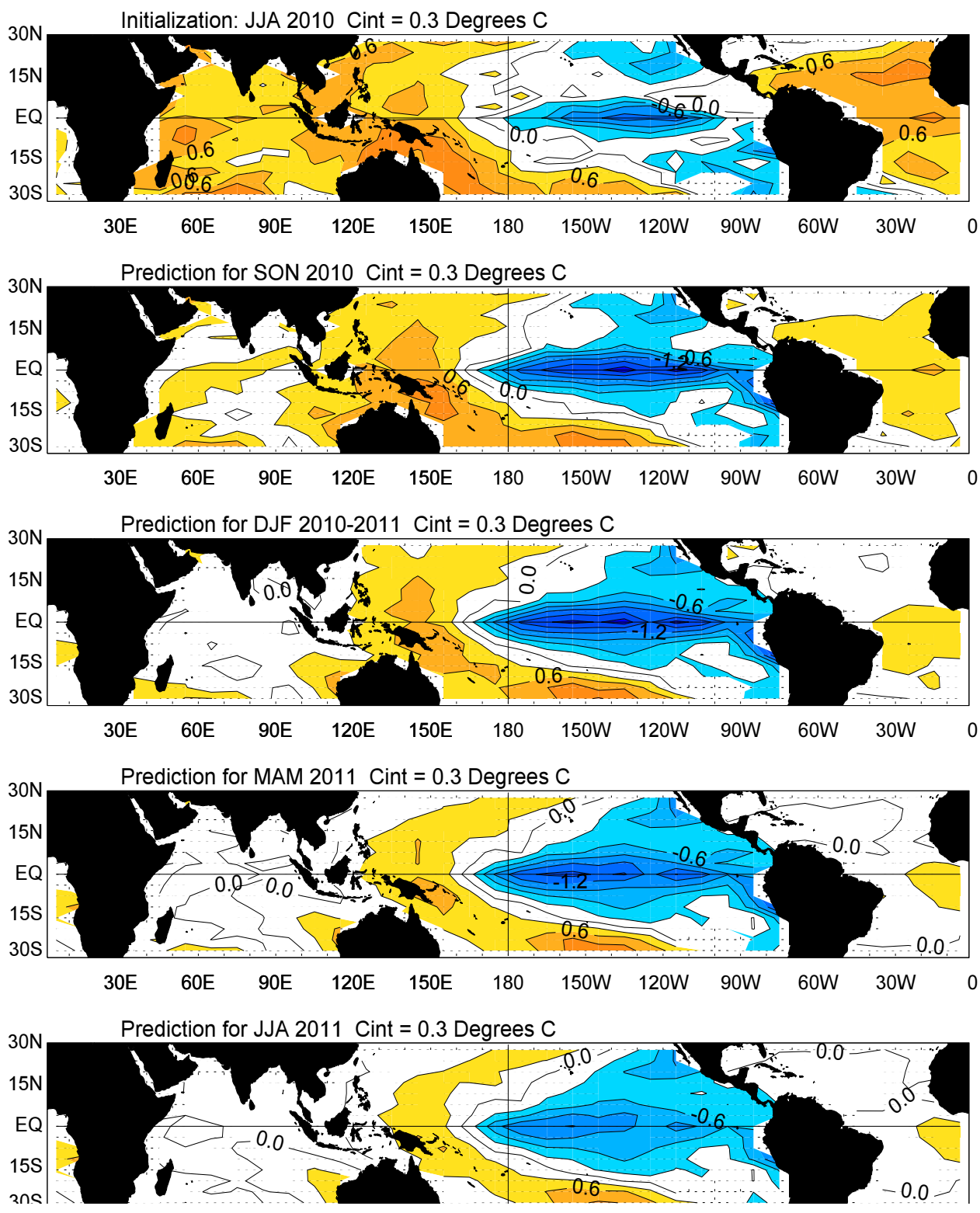


FIGURE F9. Forecast of tropical SST anomalies from the Linear Inverse Modeling technique of Penland and Magorian (1993: *J. Climate*, 6, 1067-1076). The contour interval is 0.3C. Anomalies are calculated relative to the 1951-2000 climatology and are projected onto 20 leading EOFs.

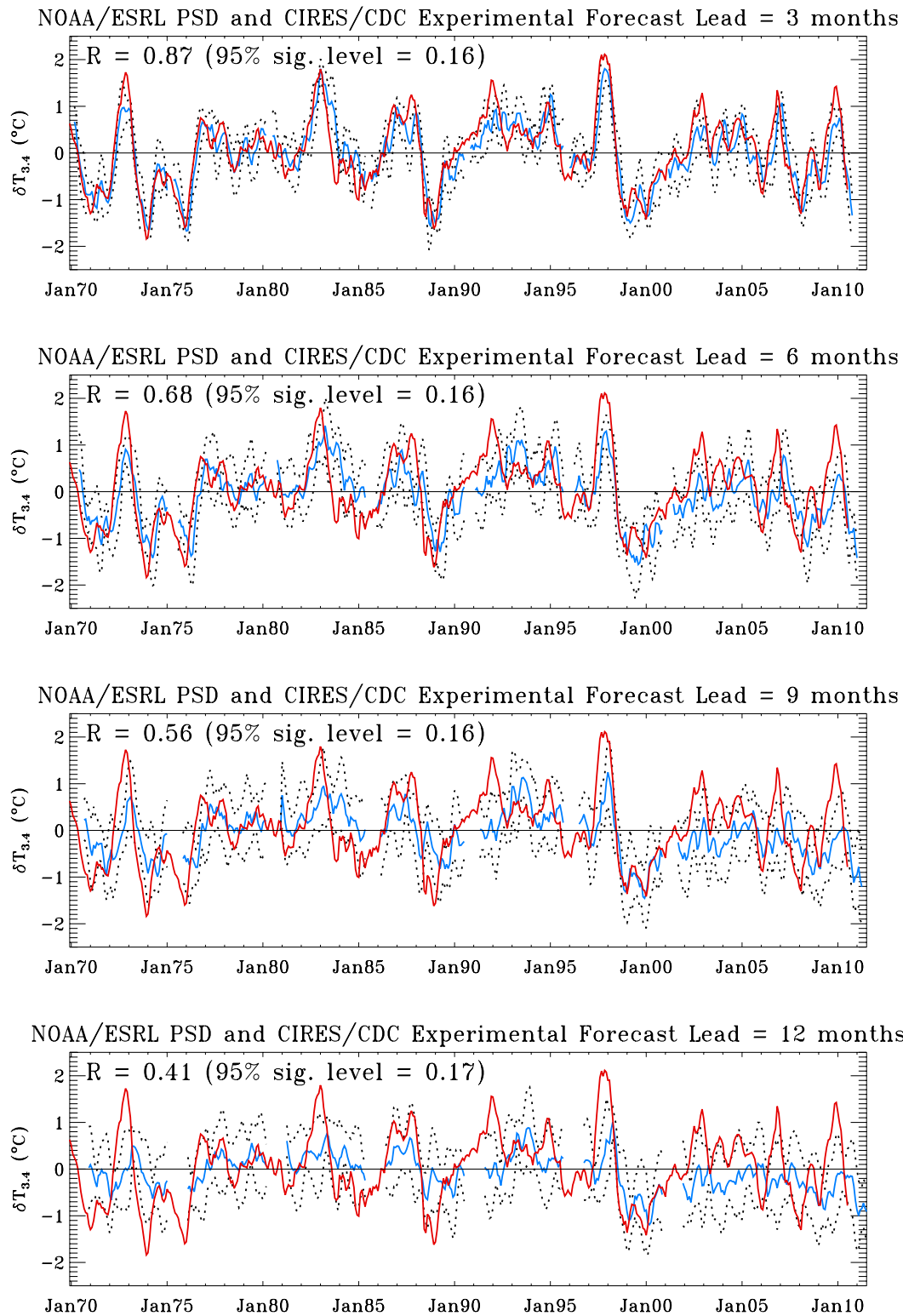


FIGURE F10. Predictions of SST anomalies in the Niño3.4 region (blue line) for leads of three months (top) to 12 months (bottom), from the Linear Inverse Modeling technique of Penland and Magorian (1993: *J. Climate*, **6**, 1067-1076). Observed SST anomalies are indicated by the red line. Anomalies are calculated relative to the 1951-2000 climatology and are projected onto 20 leading EOFs. The Niño 3.4 region spans the east-central equatorial Pacific between 5N-5S, 170W-120W.

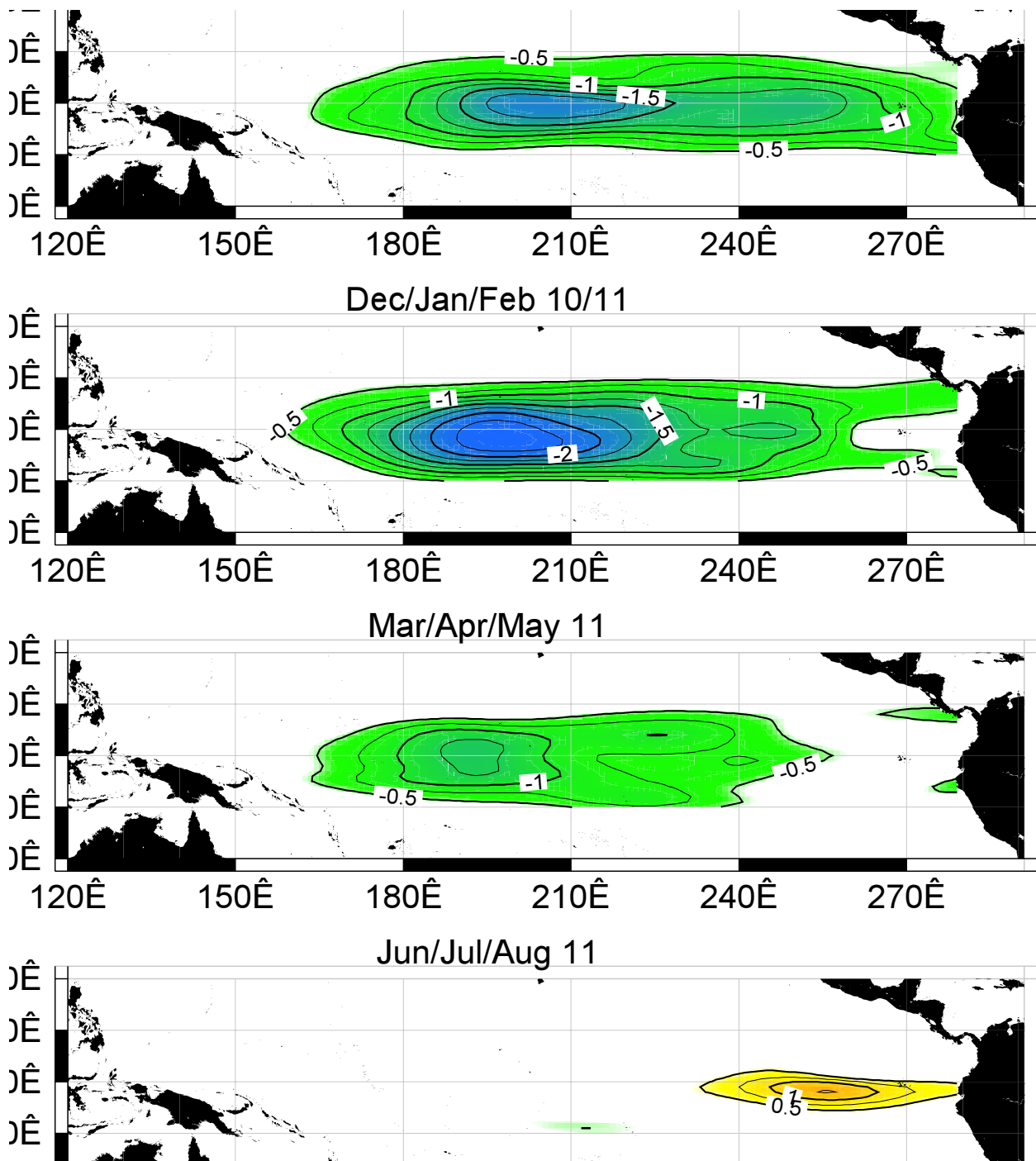


FIGURE F11. SST anomaly forecast for the equatorial Pacific from the Hybrid Coupled Model (HCM) developed by the Scripps Institution of Oceanography and the Max-Planck Institut fuer Meteorologie.

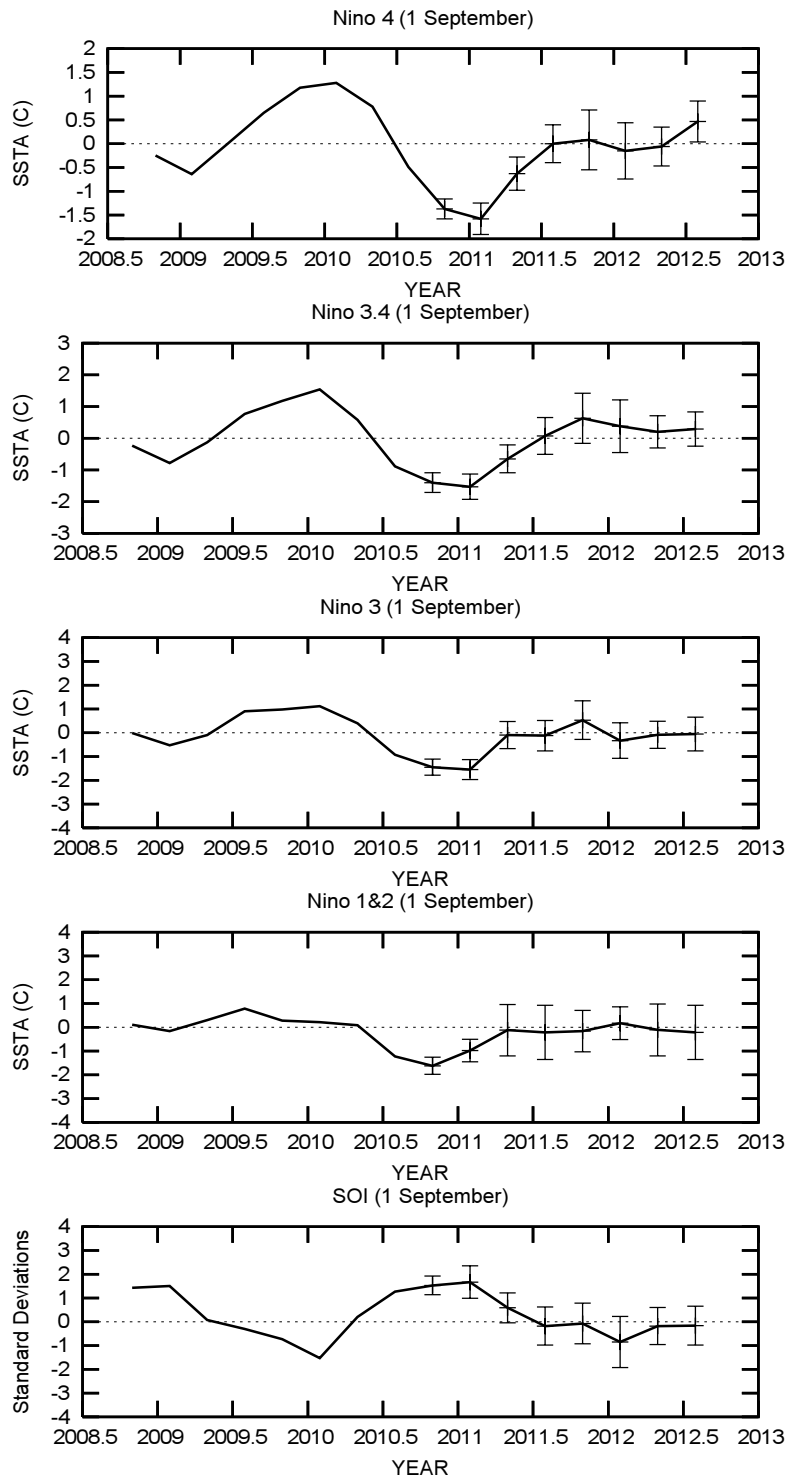


FIGURE F12. ENSO-CLIPER statistical model forecasts of three-month average sea surface temperature anomalies (green lines, deg. C) in (top panel) the Nino 4 region (5N-5S, 160E-150W), (second panel) the Nino 3.4 region (5N-5S, 170W-120W), (third panel) the Nino 3 region (5N-5S, 150W-90W), and (fourth panel) the Nino 1+2 region (0-10S, 90W-80W) (Knaff and Landsea 1997, *Wea. Forecasting*, **12**, 633-652). Bottom panel shows predictions of the three-month standardized Southern Oscillation Index (SOI, green line). Horizontal bars on green line indicate the adjusted root mean square error (RMSE). The Observed three-month average values are indicated by the thick blue line. SST anomalies are departures from the 1971-2000 base period means, and the SOI is calculated from the 1951-1980 base period means.

Model Predictions of ENSO from Aug 2010

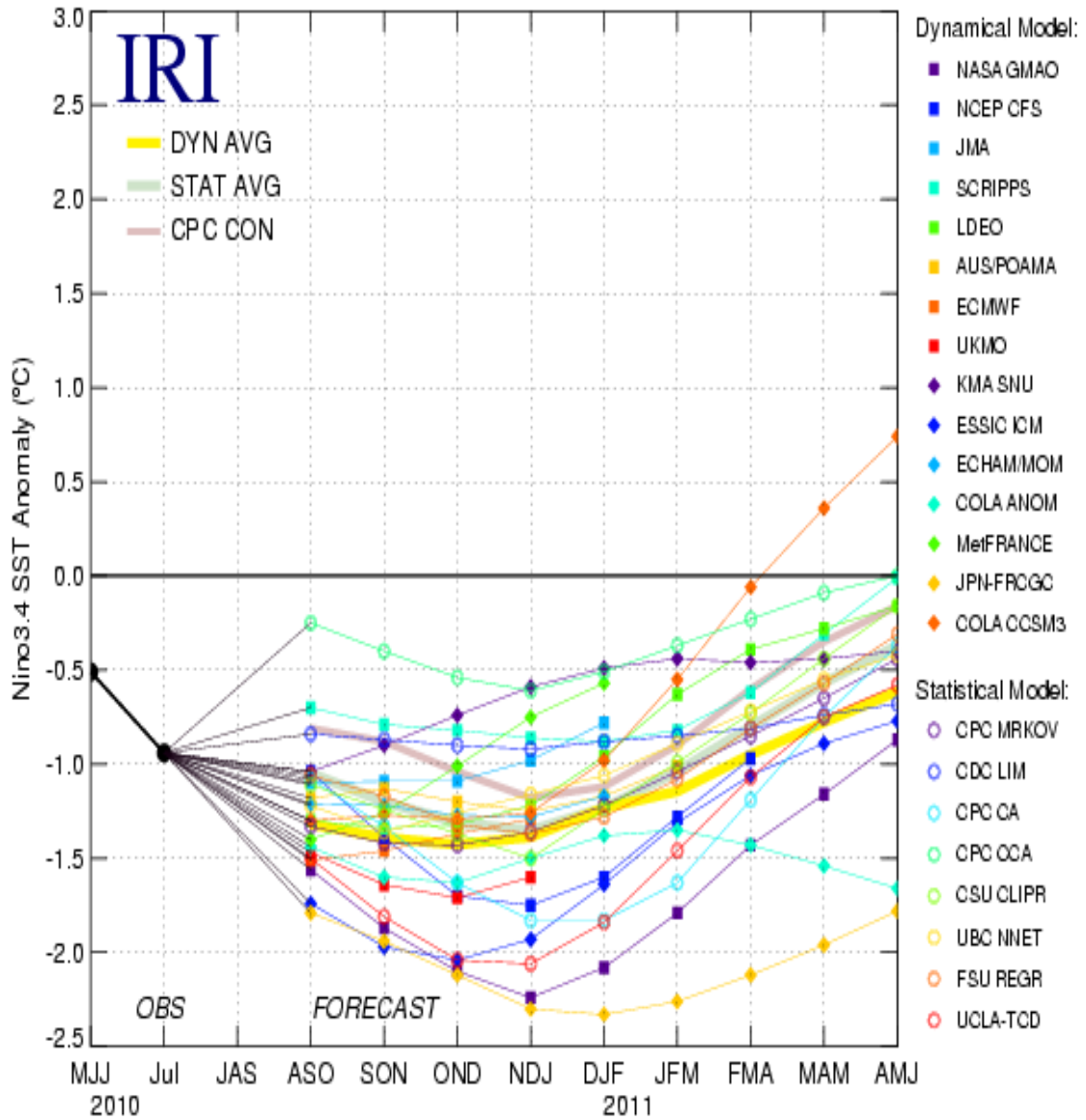


FIGURE F13. Time series of predicted sea surface temperature anomalies for the Nino 3.4 region (deg. C) from various dynamical and statistical models for nine overlapping 3-month periods. The Nino 3.4 region spans the east-central equatorial Pacific between 5N-5S, 170W-120W. Figure provided by the International Research Institute (IRI).

Extratropical Highlights – August 2010

1. Northern Hemisphere

The 500-hPa circulation during August featured above-average heights over Greenland, western Russia, eastern Asia, and the Gulf of Alaska, and below average heights over western Europe and central Siberia (**Fig. E9**). Over the subtropical Atlantic basin, the 200-hPa streamfunction pattern continued to show a pronounced inter-hemispheric symmetry during August, with anticyclonic anomalies extending from the America's to Africa in both hemispheres (**Fig. T22**). Conversely, an anomalous trough was evident across most of the tropical western North Pacific, with a similar anomaly pattern evident in the Southern Hemisphere. These signals are consistent with the combined influences of La Niña and an enhanced west African monsoon system (**Figs. T23, T24**).

The main surface temperature signals during August included warmer than average conditions across the eastern half of the United States, Mexico, western Russia, and most of China (**Fig. E1**). Monthly precipitation totals (**Fig. E3**) were above-average in northern Europe, and in the Inter-Mountain West and Gulf Coast regions of the U.S. (**Figs. E5, E6**). Monthly precipitation was below average in the mid-Atlantic, Northeast, and Pacific Northwest regions of the U.S., southwestern Europe and southwestern Russia.

a. North America

The mean 500-hPa circulation during August featured a broad and persistent ridge across the central and eastern United States (**Figs. E9**). This pattern was associated with a continuation from July of above average temperatures across the eastern half of the country, with August departures in many locations exceeding the 90th percentile of occurrences (**Fig. E1**). The mid-Atlantic and northeastern states also experienced a continuation of well below average precipitation during August (**Fig. E5**). For both regions precipitation has been below average since April. During August, ongoing precipitation deficits in the mid-Atlantic region led to the development of moderate- to-severe drought. Elsewhere, precipitation was above average in the Midwest and Gulf Coast regions of the country, and in the Inter-Mountain West where totals have been above average for nine straight months.

b. North Atlantic

Over the subtropical Atlantic, anticyclonic streamfunction anomalies at 200-hPa extended from the America's to Africa in both hemispheres (**Fig. T22**). This pronounced inter-hemispheric symmetry of the anomaly pattern was associated with an expanded area of upper-level easterly wind anomalies that extended across tropical northern Africa and the tropical North Atlantic (**Fig. T21**). It was also associated with an extensive area of low-level westerly wind anomalies across the tropical Atlantic (**Fig. T20**). These conditions lead to reduced vertical wind shear across the tropical Atlantic, and are typical of the high activity era for Atlantic hurricanes that began in 1995. This combination of conditions is consistent with an enhanced west African monsoon circulation, which was again present during August (**Figs. T23, T24**) and

has been a prominent feature of the circulation since 1995.

c. Eurasia

The 500-hPa circulation during August featured a strong and persistent ridge centered over western Russia, along with an amplified trough over northern Europe (**Fig. E9**). This pattern affected temperature and precipitation patterns from Europe to Pakistan (**Figs. E1, E3**). The strong ridge led to exceptionally warm and dry conditions in western Russia, with many areas experiencing record heat. The amplified trough contributed to well above average precipitation in northern Europe, with many areas recording totals in the upper 90th percentile of occurrences.

During part of the month the ridge in western Russia was exceptionally amplified and resembled a typical Omega-block. This blocking pattern was associated with a very strong downstream trough that extended southward from central Russia to Pakistan. This amplified trough interacted with a deep monsoonal flow of moisture coming into the Indian sub-continent, which led to extreme precipitation totals and record flooding in Pakistan.

2. Southern Hemisphere

The 500-hPa circulation during August featured a zonally-symmetric pattern of height anomalies, with above average heights in the middle latitudes and generally below average heights over Antarctica (**Fig. E15**). In the subtropics, the upper-level streamfunction pattern reflected an anomalous trough across the western and central tropical South Pacific, and an anomalous ridge extending from the eastern subtropical South Pacific to southern Africa (**Fig. T22**). A similar anomaly pattern was evident in the Northern Hemisphere. These conditions have been present since June, and likely reflect the combined influences of La Niña and an enhanced west African monsoon system. One characteristic feature of La Niña was a marked westward retraction of the South Pacific jet core, as indicated by easterly wind anomalies centered along the jet axis east of the date line near 30°S (**Fig. T21**).

TELECONNECTION INDICES

NORTH ATLANTIC NORTH PACIFIC EURASIA

| MONTH | NAO | EA | WP | EP-NP | PNA | TNH | EATL/ WRUS | SCAND | POLEUR |
|---------------|------|------|------|-------|------|------|---------------|-------|--------|
| AUG 10 | -1.2 | 1.9 | 0.1 | -2.4 | 1.1 | --- | -0.9 | -0.6 | 1.5 |
| JUL 10 | -0.4 | 2.8 | -2.9 | -0.2 | 1.4 | --- | -1.6 | 0.6 | 1.7 |
| JUN 10 | -0.8 | 0.5 | -0.3 | 1.2 | -0.2 | --- | -2.1 | -1.1 | 2.1 |
| MAY 10 | -1.5 | -1.2 | -3.1 | 0.0 | -0.9 | --- | -2.1 | 0.3 | -1.9 |
| APR 10 | -0.7 | 0.5 | 0.8 | -0.9 | 1.5 | --- | -0.5 | -0.5 | -0.5 |
| MAR 10 | -0.9 | 1.4 | 2.1 | -1.5 | 2.0 | --- | 0.8 | -0.5 | -1.4 |
| FEB 10 | -2.0 | 1.3 | 0.7 | -0.1 | 0.6 | -1.2 | -0.7 | 1.1 | -1.9 |
| JAN 10 | -1.1 | 0.9 | 0.8 | -0.7 | 1.3 | -1.2 | -0.6 | 1.2 | -0.1 |
| DEC 09 | -1.9 | 1.1 | -0.9 | --- | 0.3 | -0.6 | -0.8 | 0.5 | -1.6 |
| NOV 09 | 0.0 | 1.9 | 1.4 | -1.5 | 0.2 | --- | -0.2 | 0.7 | -0.7 |
| OCT 09 | -1.0 | 1.4 | -2.4 | 0.7 | 0.4 | --- | -0.1 | -0.9 | -2.6 |
| SEP 09 | 1.5 | 0.9 | -0.7 | -1.7 | 1.3 | --- | -0.5 | -0.8 | 0.9 |
| AUG 09 | -0.2 | 2.6 | 0.3 | -2.3 | 0.6 | --- | -0.5 | -0.5 | 0.2 |

TABLE E1-Standardized amplitudes of selected Northern Hemisphere teleconnection patterns for the most recent thirteen months (computational procedures are described in Fig. E7). Pattern names and abbreviations are North Atlantic Oscillation (NAO); East Atlantic pattern (EA); West Pacific pattern (WP); East Pacific - North Pacific pattern (EP-NP); Pacific/North American pattern (PNA); Tropical/Northern Hemisphere pattern (TNH); East Atlantic/Western Russia pattern (EATL/WRUS)-called Eurasia-2 pattern by Barnston and Livezey, 1987, *Mon. Wea. Rev.*, **115**, 1083-1126); Scandinavia pattern (SCAND)-called Eurasia-1 pattern by Barnston and Livezey (1987); and Polar Eurasia pattern (POLEUR). No value is plotted for calendar months in which the pattern does not appear as a leading mode.

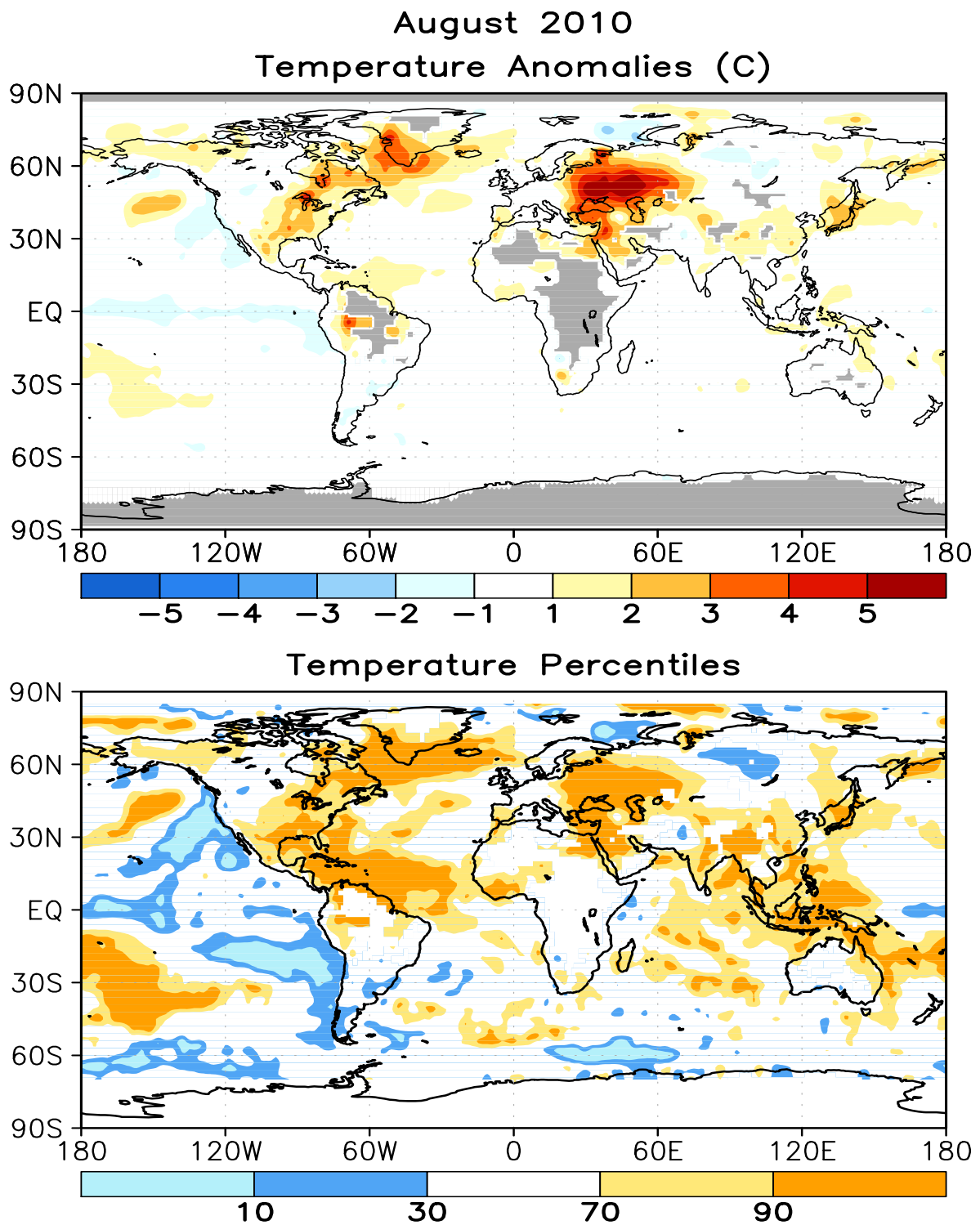


FIGURE E1. Surface temperature anomalies ($^{\circ}\text{C}$, top) and surface temperature expressed as percentiles of the normal (Gaussian) distribution fit to the 1971–2000 base period data (bottom) for AUG 2010. Analysis is based on station data over land and on SST data over the oceans (top). Anomalies for station data are departures from the 1971–2000 base period means, while SST anomalies are departures from the 1971–2000 adjusted OI climatology. (Smith and Reynolds 1998, *J. Climate*, **11**, 3320–3323). Regions with insufficient data for analysis in both figures are indicated by shading in the top figure only.

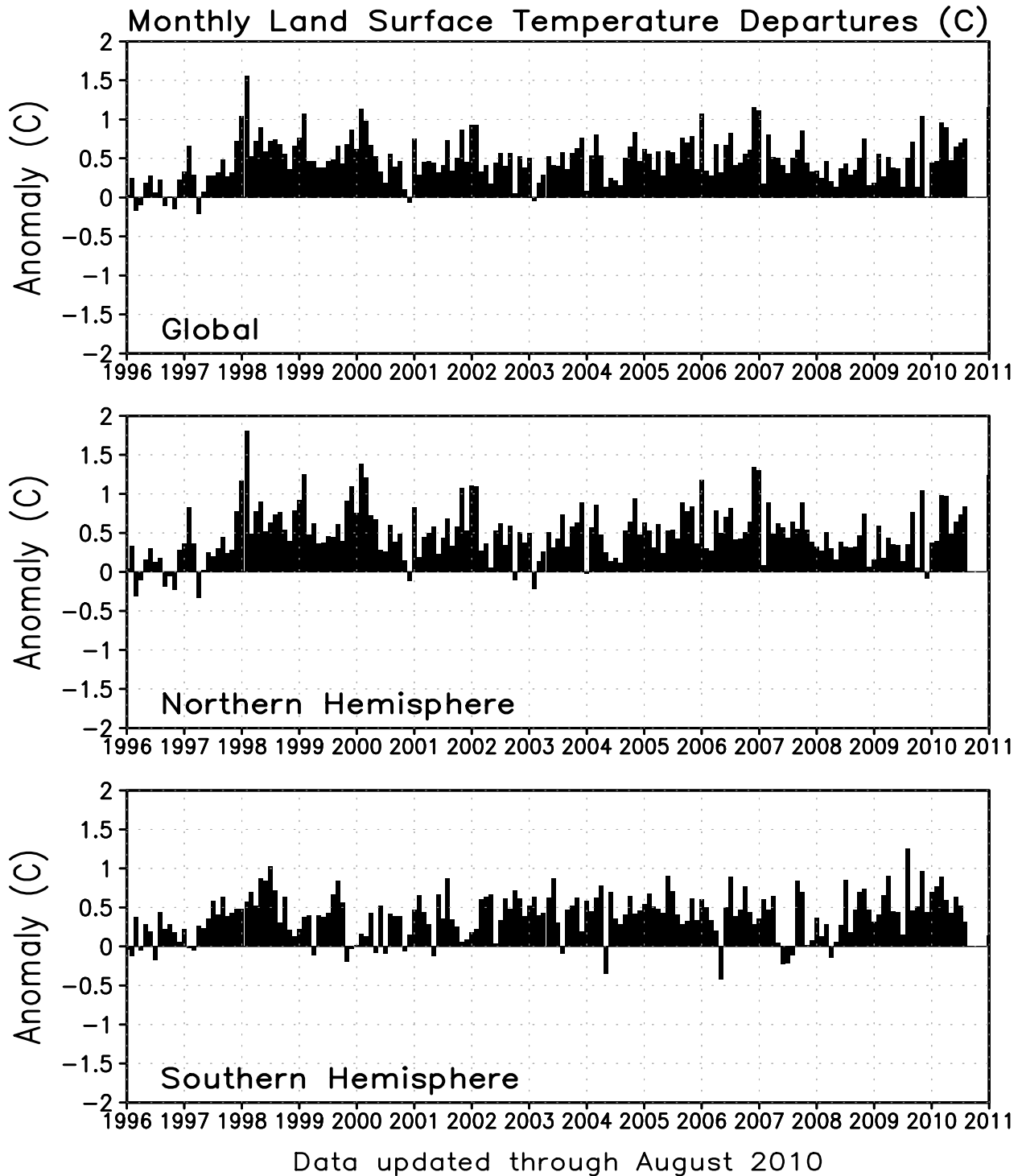


FIGURE E2. Monthly global (top), Northern Hemisphere (middle), and Southern Hemisphere (bottom) surface temperature anomalies (land only, °C) from January 1990 - present, computed as departures from the 1971–2000 base period means.

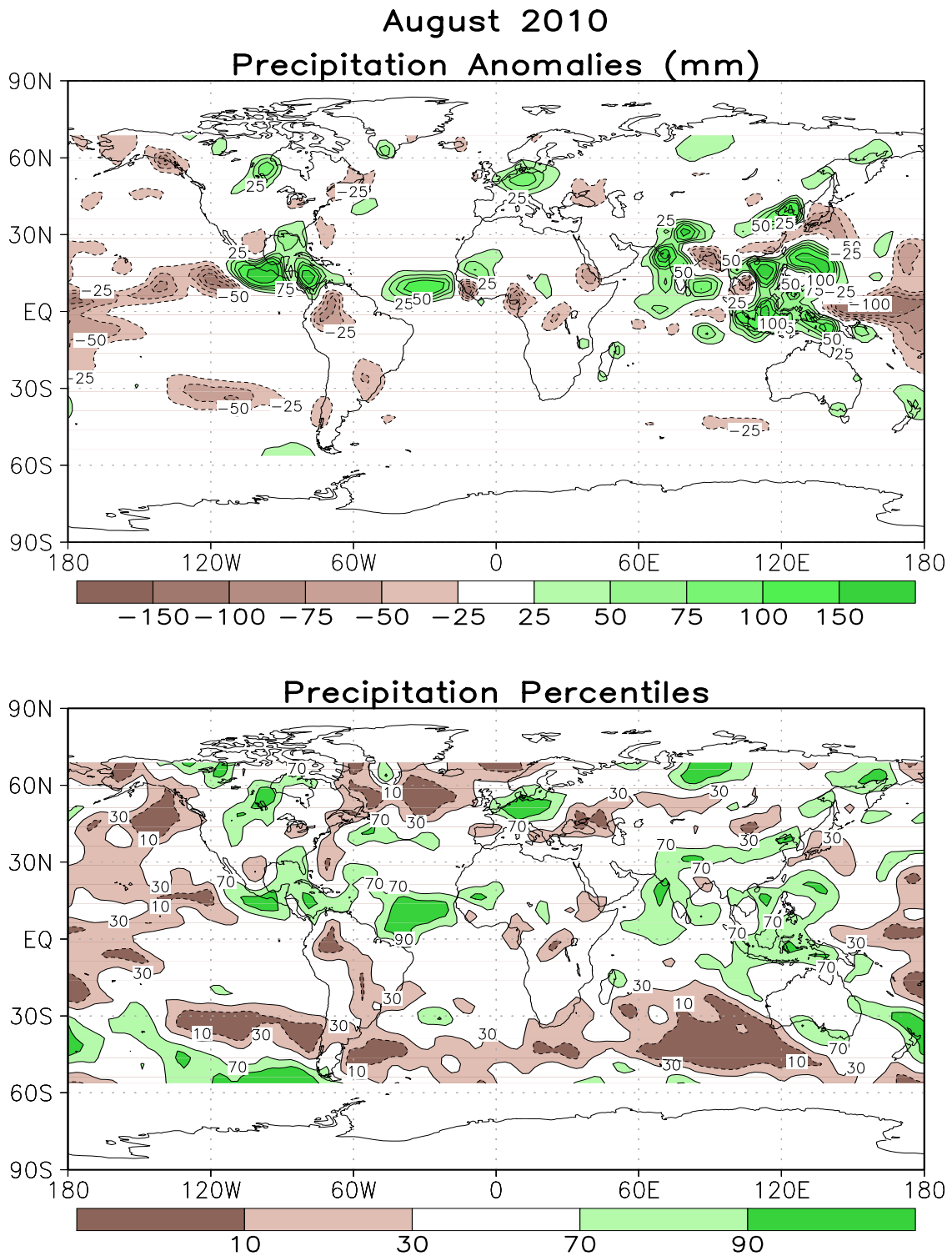


FIGURE E3. Anomalous precipitation (mm, top) and precipitation percentiles based on a Gamma distribution fit to the 1979–2000 base period data (bottom) for AUG 2010. Data are obtained from a merge of raingauge observations and satellite-derived precipitation estimates (Janowiak and Xie 1999, *J. Climate*, **12**, 3335–3342). Contours are drawn at 200, 100, 50, 25, -25, -50, -100, and -200 mm in top panel. Percentiles are not plotted in regions where mean monthly precipitation is <5mm/month.

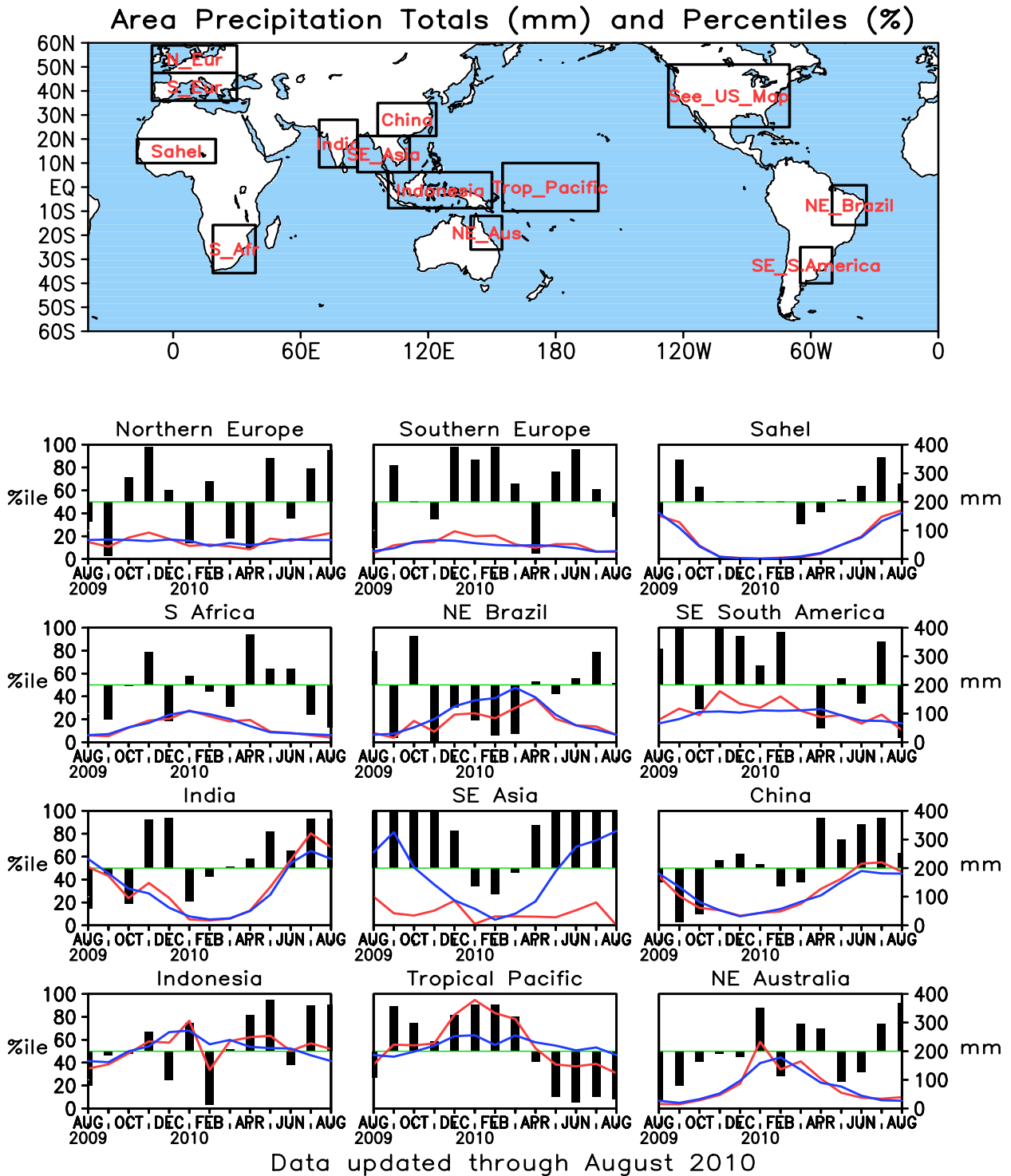


FIGURE E4. Areal estimates of monthly mean precipitation amounts (mm, solid lines) and precipitation percentiles (% , bars) for the most recent 13 months obtained from a merge of raingauge observations and satellite-derived precipitation estimates (Janowiak and Xie 1999, *J. Climate*, **12**, 3335–3342). The monthly precipitation climatology (mm, dashed lines) is from the 1979–2000 base period monthly means. Monthly percentiles are not shown if the monthly mean is less than 5 mm.

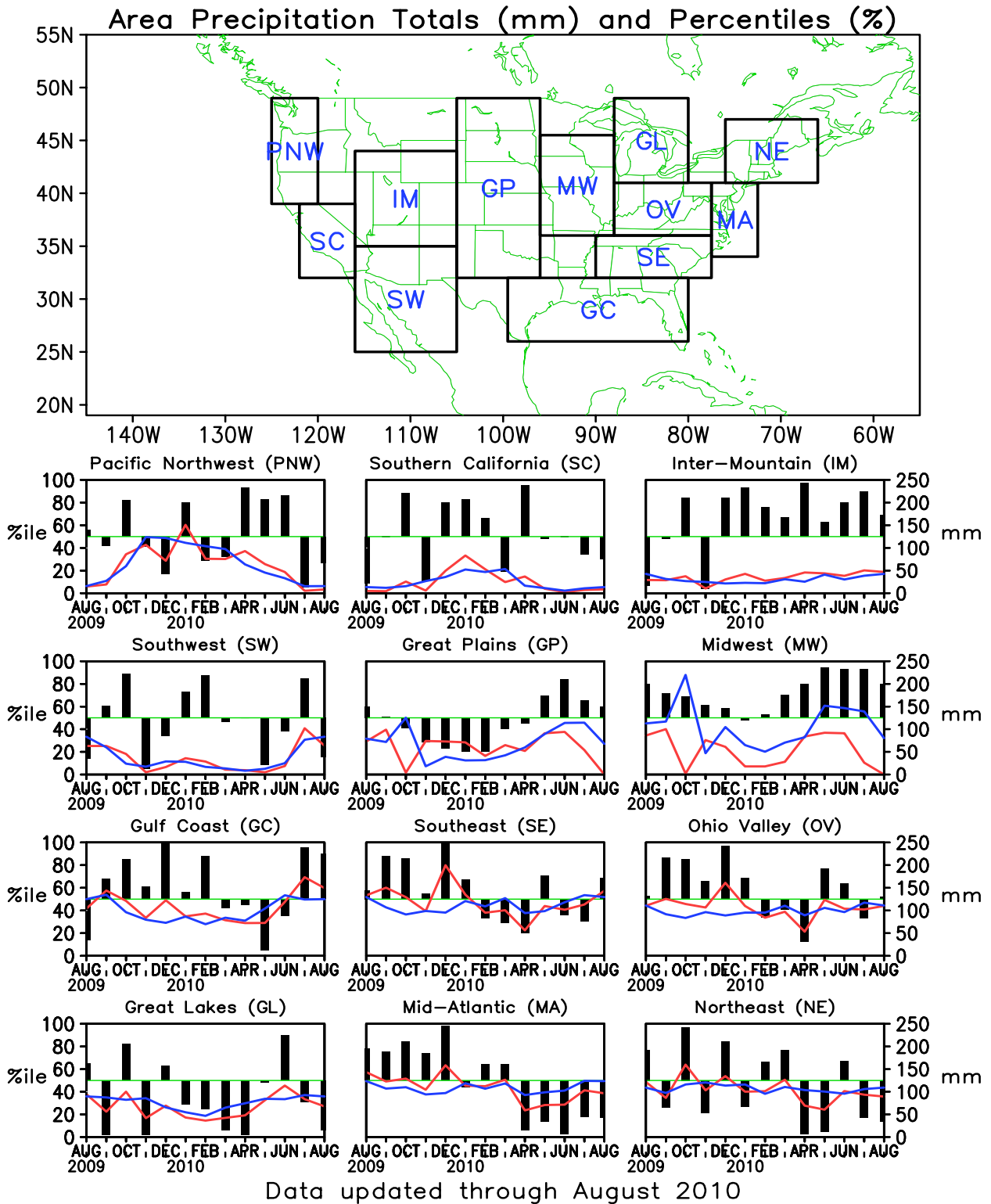


FIGURE E5. Areal estimates of monthly mean precipitation amounts (mm, solid lines) and precipitation percentiles (% , bars) for the most recent 13 months obtained from a merge of raingauge observations and satellite-derived precipitation estimates (Janowiak and Xie 1999, *J. Climate*, **12**, 3335–3342). The monthly precipitation climatology (mm, dashed lines) is from the 1979–2000 base period monthly means. Monthly percentiles are not shown if the monthly mean is less than 5 mm.

Monthly Accumulation -- August, 2010

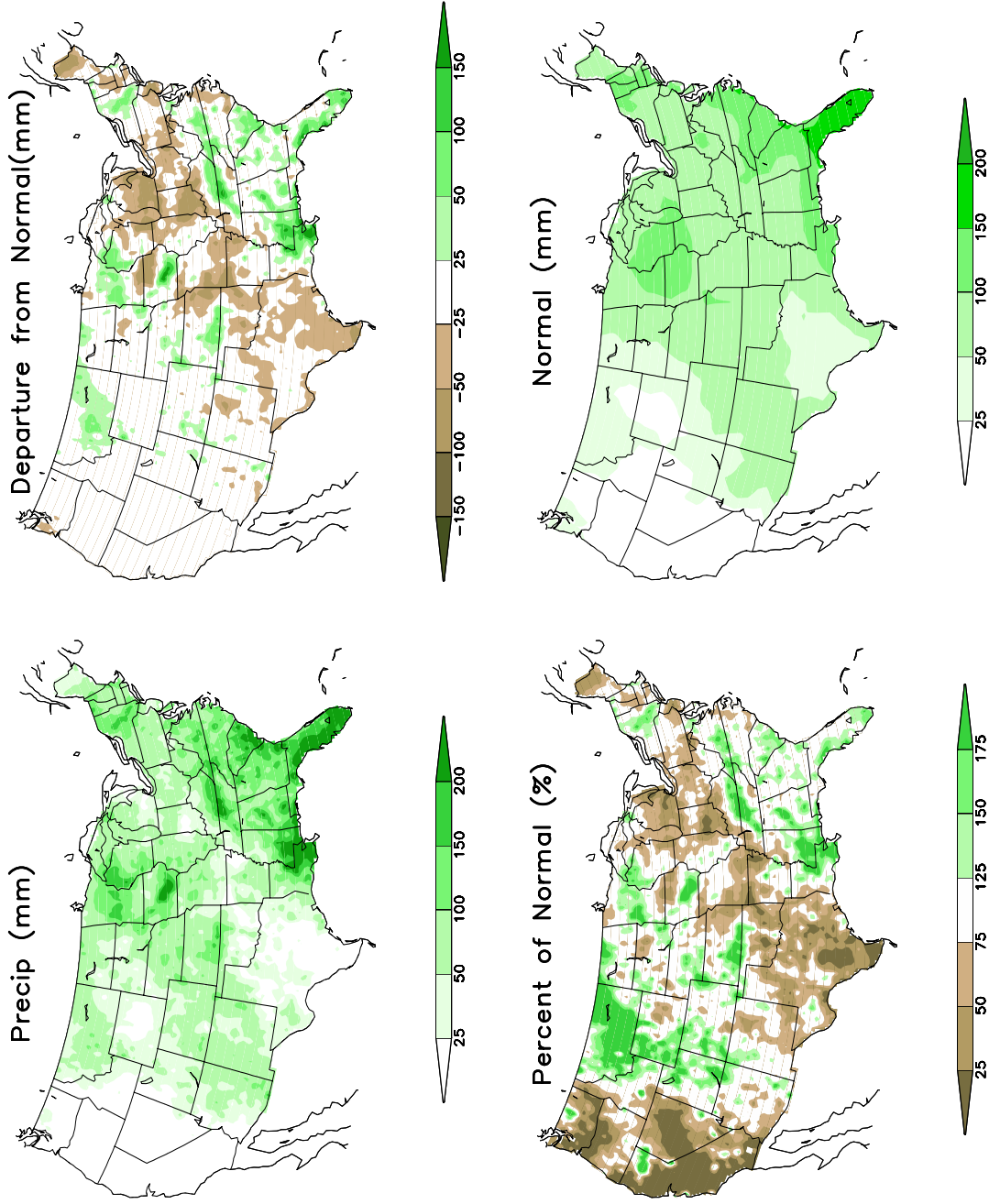
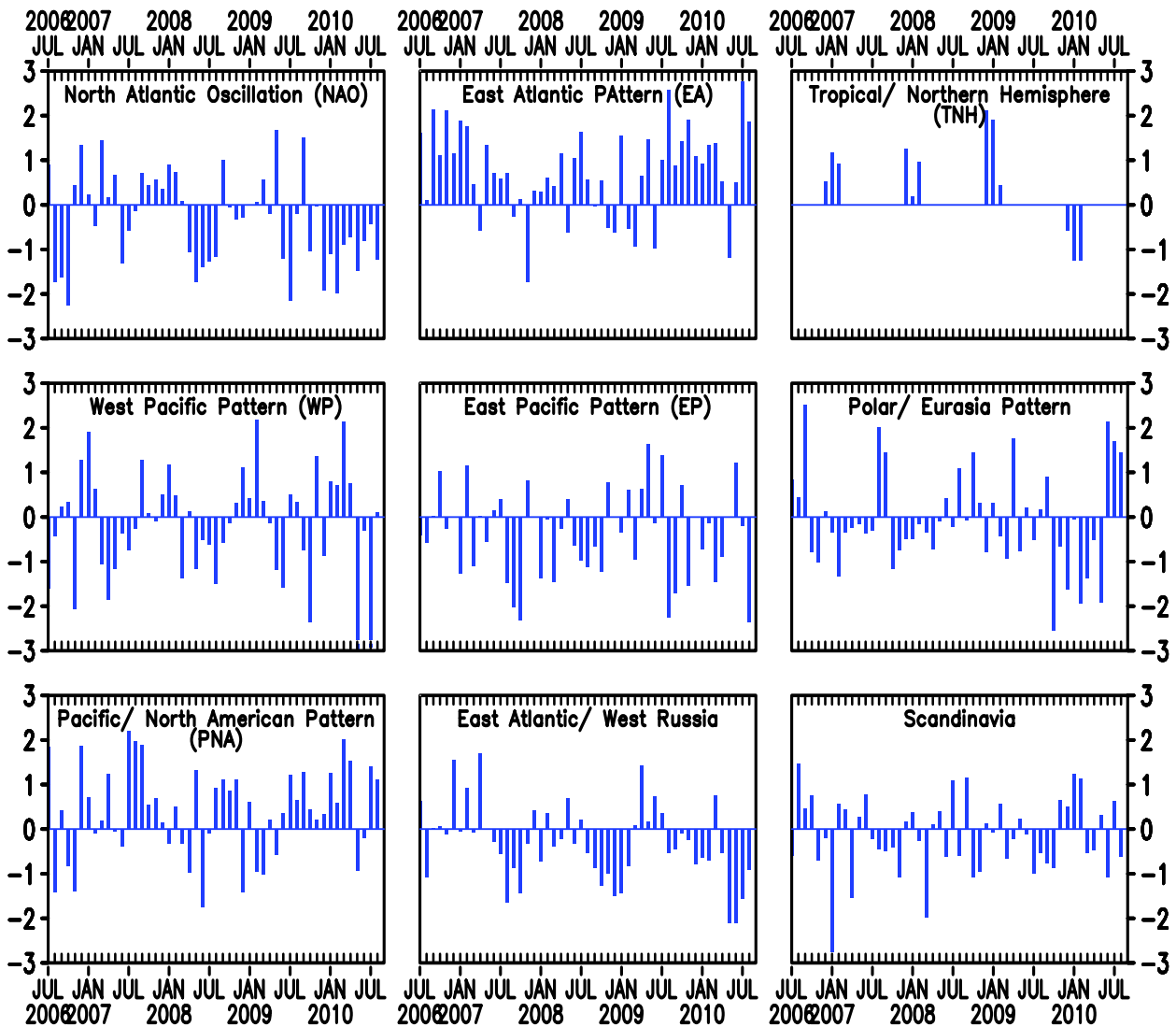


FIGURE E6. Observed precipitation (upper left), departure from average (upper right), percent of average (lower left), and average precipitation (lower right) for AUG 2010. The units are given on each panel. Base period for averages is 1971–2000. Results are based on CPC’s U. S. daily precipitation analysis, which is available at <http://www.cpc.ncep.noaa.gov/products/precip/realtime>.

Monthly Teleconnection Indices



Data updated through August 2010

FIGURE E7. Standardized monthly Northern Hemisphere teleconnection indices. The teleconnection patterns are calculated from a Rotated Principal Component Analysis (RPCA) applied to monthly standardized 500-hPa height anomalies during January 1950 – December 2000. To obtain these patterns, ten leading un-rotated modes are first calculated for each calendar month by using the monthly height anomaly fields for the three-month period centered on that month: [i.e., The July modes are calculated from the June, July, and August standardized monthly anomalies]. A Varimax spatial rotation of the ten leading un-rotated modes for each calendar month results in 120 rotated modes (12 months x 10 modes per month) that yield ten primary teleconnection patterns. The teleconnection indices are calculated by first projecting the standardized monthly anomalies onto the teleconnection patterns corresponding to that month (eight or nine teleconnection patterns are seen in each calendar month). The indices are then solved for simultaneously using a Least-Squares approach. In this approach, the indices are the solution to the Least-Squares system of equations which explains the maximum spatial structure of the observed height anomaly field during the month. The indices are then standardized for each pattern and calendar month independently. No index value exists when the teleconnection pattern does not appear as one of the ten leading rotated EOF's valid for that month.

August 2010
Sea-Level Pressure and Anomaly

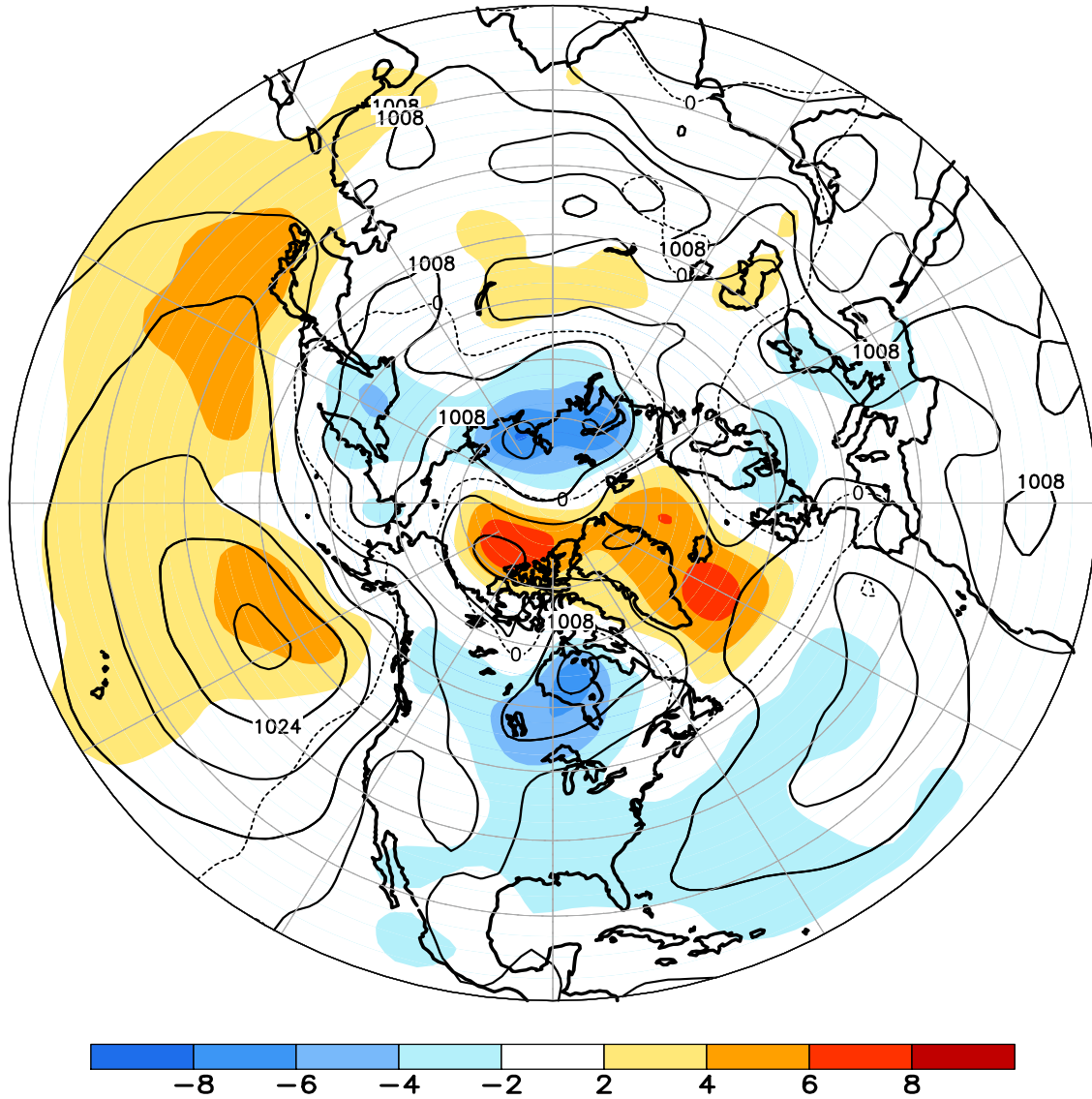


FIGURE E8. Northern Hemisphere mean and anomalous sea level pressure (CDAS/Reanalysis) for AUG 2010. Mean values are denoted by solid contours drawn at an interval of 4 hPa. Anomaly contour interval is 2 hPa with values less (greater) than -2 hPa (2 hPa) indicated by dark (light) shading. Anomalies are calculated as departures from the 1979-95 base period monthly means.

August 2010
500-hPa Height and Anomaly

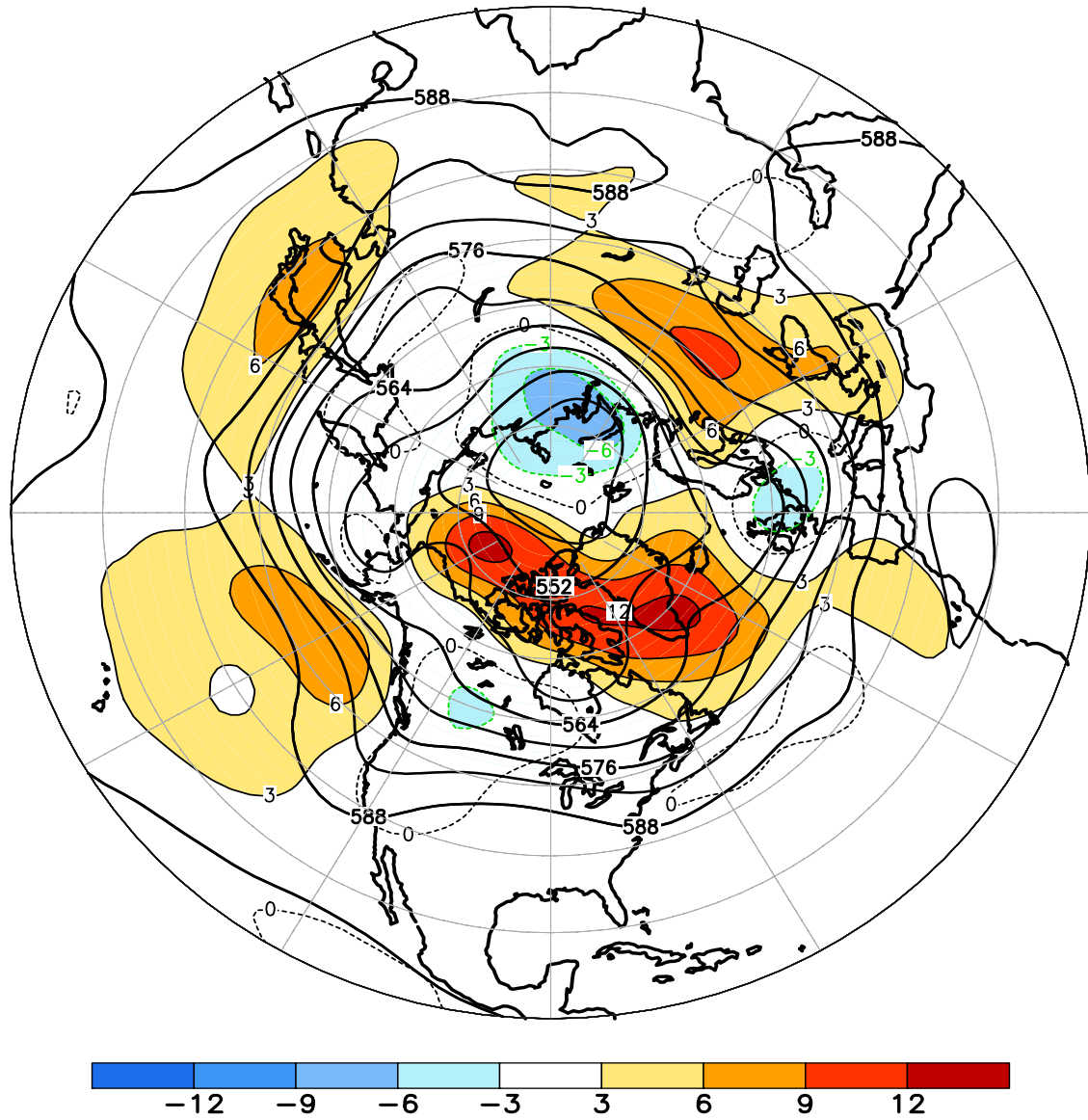
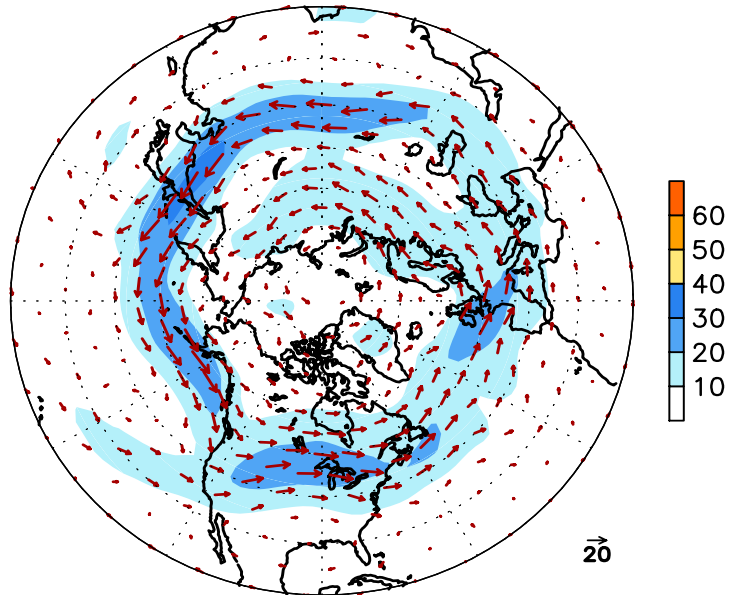


FIGURE E9. Northern Hemisphere mean and anomalous 500-hPa geopotential height (CDAS/Reanalysis) for AUG 2010. Mean heights are denoted by solid contours drawn at an interval of 6 dam. Anomaly contour interval is 3 dam with values less (greater) than -3 dam (3 dam) indicated by dark (light) shading. Anomalies are calculated as departures from the 1979-95 base period monthly means.

August 2010
300-hPa Wind



300-hPa Wind Anomaly

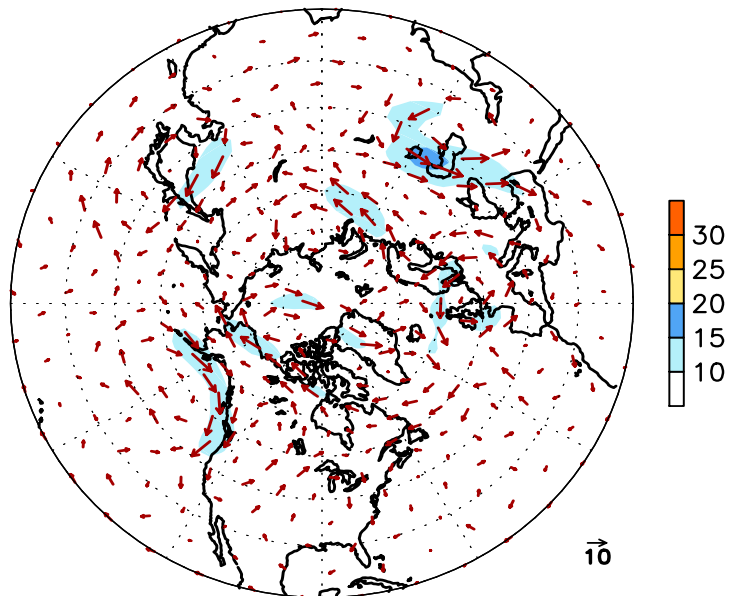


FIGURE E10. Northern Hemisphere mean (left) and anomalous (right) 300-hPa vector wind (CDAS/Reanalysis) for AUG 2010. Mean (anomaly) isotach contour interval is 10 (5) ms^{-1} . Values greater than 30 ms^{-1} (left) and 10 ms^{-1} (rights) are shaded. Anomalies are departures from the 1979-95 base period monthly means.

August 2010
500-hPa: Percentage of Anomaly Days

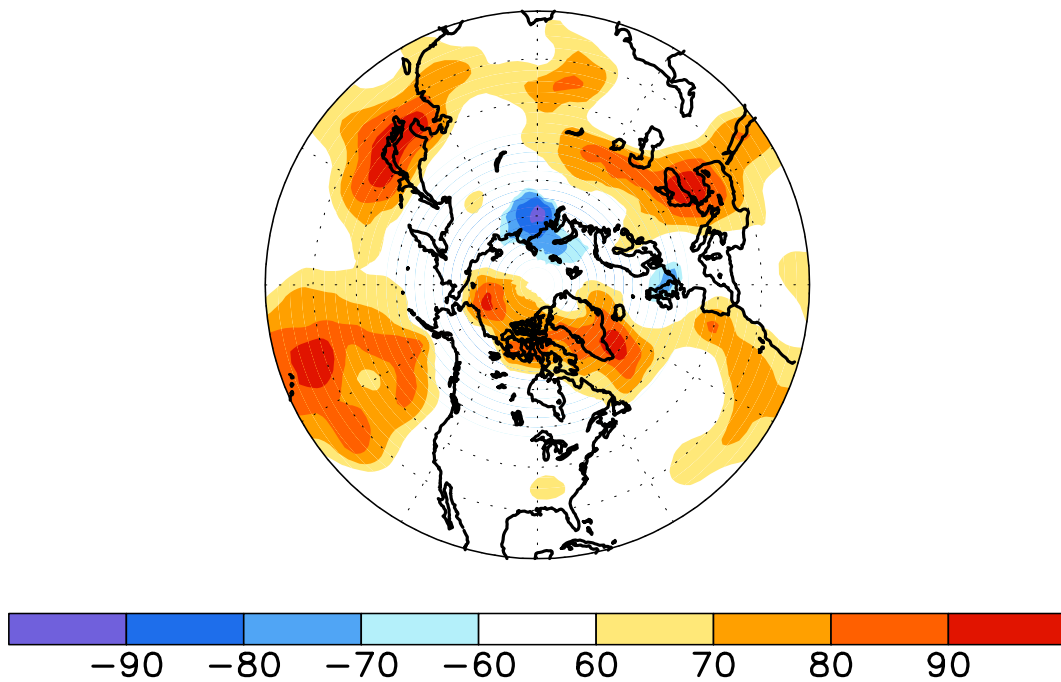


FIGURE E11. Northern Hemisphere percentage of days during AUG 2010 in which 500-hPa height anomalies greater than 15 m (red) and less than -15 m (blue) were observed. Values greater than 70% are shaded and contour interval is 20%.

August 2010
500-hPa Height Anomalies: 40.0N

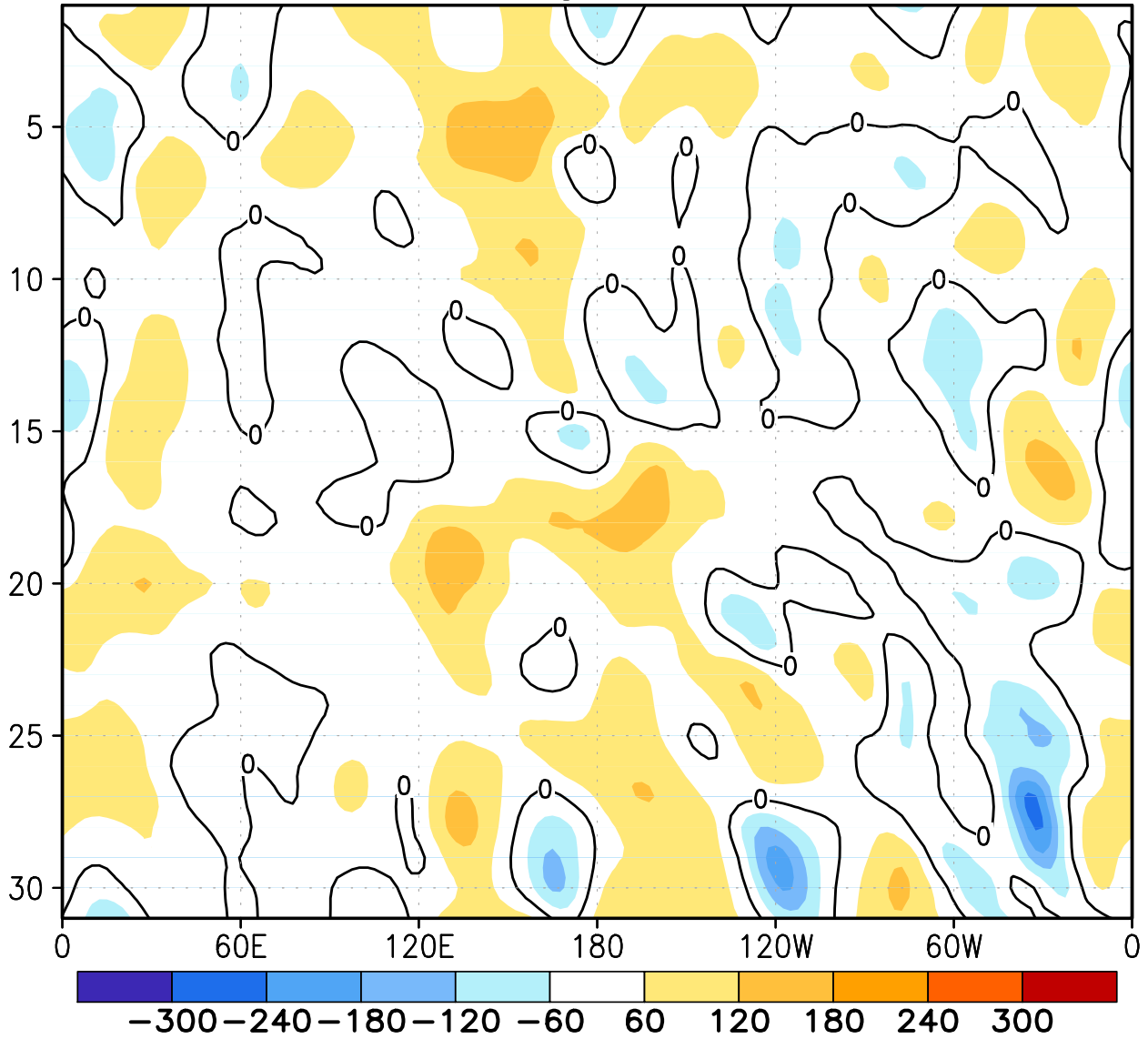
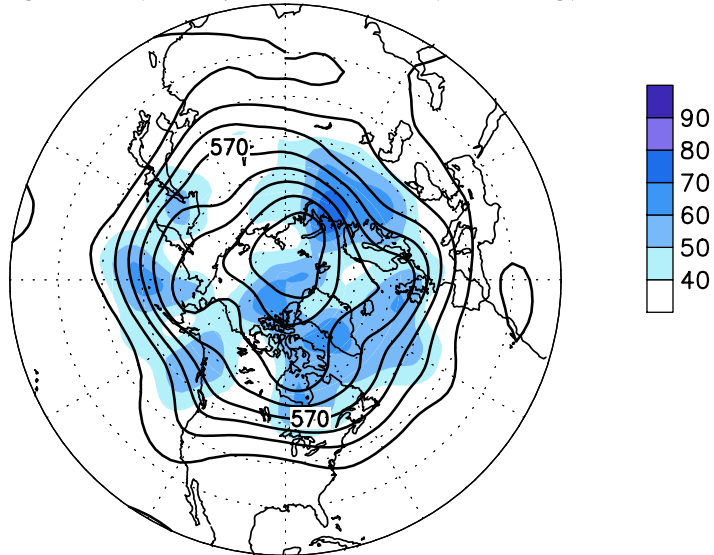


FIGURE E12. Northern Hemisphere: Daily 500-hPa height anomalies for AUG 2010 averaged over the 5° latitude band centered on 40°N. Positive values are indicated by solid contours and dark shading. Negative values are indicated by dashed contours and light shading. Contour interval is 60 m. Anomalies are departures from the 1979-95 base period daily means.

August 2010
 500-hPa Heights (Contours)
 High Frequency Std. Dev. (Shading)



500-hPa Heights (Contours)
 Normalized High Frequency Variance (Shading)

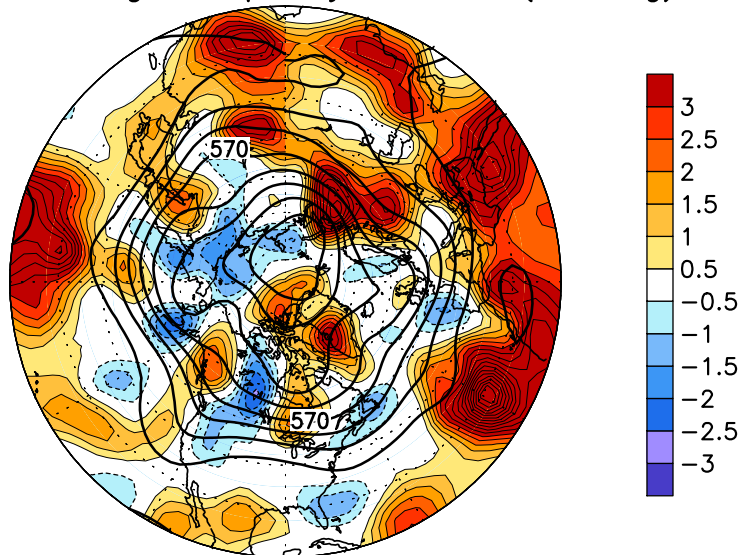


FIGURE E13. Northern Hemisphere 500-hPa heights (thick contours, interval is 6 dam) overlaid with (Top) Standard deviation of 10-day high-pass (HP) filtered height anomalies and (Bottom) Normalized anomalous variance of 10-day HP filtered height anomalies. A Lanczos filter is used to calculate the HP filtered anomalies. Anomalies are departures from the 1979-2000 daily means.

August 2010
Sea-Level Pressure and Anomaly

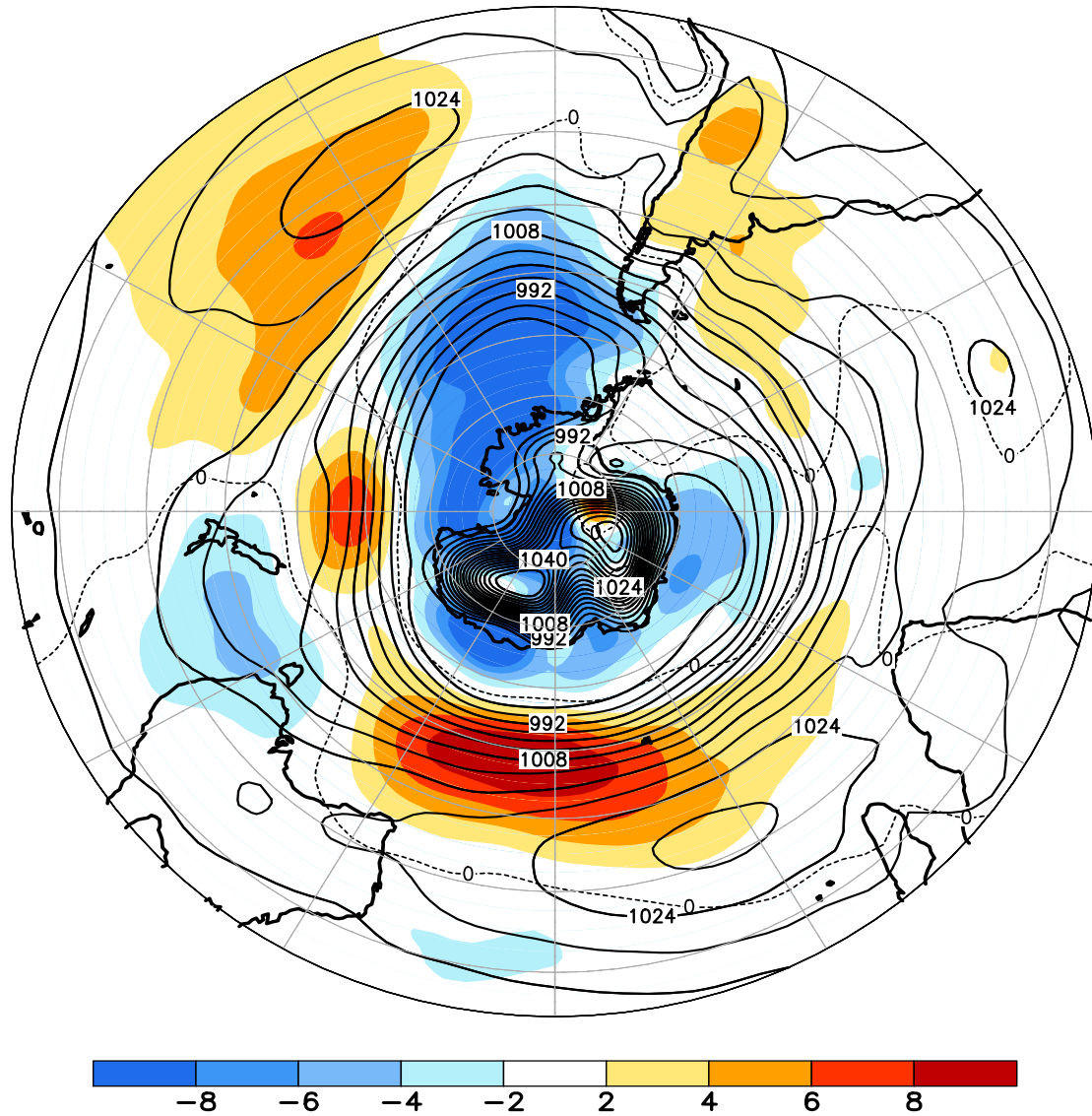


FIGURE E14. Southern Hemisphere mean and anomalous sea level pressure(CDAS/Reanalysis) for AUG 2010. Mean values are denoted by solid contours drawn at an interval of 4 hPa. Anomaly contour interval is 2 hPa with values less (greater) than -2 hPa (2 hPa) indicated by dark (light) shading. Anomalies are calculated as departures from the 1979-95 base period monthly means.

August 2010
500-hPa Height and Anomaly

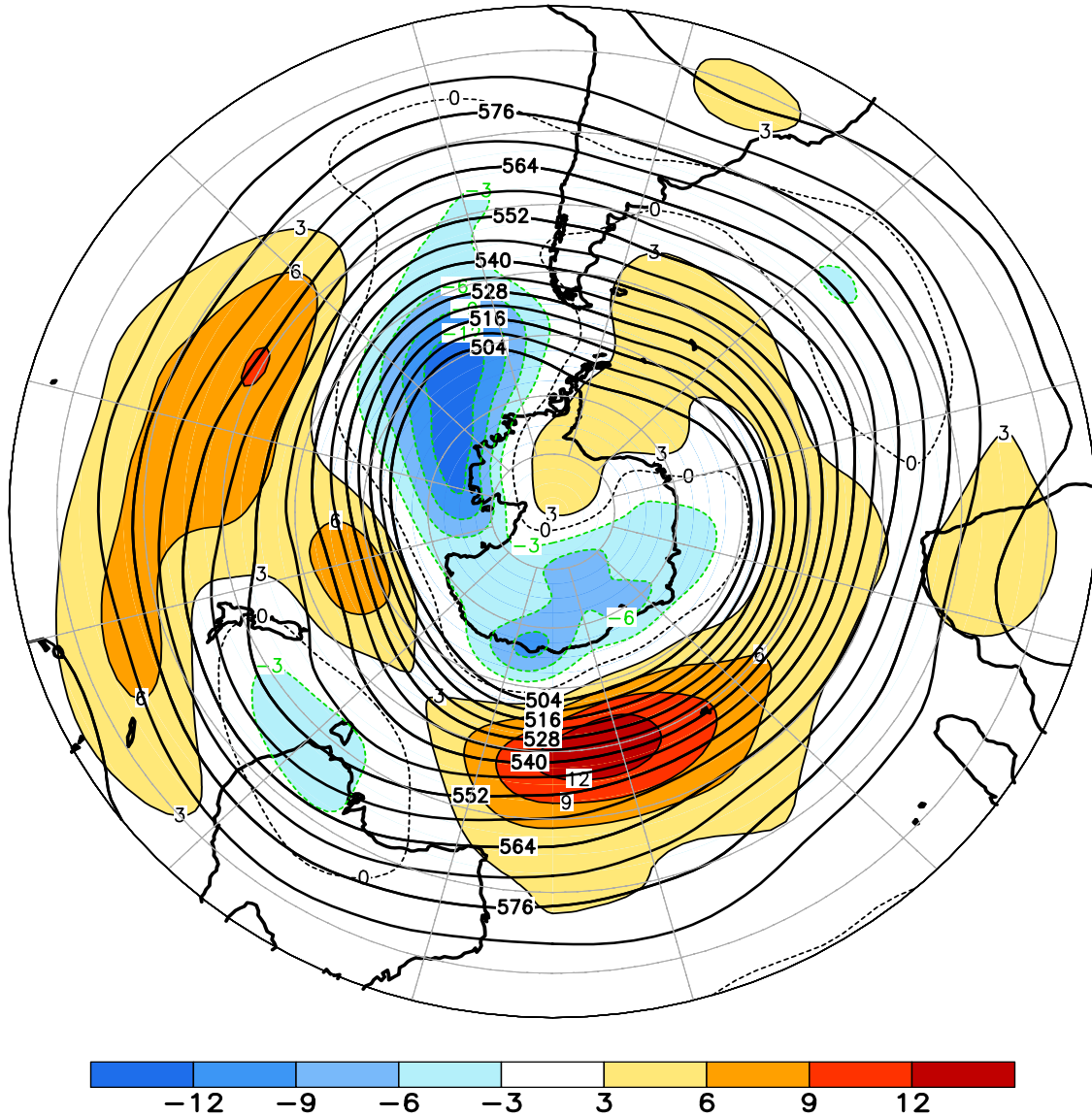
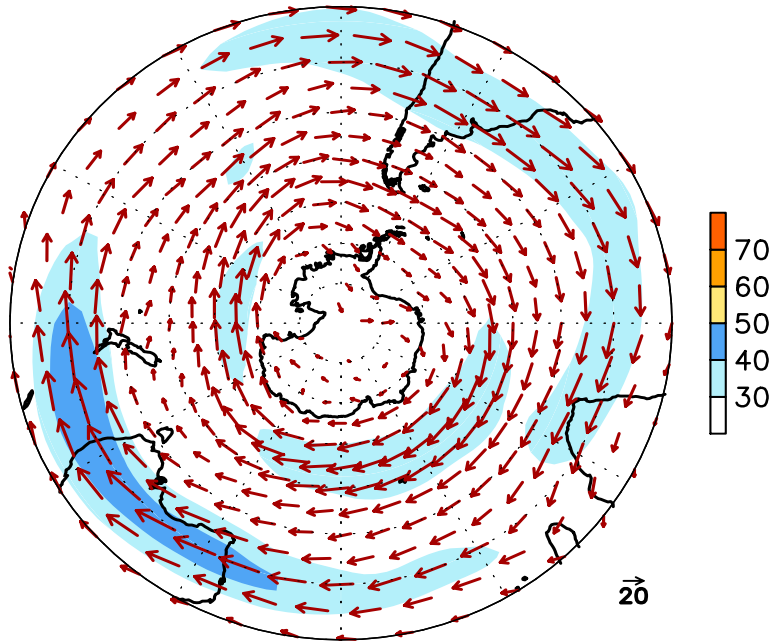


FIGURE E15. Southern Hemisphere mean and anomalous 500-hPa geopotential height (CDAS/Reanalysis) for AUG 2010. Mean heights are denoted by solid contours drawn at an interval of 6 dam. Anomaly contour interval is 3 dam with values less (greater) than -3 dam (3 dam) indicated by dark (light) shading. Anomalies are calculated as departures from the 1979-95 base period monthly means.

August 2010
300-hPa Wind



300-hPa Wind Anomaly

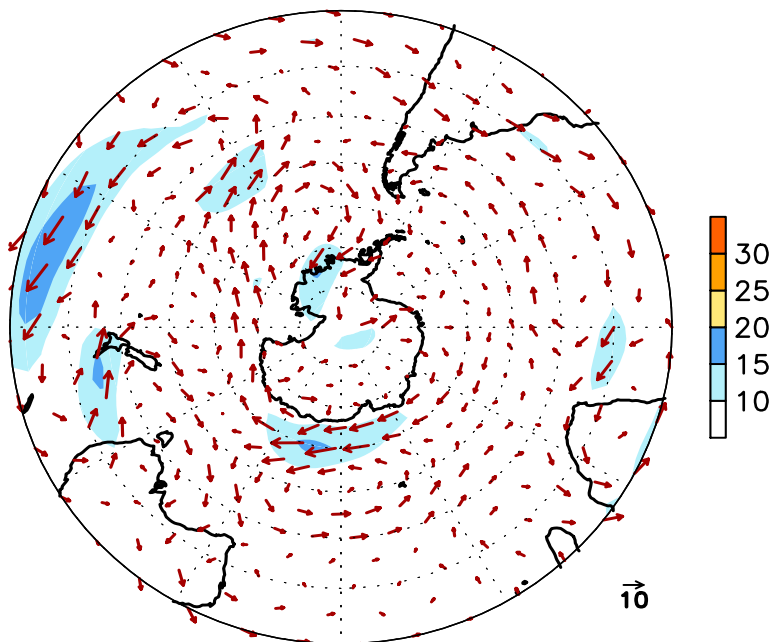


FIGURE E16. Southern Hemisphere mean (left) and anomalous (right) 300-hPa vector wind (CDAS/Reanalysis) for AUG 2010. Mean (anomaly) isotach contour interval is 10 (5) ms^{-1} . Values greater than 30 ms^{-1} (left) and 10 ms^{-1} (rights) are shaded. Anomalies are departures from the 1979-95 base period monthly means.

August 2010
500-hPa: Percentage of Anomaly Days

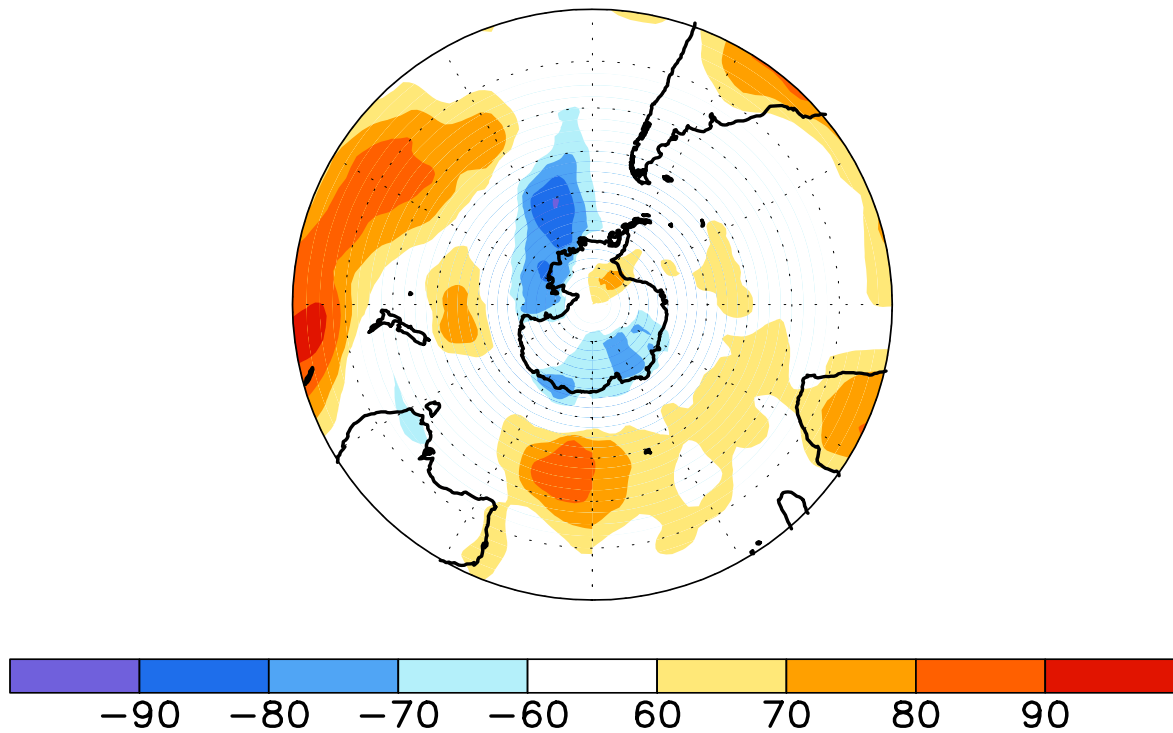


FIGURE E17. Southern Hemisphere percentage of days during AUG 2010 in which 500-hPa height anomalies greater than 15 m (red) and less than -15 m (blue) were observed. Values greater than 70% are shaded and contour interval is 20%.

August 2010
500-hPa Height Anomalies: 40.0S

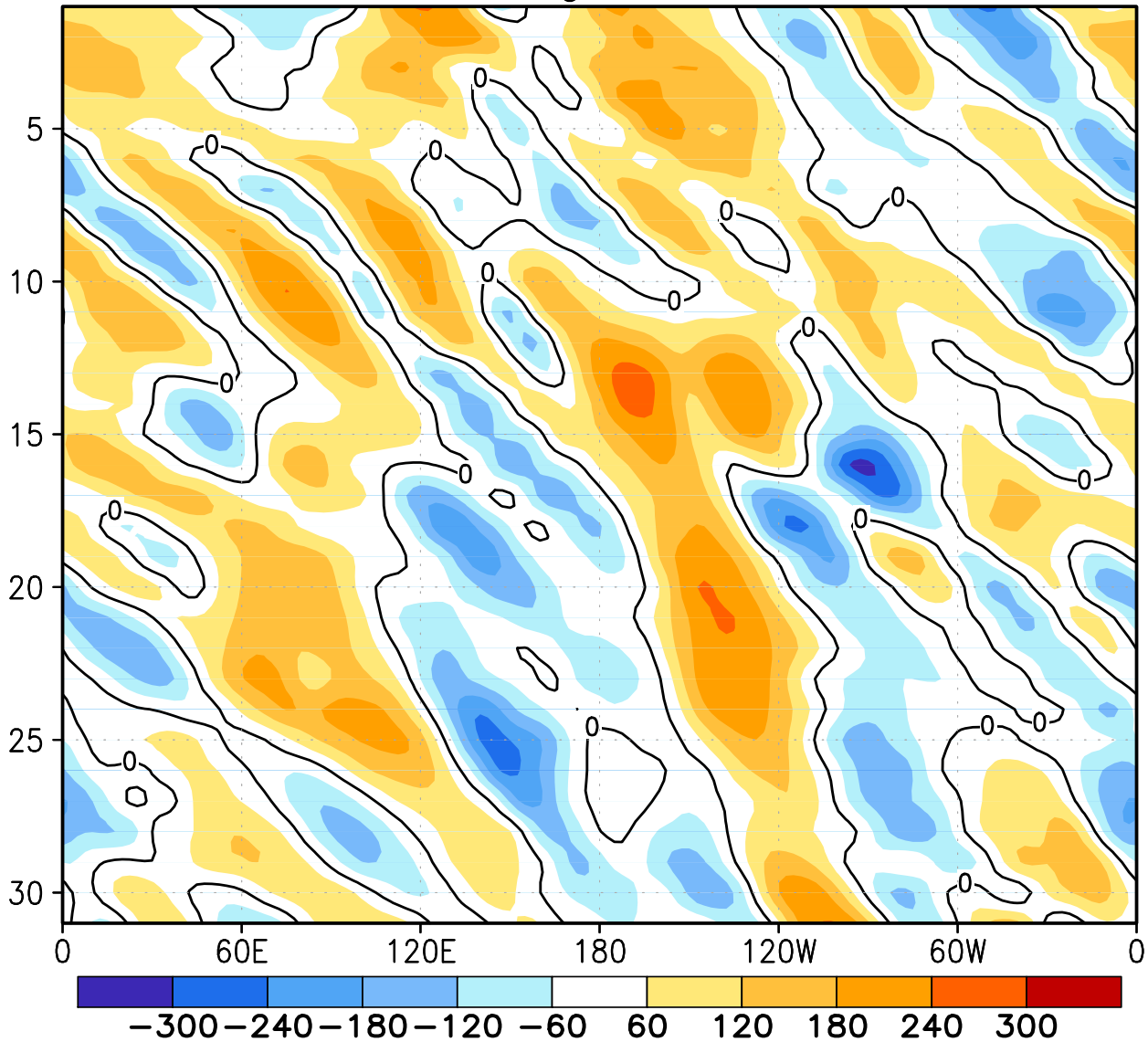


FIGURE E18. Southern Hemisphere: Daily 500-hPa height anomalies for AUG 2010 averaged over the 5° latitude band centered on 40°S. Positive values are indicated by solid contours and dark shading. Negative values are indicated by dashed contours and light shading. Contour interval is 60 m. Anomalies are departures from the 1979-95 base period daily means.

August 2010
Height Anomalies

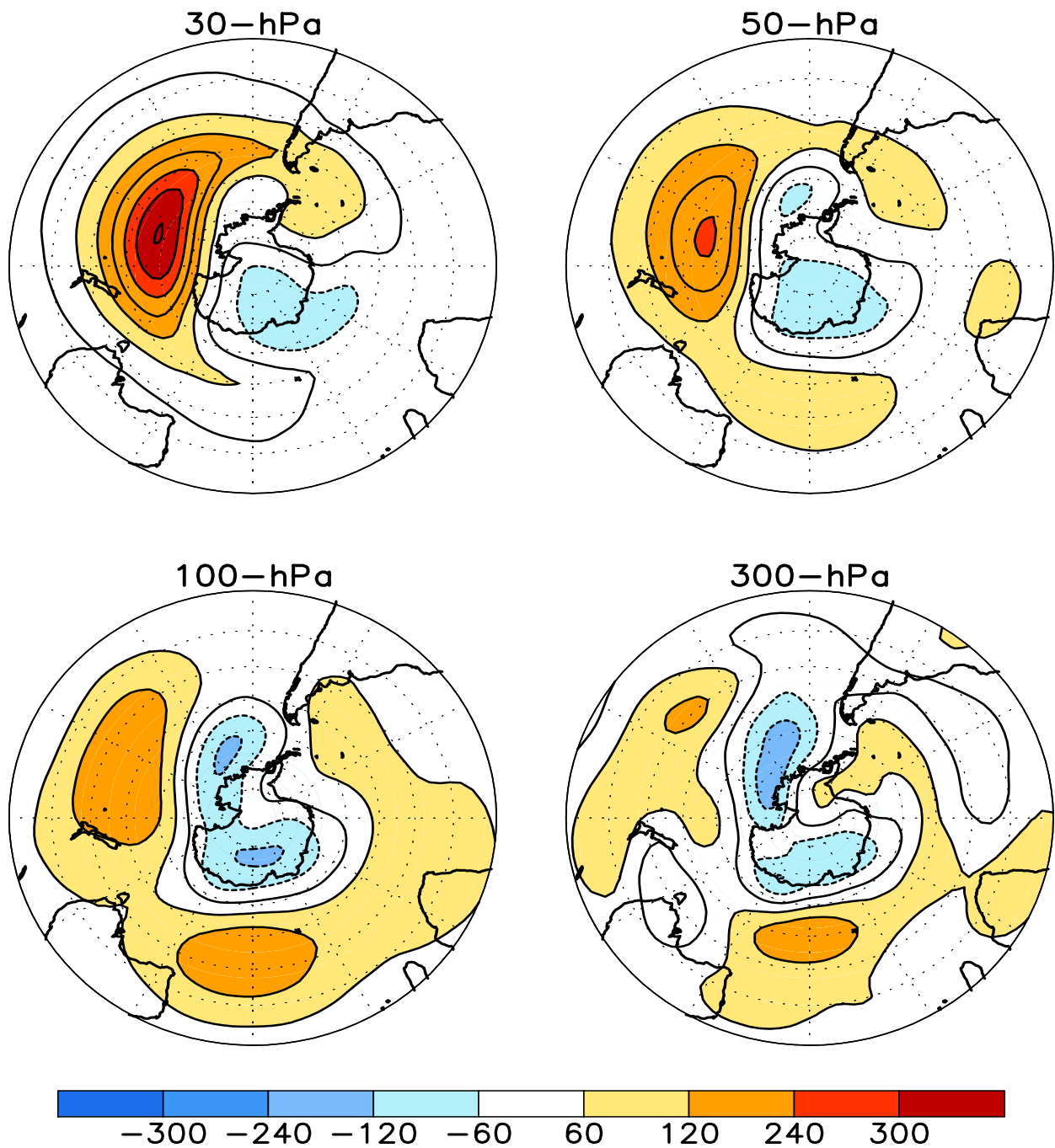


FIGURE S1. Stratospheric height anomalies (m) at selected levels for AUG 2010. Positive values are indicated by solid contours and dark shading. Negative values are indicated by dashed contours and light shading. Contour interval is 60 m. Anomalies are calculated from the 1979–95 base period means. Winter Hemisphere is shown.

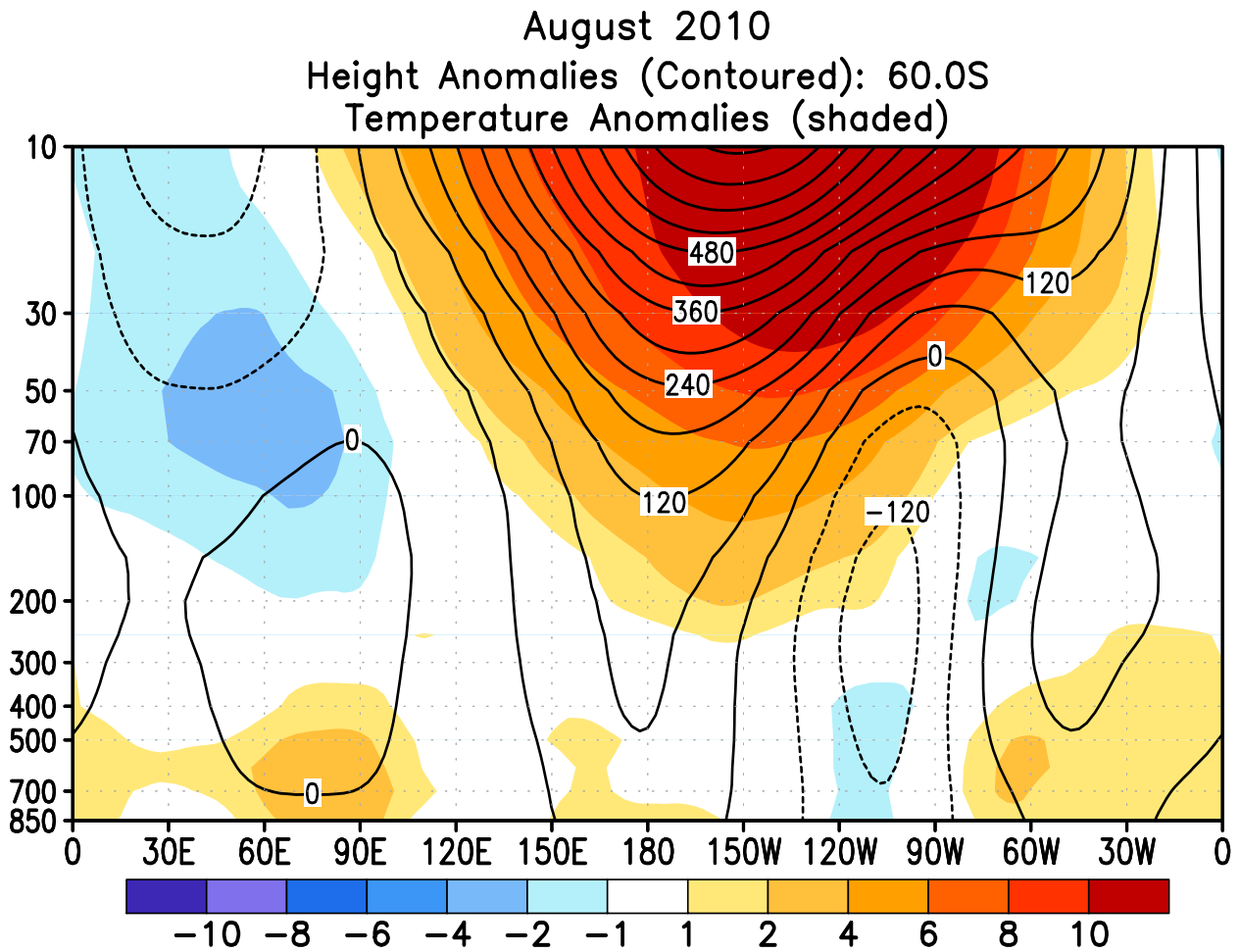


FIGURE S2. Height-longitude sections during AUG 2010 for height anomalies (contour) and temperature anomalies (shaded). In both panels, positive values are indicated by solid contours and dark shading, while negative anomalies are indicated by dashed contours and light shading. Contour interval for height anomalies is 60 m and for temperature anomalies is 2°C. Anomalies are calculated from the 1979–95 base period monthly means. Winter Hemisphere is shown.

50hPa JJA Mean Temperature Anomalies

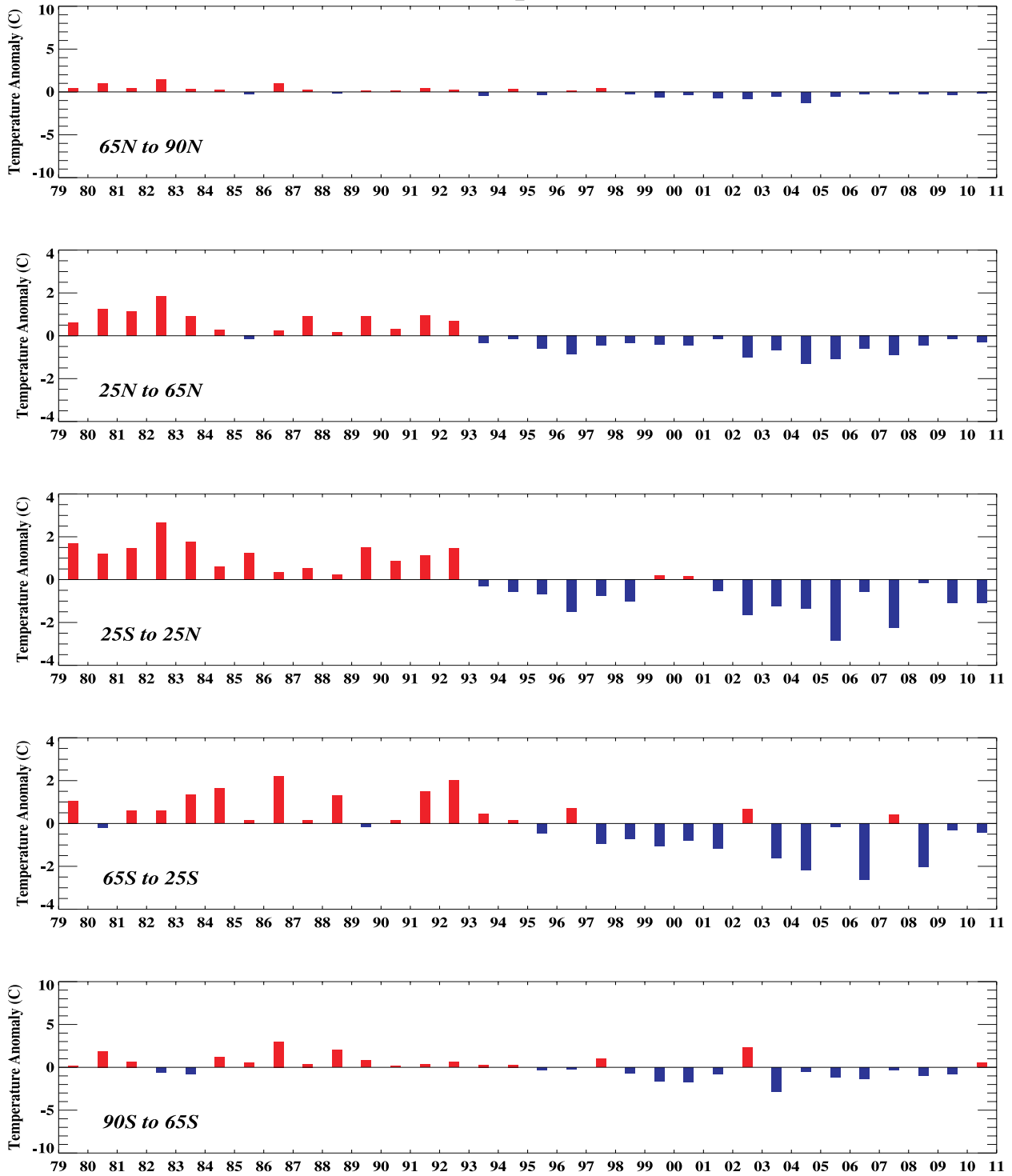


FIGURE S3. Seasonal mean temperature anomalies at 50-hPa for the latitude bands 65°–90°N, 25°–65°N, 25°N–25°S, 25°–65°S, 65°–90°S. The seasonal mean is comprised of the most recent three months. Zonal anomalies are taken from the mean of the entire data set.

Zonal Mean Temperature for 2009 & 2010

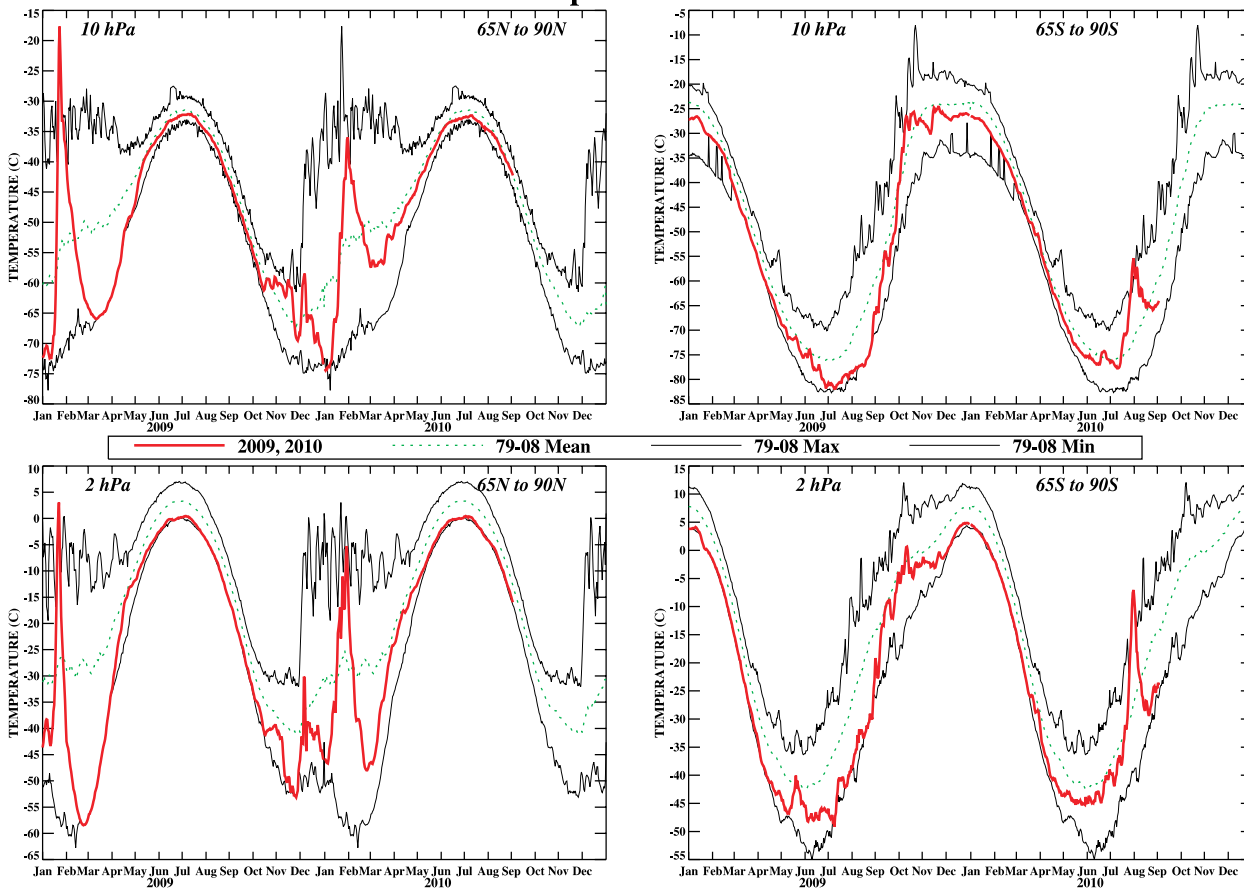


FIGURE S4. Daily mean temperatures at 10-hPa and 2-hPa (thick line) in the region 65°–90°N and 65°–90°S for the past two years. Dashed line depicts the 1979–99 base period daily mean. Thin solid lines depict the daily extreme maximum and minimum temperatures.

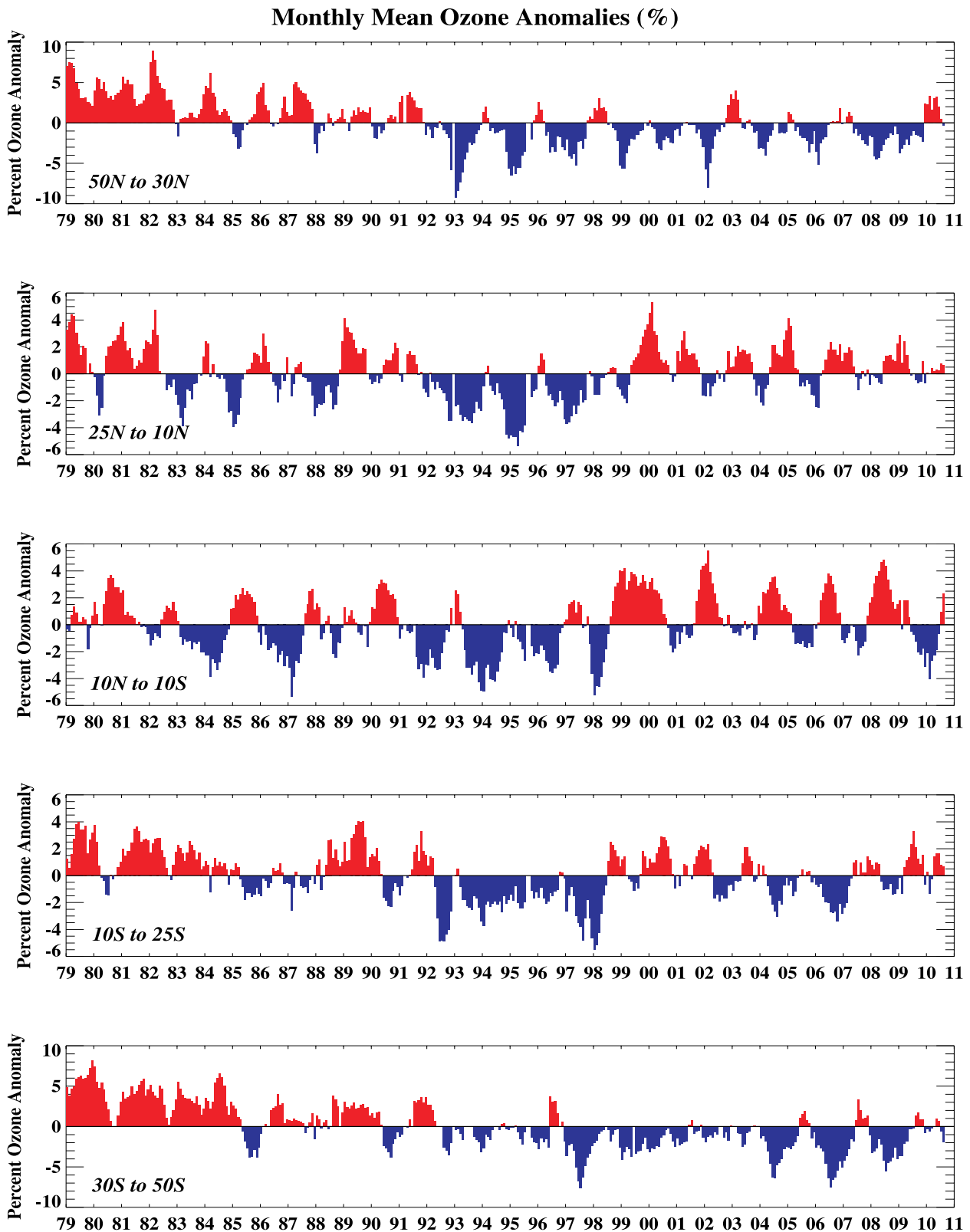


FIGURE S5. Monthly ozone anomalies (percent) from the long term monthly means for five zones: 50N-30N (NH mid-latitudes), 25N-10N (NH tropical surf zone), 10N-10S (Equatorial-QBO zone), 10S-25S (SH tropical surf zone), and 30S-50S (SH mid-latitudes). The long term monthly means are determined from the entire data set beginning in 1979.

AUGUST PERCENT DIFF (2010 - AVG(79-86))

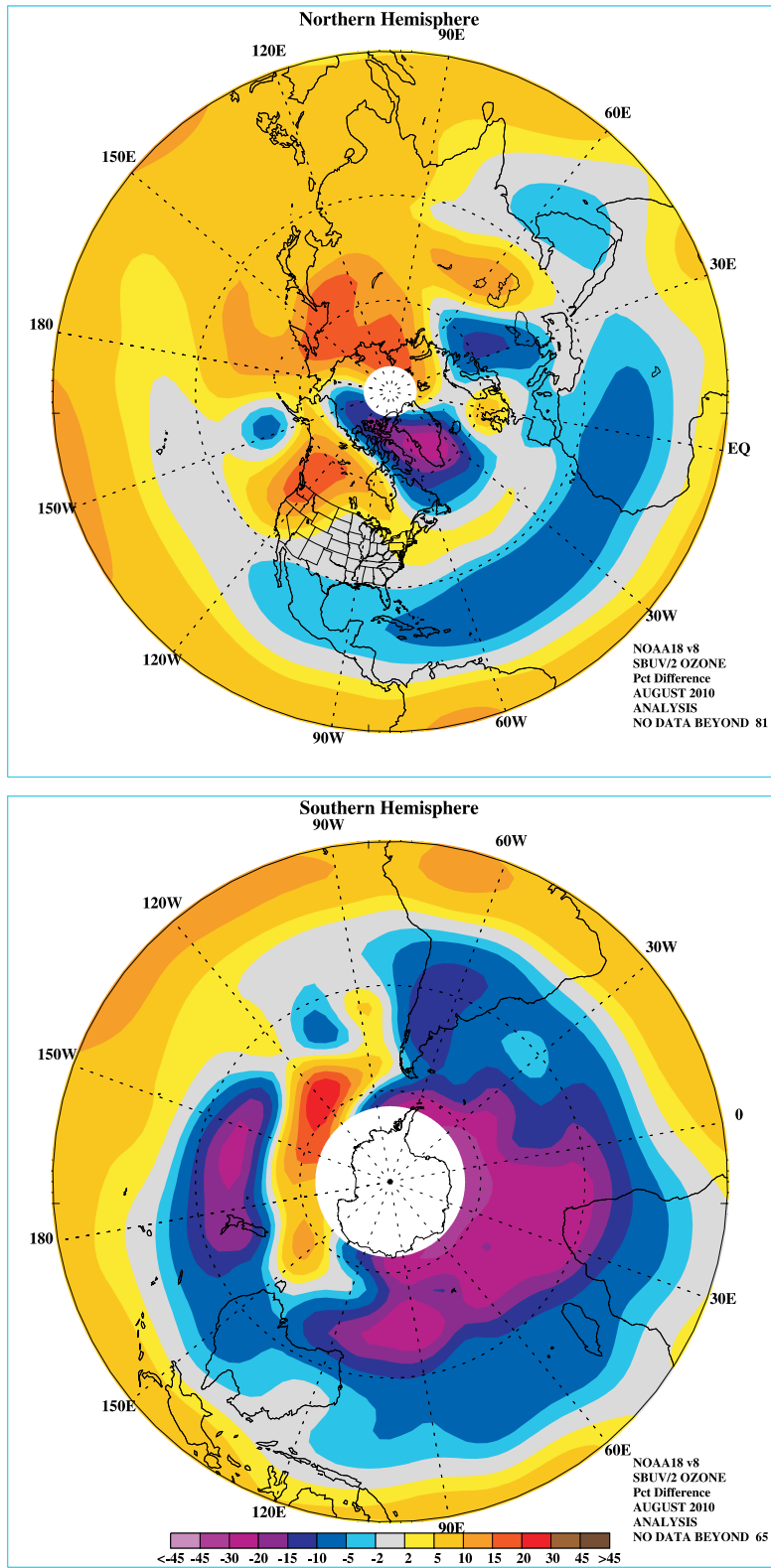


FIGURE S6. Northern (top) and Southern (bottom) Hemisphere total ozone anomaly (percent difference from monthly mean for the period 1979–86). The region near the winter pole has no SBUV/2 data.

Fz at 100 hPa (Aug. 2010)

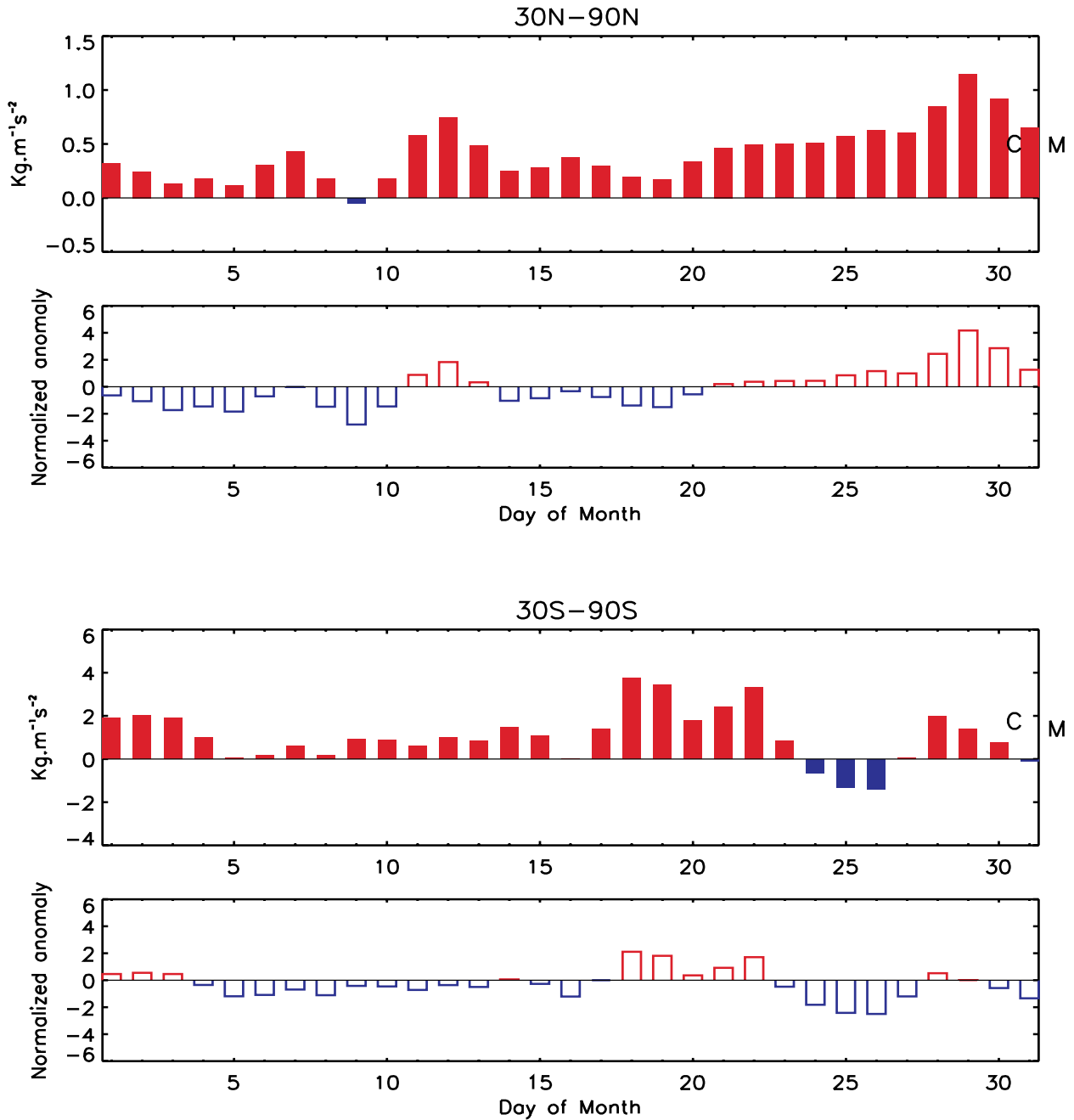


FIGURE S7. Daily vertical component of EP flux (which is proportional to the poleward transport of heat or upward transport of potential energy by planetary wave) at 100 hPa averaged over (top) 30°N–90°N and (bottom) 30°S–90°S for AUG 2010. The EP flux unit ($\text{kg m}^{-1} \text{s}^{-2}$) has been scaled by multiplying a factor of the Brunt Vaisala frequency divided by the Coriolis parameter and the radius of the earth. The letter 'M' indicates the current monthly mean value and the letter 'C' indicates the climatological mean value. Additionally, the normalized departures from the monthly climatological EP flux values are shown.

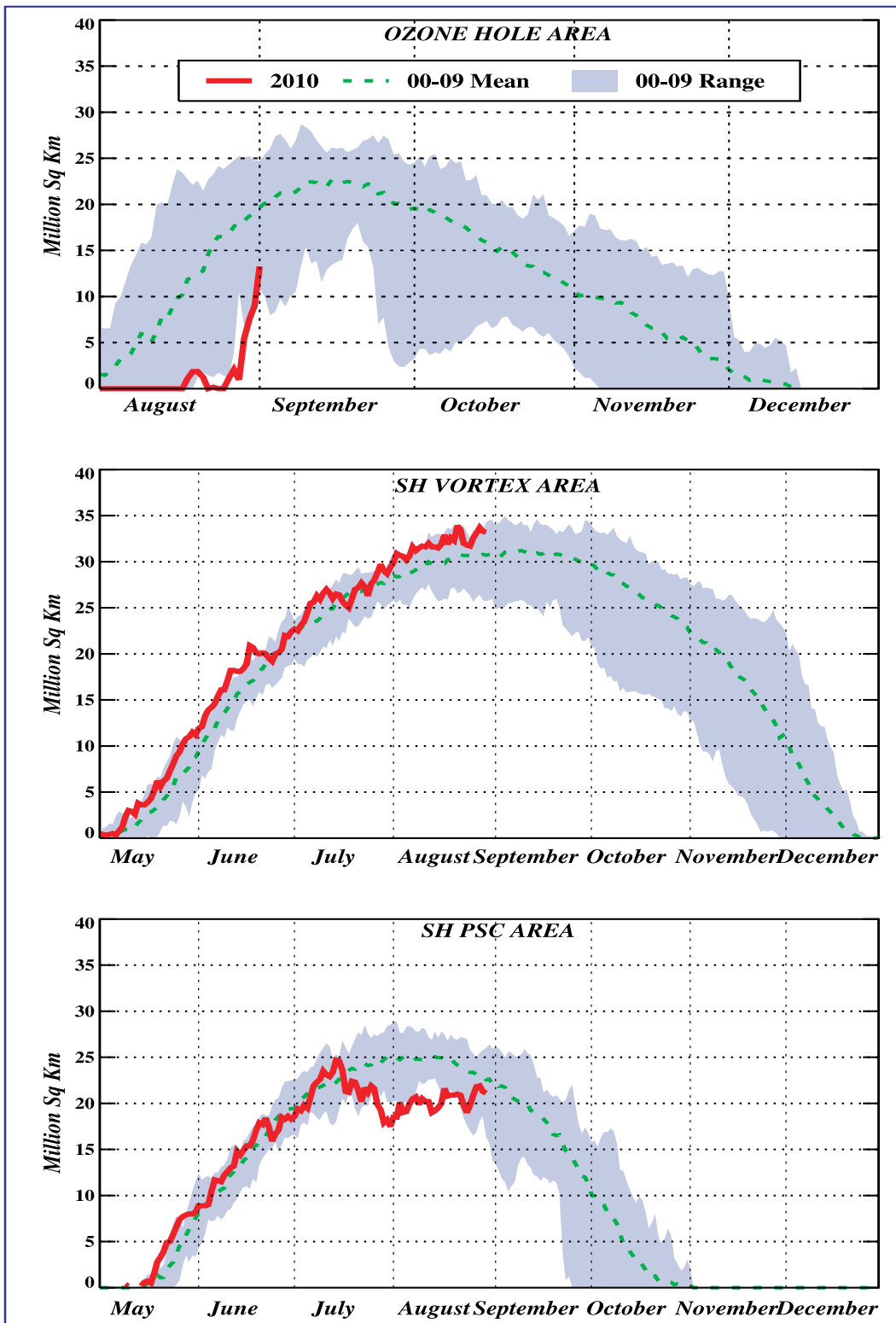


FIGURE S8. Daily time series showing the size of the SH polar vortex (representing the area enclosed by the 32 PVU contour on the 450K isentropic surface), and the areal coverage of temperatures < -78C on the 450K isentropic surface.

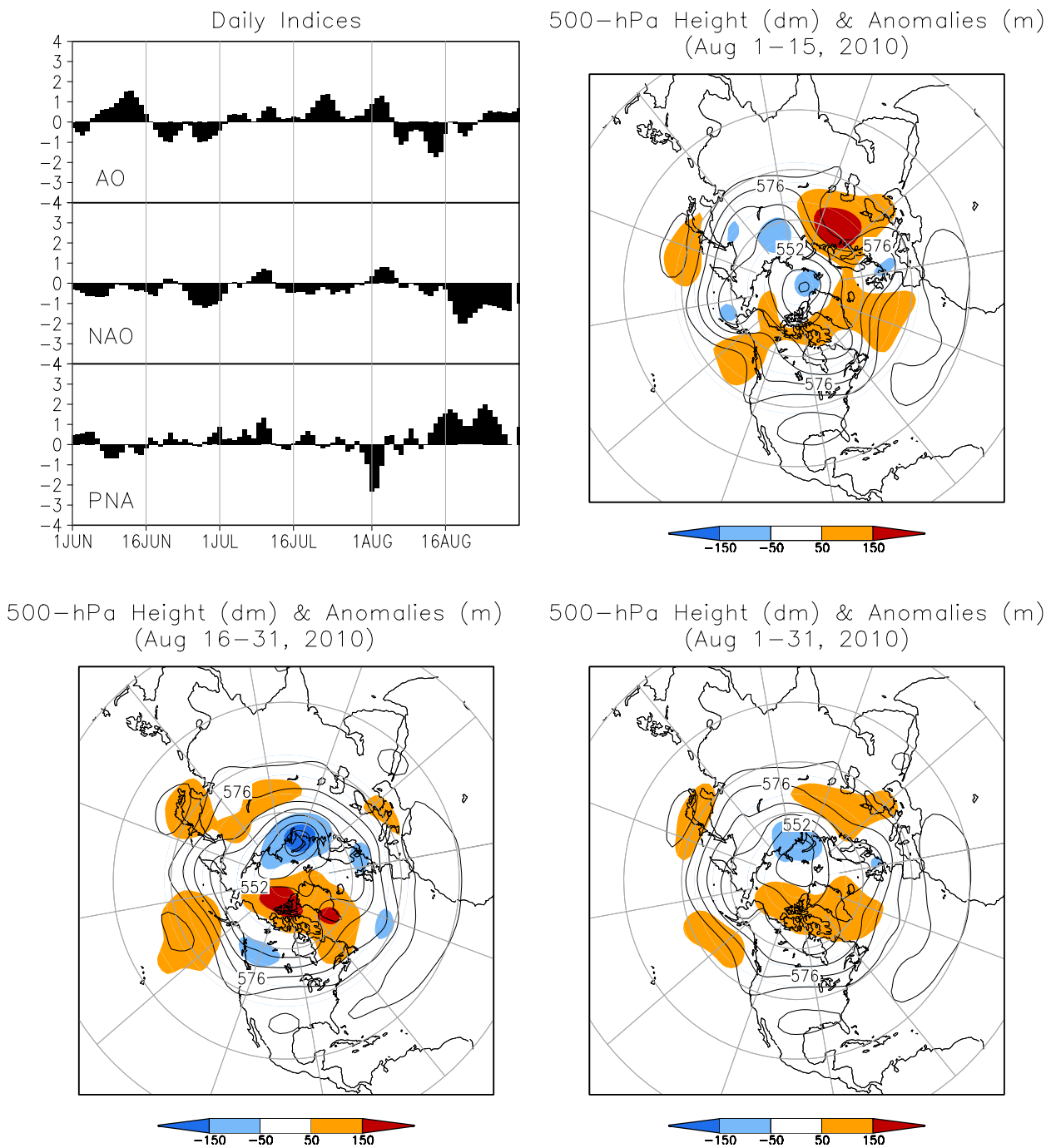


FIGURE A2.1. (a) Daily amplitudes of the Arctic Oscillation (AO) the North Atlantic Oscillation (NAO), and the Pacific-North American (PNA) pattern. The pattern amplitudes for the AO, (NAO, PNA) are calculated by projecting the daily 1000-hPa (500-hPa) height anomaly field onto the leading EOF obtained from standardized time-series of daily 1000-hPa (500-hPa) height for all months of the year. The base period is 1979–2000.

(b-d) Northern Hemisphere mean and anomalous 500-hPa geopotential height (CDAS/Reanalysis) for selected periods during AUG 2010 are shown in the remaining 3 panels. Mean heights are denoted by solid contours drawn at an interval of 8 dam. Dark (light) shading corresponds to anomalies greater than 50 m (less than -50 m). Anomalies are calculated as departures from the 1979–95 base period daily means.

**SSM/I/S Snow Cover for Aug 2010
anomaly based on departure from SSM/I 1987–2006 baseline**

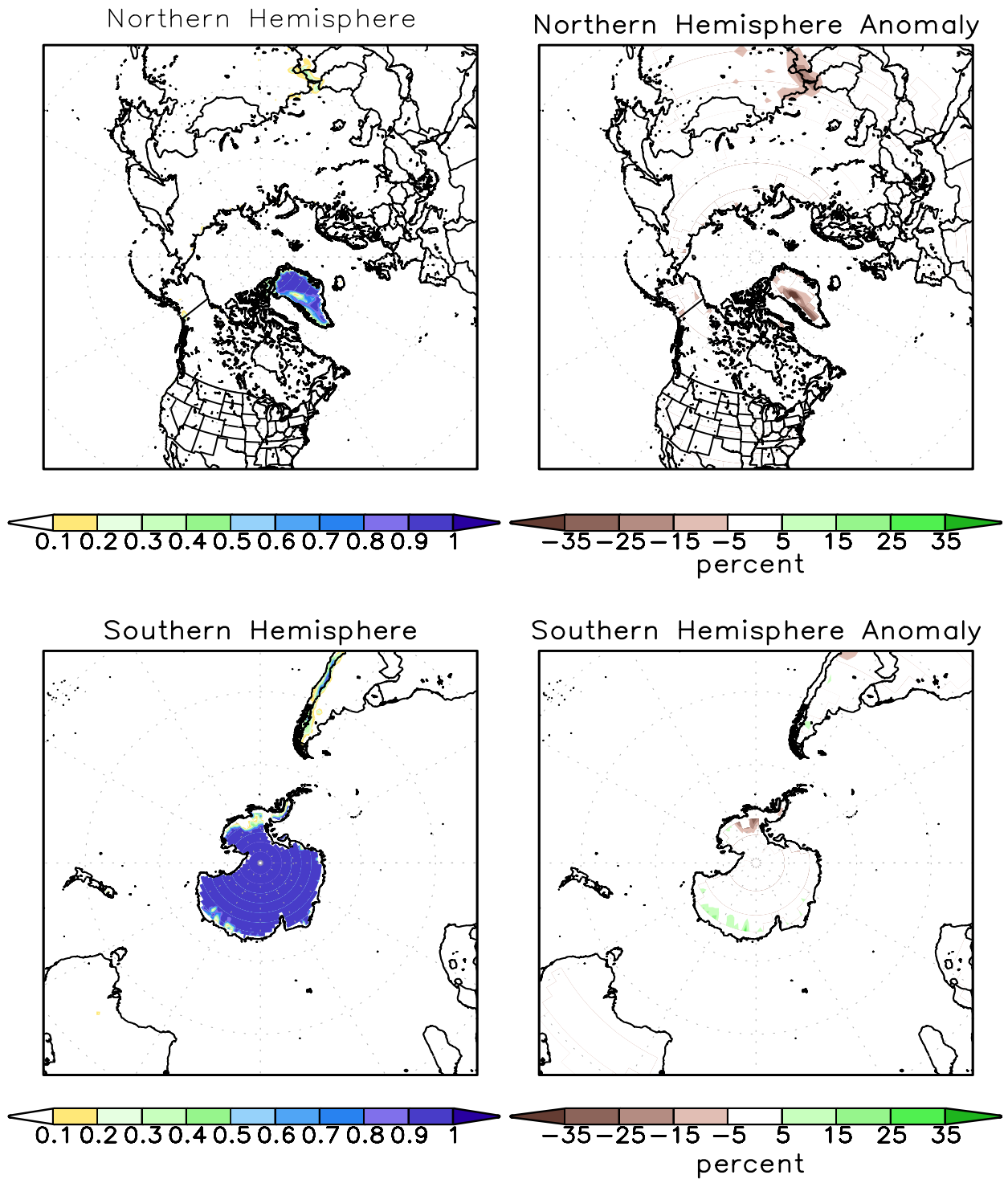


FIGURE A2.2. SSM/I derived snow cover frequency (%) (left) and snow cover anomaly (%) (right) for the month of AUG 2010 based on 1987 - 2006 base period for the Northern Hemisphere (top) and Southern Hemisphere (bottom). It is generated using the algorithm described by Ferraro et. al, 1996, Bull. Amer. Meteor. Soc., vol 77, 891-905.